AN INVESTIGATION INTO THE WAKE FLOW

BEHIND

CIRCULAR CYLINDERS FITTED WITH SLAT DEVICES

by

Anastasios Kokkalis, B.Sc.

Thesis presented for the degree of M.Sc.

to the Faculty of Engineering,

The University of Glasgow.

Department of Aeronautics and

Fluid Mechanics.   April, 1983.

ACKNOWLEDGEMENTS

LIST OF CONTENTS

List of Figures

List of Diagrams

List of Tables

Nomenclature

A, B, C	Coefficients of hot-wire characteristics
a, b	Constants
a_v	Longitudinal vortex spacing
C( )	Phase speed
C_2	Linearization constant
C_{xy}	Co-spectral density function
C_p	Specific heat at constant pressure
D	External diameter of plain circular cylindrical model
d	Diameter of the hot-wire
E	Voltage
E( )	Wake Energy
E[| |]	Expected value operator of a Fourier Transform
Ein	Non-linear voltage input
Eout	Linear voltage output
E_{REF}	Reference voltage
e	Exponent
F( )	General function of
F^{-1}( )	Inverse of general function
f	Frequency content of a record
f_c	Filter cut-off frequency
f_s	Frequency of digital sampling
f_v	Frequency of vortex shedding
Gx	Auto-spectral power function
Gxy	Cross-spectral power function
H	Width of wind tunnel
h	Time interval between two digitally sampled values

j	Imaginary part of a complex number
K1, K2, K3	Linearization constants
k_f	Coefficient of thermal conductivity
L	Characteristic length of a model
l	Area of a hot-wire
l_o	Spacing between two single hot-wires along the X-direction
m	Maximum lag value
N	Total number of digitally recorded data values
Nu	Nusselt number
n	Set of data values
Pr	Prandtl number
Q	Rate of heat transfer
Q_{xy}	Quandrature spectral density function
R	Electrical resistance of a hot-wire
Re	Reynolds number
Rx	Auto-correlation function
R_{xy}	Cross-correlation function
r	Lag number
S	General transfer function
St	Strouthal number
T	Total sampling time
To	Reference temperature
Tr	Total analogue-to-digital conversion time
T_w	Wall or body temperature
t	Time

t_r	Reference time
U	Mean flow velocity component along the X-direction
U_{eff}	Effective cooling velocity
U_o	Mean free stream flow velocity
Ur	Vortex convection velocity
u'	Fluctuating velocity component along the X-direction
V	Mean flow velocity component along the Y-direction
Vr	Reduced flow velocity
v'	Fluctuating velocity component along the Y-direction
W	Mean flow velocity component along the Z-direction
w'	Fluctuating velocity component along the Z-direction
X,Y,Z	Orthogonal system of reference axis
x( ), y( )	Time history (analogue) records of analogue signals
α	Open area ratio
α_1	Angle
β	Non-dimensional width of a slat
γ	Non-dimensional of the gap between the slat device and the body
γ_{xy}^2	Squared coherence
Δ	Very small rate of increament

θ	Angle formed between the XZ-plane and the hot-wire
θ_0	Opening angle of the partially slatted device
θ_{xy}	Phase angle
η	Index
λ	Wavelength of a velocity purturbation
μ	Dynamic viscosity of a fluid
ν	Kinematic viscosity of a fluid
π	3.1414141.......
ρ	Density of a fluid
ρ_x	Auto-correlation coefficient function
ρ_{xy}	Cross-correlation coefficient function
$\sum$	Summation
τ	Time delay of an analogue signal
Φ	Angle of orientation of the large openings w.r.t. direction of mean flow
φ	Angle formed between the XY-orthogonal plane and the hot-wire

Suffices

( )	Function of
——	Time mean value
$'$	Fluctuant component of a quantity

SUMMARY

In this experimental study, two types of slat models were used to fit on a circular cylinder; a fully slatted (slats placed evenly around the cylinder) and a partially slatted model (slat system leaving larger openings at the front and at the rear of the cylinder). Hot wire anemometric technique was used to study the wake flow within the downstream region between 3 cylinder diameters to 6 cylinder diameters, measured from the centre of the model, and in a plane about 6.5 diameters from the free end of the model. The model has a length-to-diameter ratio of 10, and the Reynolds number for the experiment was about Re=3x10^4. A number of flow measurements were undertaken, namely, the mean flow velocity in the stream direction (X-direction), and the fluctuating velocity components in the X-direction and in the transverse direction (Y-direction). The fluctuating velocity component in the longitudinal direction (Z-direction) was assumed to be extremely small. From these direct measurements, flow parameters such as turbulence intensities, power spectra, cross-correlations, phase angle, squared coherence, vortex convection velocity and vortex longitudinal spacing were derived on the basis of statistical and F.F.T. techniques. Special computer programs were written for the calculation of the above flow parameters. Flow measurements behind the basic model without the slat device incorporated were also taken for the purpose of making comparisons. Many points in the flow field in this region have been examined. For discussion, only selected results are presented in this thesis.

Two worthwhile features have resulted from the flow measurements behind a plain circular cylinder. It confirms, when comparing results with those determined by other investigators on plain circular cylinders, that the present measurements and analysis are reliable. Furthermore the results reveal, as expected, the flow pattern to be that of a regular vortex street. The vortices are formed very close to the body and are shed at a frequency close to the Strouhal frequency for a stationary cylinder. These vortices, formed and shed very close to the body, are undoubtedly responsible for the cause of vortex induced excitations.

The flow behind the cylinder model is found to be greatly modified by the presence of the slat device. With the fully slatted model, the two shear layers sprung out from the separation points are found to be very much strengthened and to have acquired, therefore, some extra degree of stability, for the formation of vortices from these layers do not take place until further downstream. Measurements have indicated that the first appearance of vortex formation occurs at a point about 3.6 diameters downstream. A regular vortex street pattern is evident beyond 3.6 diameters, having a reduced vortex frequency by about 20% compared with that of a plain stationary circular cylinder. With the partially slatted model, in which a greater amount of frontal flow is admitted to the slatted region for flow ejection at the rear of the model, no regular vortex formation was evident within the measured region of the wake. The separated shear layers are found to be very stable and to bear no sign of rolling up into

vortices. Any vortex formation can only take place beyond the 6.0D distance downstream, since up to that distance in the wake there is no evidence of narrow-band energy peaks nor any obvious correlation.

From this study it is confirmed that the effectivness of a system being able to suppress vortex induced oscillation lies in its ability to modify the wake flow in such a way that the formation of vortices, after flow separation, is removed from the body surface. The flow mechanism revealed by the present study shows that the slat devices investigated are capable of doing that.

CHAPTER 1

INTRODUCTION

Introduction

Depending entirely on air and water for existance, man has always been interested in fluid motion and the phenomena of such motion around obstacles. The whirling and swirling vortex motions seen usually behind bluff bodies may well have inspired artists in bygone days to conceive those ideas of chains and spirals in their murals and ornamentations. Leonardo da Vinci's sketch of vortical flow behing an obstacle is one such example(1).

However, it is only in the last hundred years or so that a systematic study of the bluff body - fluid flow interaction has taken place. As a result of these investigations, a wealth of knowledge about bluff body flow has been accumulated so that general flow activities behind a circular cylinder can now be fairly well understood. With a bluff body, the streamlines run close to the surface of the forward part but will break away at some point where the flow can no longer be able to overcome the rising pressure. The breaking-away of streamlines from the body surface is called boundary layer separation. The factors which contribute to this are:

(i) The viscosity of a real fluid, and

(ii) The presence of a high pressure gradient.

Once the boundary layers have separated from the body surface and become unstable, they roll up into discrete vortices. The asymmetric arrangement of vortices is more stable than the symmetric one(2,3). When growing, the vortices will draw-in fluid flow from the neighbouring flow region including that at the back of the body (base region). Several investigators have indicated that there seems to be a complex relationship between the base

2

pressure, the reverse entrained flow, the vorticity shed and the distance to the vortex formation(4,5,6).

When vortices are formed and shed from alternative sides of the bluff body, we have the well known phenomenon termed as "vortex street". For a given bluff body section, the shedding frequency (f_v) of pairs of vortices is a function of the mean flow velocity (Uo), a body characteristic length (D) and Reynolds number Re. This relationship is embraced in a non-dimensional term denoted by the Strouhal number $St = (f_v D)/Uo$. The general relationship between St and Re for cylinders of circular cross-section is well documented (7,8,9) Diag.1, but absolute values of St also depend upon cylinder surface roughness, length/diameter ratio and flow turbulence levels.
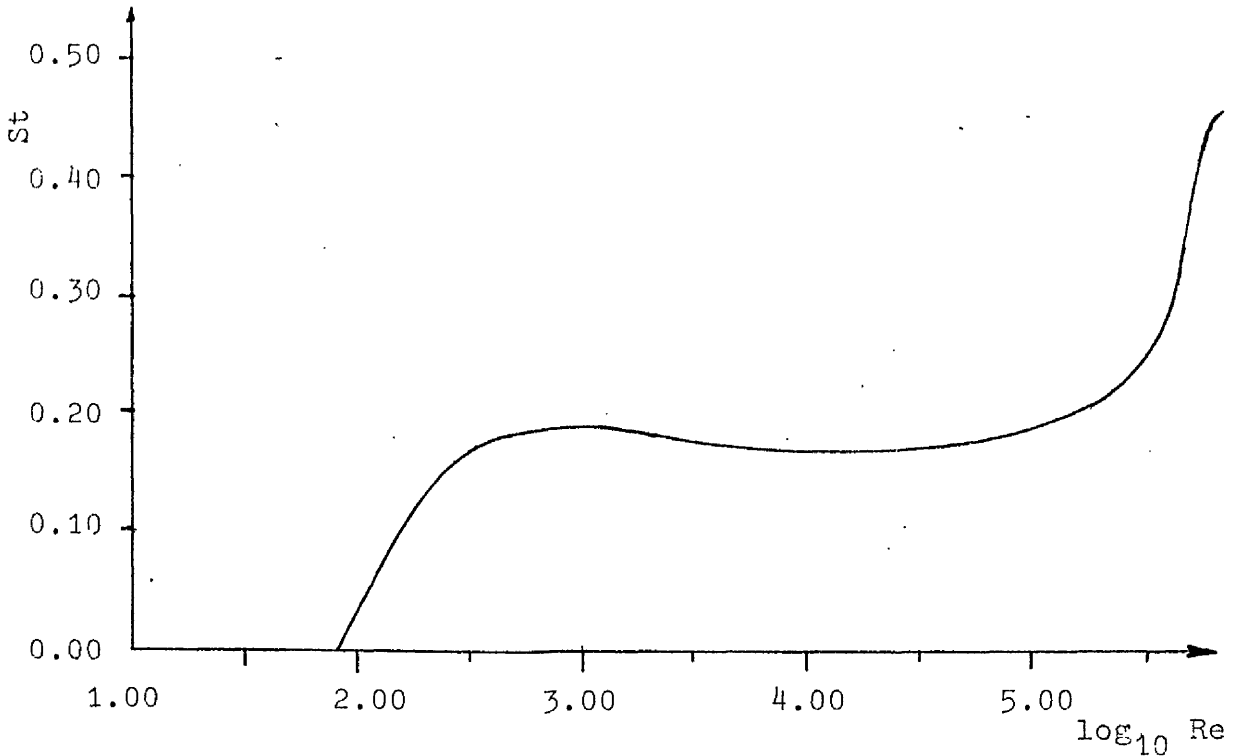
DIAGRAM 1: Variation of Strouthal number with Reynolds number.

3

Whenever a vortex is shed from the bluff body, it alters the local pressure distribution, and the body experiences a time varying force at the frequency of vortex shedding. Also, the presence of vortices in the near wake is the main cause of high pressure drag and they can also excite a leeward structure to buffeting oscillation. Many structures of engineering importance are usually slender with a bluff cross section and are prone to suffer this kind of adverse effect. If the structure is flexible or flexibly mounted, interactions can arise between the vortex shedding mechanism and the structure deflections. Under certain conditions, sustained oscillations can be excited over a flow speed range and the structure oscillates at a frequency close to its natural frequency. This is called the "lock-in" effect and at this condition it is the structure itself that controls the vortex shedding frequency. Because of this, shedding of periodic vortices can persist up to the supercritical Re range. Such oscillations are classed as self-excited or self-controlled.

In air flow, bluff cross section structures oscillate almost invariably in a direction normal to air flow, with any in-line oscillations occurring being relatively small. In water flow, structures are excited to oscillate in both in-line and cross-flow directions. Since any type of vortex-excited oscillations can often cause costly structural failures, various aerodynamic means have been devised in order to suppress them. The devices can be classified in the following catagories according to the different working principles they employ:

(i) **Surface protrusions.** A well known device of this category is that of the Helical strakes as proposed by Scrutton and

4

Walsh(10). They considered the device to operate on the principle of disrupting the correlation of the aerodynamic exciting forces along the length of the structure. In this way a three dimensional flow is introduced which interferes with the periodicity of the asymmetrical shedding of two dimensional vortices.

Other devices belonging to this category are fins. wires, studs or spheres, etc placed upon the body surface.

(ii) **Shrouds.** A typical device of this category is the perforated shroud, first proposed by Price(11). He suggested that the shroud breaks up the flow into a large number of small vortices. with the result of minimising the periodic asymmetry of flow about the cylinder.

Other devices in this category are the fine mesh gauze shroud, the axial rod shroud etc. The device under investigation, i.e. the slat device, could be also placed in this category.

(iii) **Nearwake stabilisers.** These affect the region of flow where the two entrainment layers coming from the opposite sides of the bluff body meet and interact. Devices belonging to this category are the Splitter and saw-tooth plates, guiding plates and vanes, base bleed. slits cut along the cylinder, etc.

An excellent review of the devices described above, as well as many others, can be found in Ref. 12.

A recent development in the area of suppressing vortex-excited oscillations is the Slat device. It consists of a number of longitudinally placed slats, evenly disposed around the bluff

5

body(13). For flows with a fixed direction, the effectiveness of the device can be further enhanced by providing the device with larger front and rear openings. The latter set-up will be referred to as Partially-Slatted-System. A detailed description of both devices. i.e. the Fully Slatted and Partially-Slatted, will be presented in the next chapter.

The effectiveness of the slat device in suppressing vortex-excited oscillations has been confirmed both in laboratory and practical investigations (14,15). Also a comparative study between the perforated shroud, the helical strakes and the slat device regarding their relative effectiveness in suppressing vortex-induced oscillations(12,13), showed the superiority of the slat device (especially the Partially-Slatted-system) over the other two formentioned devices, in suppressing vortex-excited oscillation especially at low damping coefficients (16). A number of reasons regarding the effectiveness of the slat device have been suggested (15,17). Some of these reasons have so far been confirmed indirectly by the various different experimental investigations carried out for a variety of practical purposes. However, it is desirable to take a step further and examine the cause for the effective performance of the slat device. One way of carrying-out this, is to examine the near wake flow in greater detail. Since the activity of the near wake is closely related to the flow behavior around the body, it is possible to interpret the dynamic influence of the flow on the body by carrying out detailed observations within this region. Thus by using circular cylindrical models fitted with and without the slat devices, it is possible to observe the flow modification rendered by the

6

presence of the devices, at least in the near wake region. For this purpose the hot-wire technique has been adopted. Although this might not be the best available technique for measurements in the wake of a body, it has been used extensively for flow measurement purposes and its shortcomings are generally known. The results of the hot-wire measurements are analysed through a digital electronic computer and are presented in the form of mean velocity ratios, Turbulence intensities, Power Spectra, Cross-correlation of velocities in space, Vortex convection velocities and length of Vortex longitudinal spacing.

In order to ascertain that the technique and further analysis of results employed is reliable, the results obtained from a plain circular cylindrical model in this investigation were first compared with known results obtained by other investigators (18,19).

Further discussions regarding the slat device, the statistical approach used for the analysis of the experimental data as well as the technique used to obtain that data, and finally, the discussion and conclusions reached regarding the flow mechanism behind the slat-cylinder combination, will be given in subsequent chapters.

7

CHAPTER 2

SLAT DEVICES

2.1 Flow separation control

In the previous chapter we discussed how the formation of vortices behind a bluff body is a result of flow separation. Thus, the control of flow separation from the bluff body surface can be regarded as an essential step towards reducing the adverse effects. such as vortex-induced oscillations. high pressure drag. etc, due to vortex shedding. If flow separation cannot be avoided and vortices do form, beneficial results can still be obtained by placing restrictions upon the movement of the vortices or by reducing their strength or by destroying their periodic occurrence.

Various methods have been devised for the control of flow separation. Discussion here will be restricted to widely used ones only.

One such method is to streamline the bluff body so that no flow separation takes place. Although this appears to be a very simple approach, it is not always convenient to be carried out in practice.

Another method is to reduce the effects of the adverse pressure gradient on the rear of the bluff body This can be achieved by reducing the thickness of the boundary layer present by using the suction technique (Diag.2). In this way, the work done by the fluid flow in overcoming the boundary layer "frictional" effects would be less and separation can thus be delayed. The application of boundary layer suction method has a serious drawback in that an external power supply is needed.

Another method of controlling flow separation is that of boundary layer re-energisation. One of the primary reasons for

boundary layer separation taking place is that the fluid adjoicing the body surface has insufficient momentum to overcome the adverse pressure gradient. By means of blowing high energy fluid into the boundary layer, the boundary layer can be invigorated to move further and thus delaying separation. In a passive system, high energy fluid can be extracted from the high pressure field of the body to do the job by directing the high energy flow to the regions where re-energisation of the boundary layer is required.

Once flow separation has taken place, the main stream of fluid near the rear body-surface is forced away from as shown in Diag.3, giving rise to a drastic change of the flow field around the body resulting often in high pressure drag, oscillations caused by vortex shedding and in buffeting of bodies placed in its wake. If the movement of the flow after separation could be restricted somewhat, then some of the formentioned adverse effects could be lessened.

One way of restraining the separated boundary layer is the use of flow bounding surfaced which have the ability of guiding the flow along a desired course. For instance, the flow could be guided to follow the potential flow streamlines, as in Diag.4. In this arrangement, high energy flow from the forward part of the body is guided through the channels formed between the bounding surfaces and ejected at the rear part of the body. The flow bounding surfaces are so shaped so as to force the flow to follow the potential flow streamlines and thus avoid any flow separation from taking place. However this arrangement is impractical due

to the high viscous drag it involves. By reducing the flow bounding surface to a single layer placed near the body surface. as in Diag.5, the problem of high viscous drag could be reduced. Yet to rely on a single layer of flow bounding surface to restrain the flow from breaking away from the body surface would certainly result in flow separation and thus the formation of vortices occurring at the outside surface of the flow bounding surface. The resulting situation would not be very much better than that of a plain cylinder. We contemplate therefore that the concept of energy injection for flow stabilisation can aid in resolving the problem. Through the action of flow ejection from an inner flow region across a flow bounding surface to an outer flow region, it is hopeful that some recovery of the potential flow characteristics can be realised.

The above ideas were therefore adopted in the design of the flow stabilising device under investigation.

2.2 Slat device

The slat device was developed to provide the flow around a bluff body with sufficient stability so that the adverse effects of structural self-induced oscillations, associated with vortex shedding, could be alleviated. The device is a passive self-regulating system which relies on the extraction of high energy fluid from the frontal high pressure field and ejecting it into the boundary layers at the sides as well as at the rear region of the body.

The device essentially consists of a number of slats which are longitudinally placed around the periphery of the body. They

11

are kept at a distance from the body surface and have regular openings or slots between them so that fluid flow can take place. The bounding surfaces employed, by virtue of their geometrical shape, offer little obstruction to the flow passage and consequently a stable and vigorous inner flow may be maintained. For convenience, the slat system can be fully defined by four geometric parameters at a given section of the structure. These parameters are:

(i)   The open area ratio, α ,

(ii) The non-dimensional width of the slats, β ,

(iii) The non-dimensional gap distance between the slats and the adjacent body surface, γ , and

(iv) The slat thickness-to-width ratio, δ .

Parameters (ii) and (iii) are referred to an effective body length D (e.g. for a circular cylinder D is the diameter of the section). A general cross-sectional lay-out of the slat system placed around a circular cylinder is shown in Diag. 6 . Experimental investigations conducted by Wong(13) on the suppression of flow induced vibrations of circular cylinders have shown that best results are obtained when, the open area ratio $\alpha = 0.4$, the non-dimensional slat width $\beta = D/11.5$ and the slat-to-cylinder gap $\gamma = D/7$. The thickness-to-width ration should not exceed the value of $\delta < 0.15$. Further results obtained by Wong (14) and by Wong and Kokkalis (16) have shown that the parameter values proposed above do give satisfactory results.

For the case of a flow having a fixed direction, the effectiveness of the slat device can further be enhanced with the provision of large front and rear openings, the configurations of

12

whichis shown in Diag.7 . The angle subtending the opening is described by θ_0 and the opening's orientation to the direction of flow by ϕ . Investigations by Wong (14) have shown that for optimum conditions regarding the suppression of flow induced vibrations, the value of θ_0 should be around 31° degrees, so as to coincide with the frontal area of high flow pressure, and the value of ϕ should be less than 30° degrees. Wong and Kokkalis (16) have also found that under very low damping coefficients (K=1.8), the slat device has a superiority over the perforated shroud device (10) and the helical strakes device (11) and that of subcritical Reynolds number, the drag coefficient is reduced at least by 15% when compared with that of the plain cylinder, whereas with the partial-slat device, drag improvement by as much as 25%.

2.3 The function of the slat device

In an attempt to explain the reasons for the slat device being able to suppress vortex-induced oscillations, Wong and Cox (17) and Wong (15) have made some suggestions regarding the flow around the slat device. Although they based their reasoning on experimental observations carried out for various practical purposes and not on detailed measurements of the wake flow, it shows a high insight of the flow field and highlights some of the complex flow mechanisms involved.

For convenience, they divided the flow field around the body into three flow regions, as shown in Diag.8, and treated the flow through the slats as being in general two-dimensional.

As the fluid approaches the body in the high pressure Region

13

I, part of it flows between the slats and the body surface. Due to forced mixing at this stage, a high intensity turbulent flow is set up which forces its way round the structure. Some of this inner flow will be ejected in Region II, where the external pressure is low and the remainder will be ejected through the slats at the base Region III.

The slats in Region II are acting as flow bounding surfaces. They prevent early flow separation from the body surface and restrict any vortex growth to take place within the passage. Outside the slats, their downwash effect is likely to delay the outer flow from breaking away and the fluid ejection between them provide counterflows which to some extent prohibit the formation of large scale vortices from taking place close to the slat-body combination.

Finally, in Region III, fluid is ejected into the base area and acts as "base bleed". This base bleed tends to increase the distance of the vortex formation region, thus lessening the effects of the vortices on the body which generates them. They considered this to be one of the reasons for the reduction of oscillations. Also, the increase in base pressure helped to reduce the overall drag coefficient.

The advantage of removing the slats from Region I and III, as in the Partially-slatted device, is to enable more high energy fluid to enter the channel provided between the slats and the body surface. However, the removal of slats from Region I and III could only be advantageous in unidirectional flows, as has already been demonstrated by Wong (14). Wong (15) concluded that

the reason for the slat device being so effective in suppressing vortex-induced oscillations lay in the capacity of the device in embracing various methods of flow separation control, such as forced flow mixing, boundary layer energisation, base bleed,etc. However it is desirable to take a step further and examine in detail the real means for the effective performance of the slat device. This will be carried out by means of taking measurements of the velocity field using hot-wire anemometry. It is hoped that the measurement of mean and fluctuant flow velocities will give us a better understanding of the complex flow processes involved in the suppression of vortex shedding behind a circular cylinder fitted with and without the mentioned devices.

ATTACHED FLOW
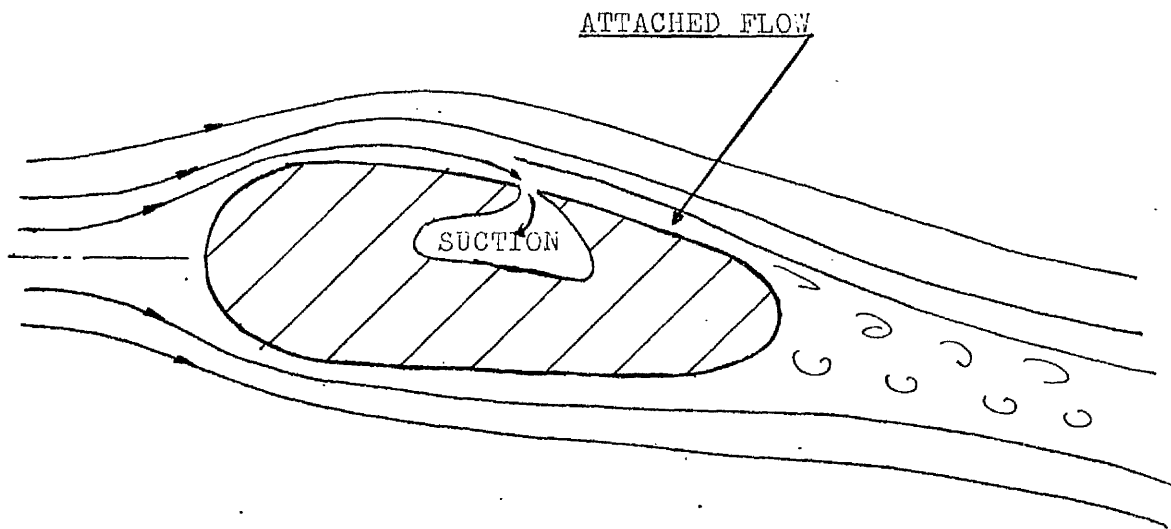
SUCTION

Diagram 2: Control of flow separation using the flow suction technique.
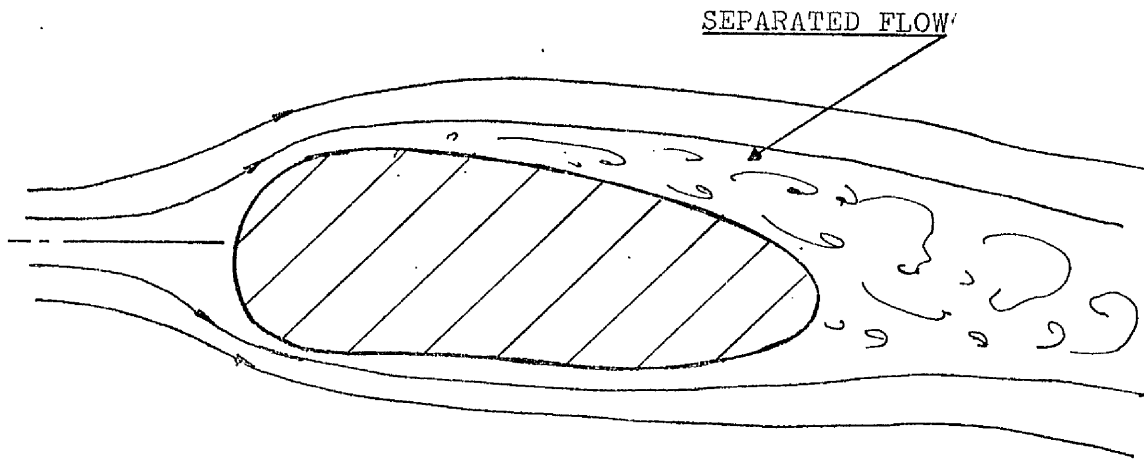
Diagram 3 :. Flow separetion in the rear of a bluff body.

U_o →
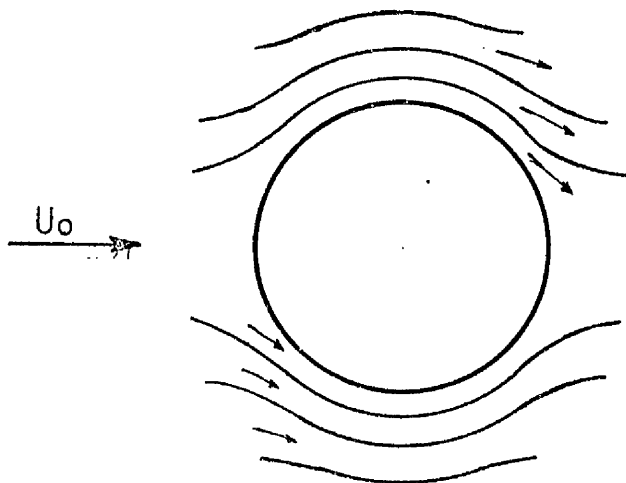
Diagram 4 : Many layers of flow bounding surfaces lying along the streamlines.

U_o →
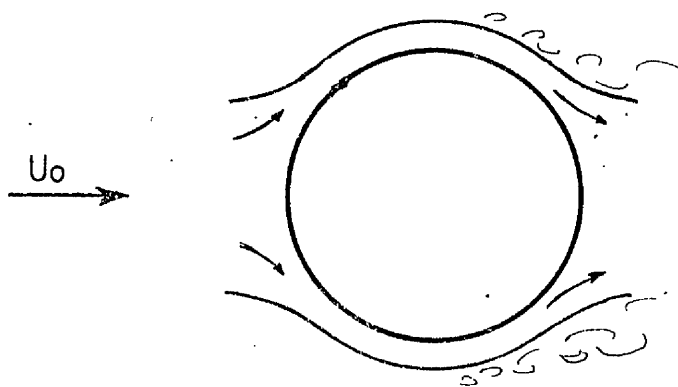
Diagram 5 : Single layer of flow bounding surfaces lying along the streamlines

16
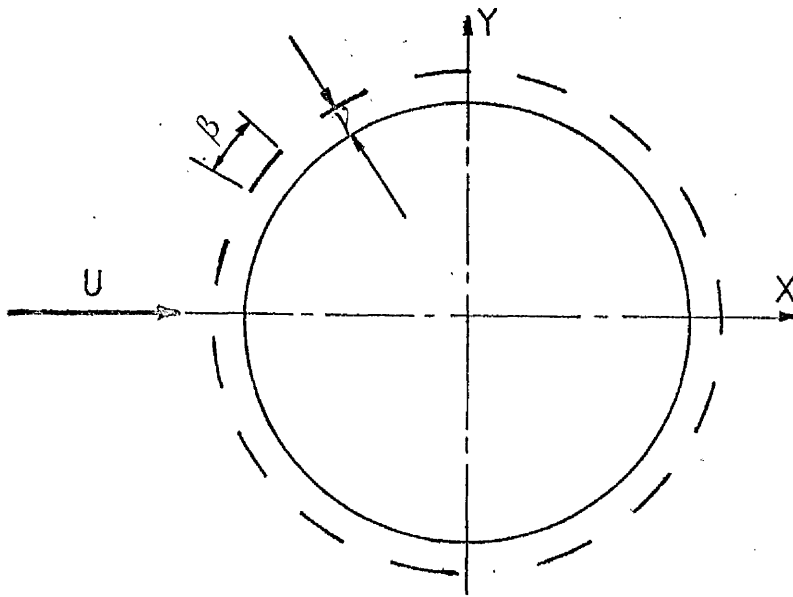
Diagram 6: Cross-sectional view of the fully slatted device
placed around a circular cylinder.
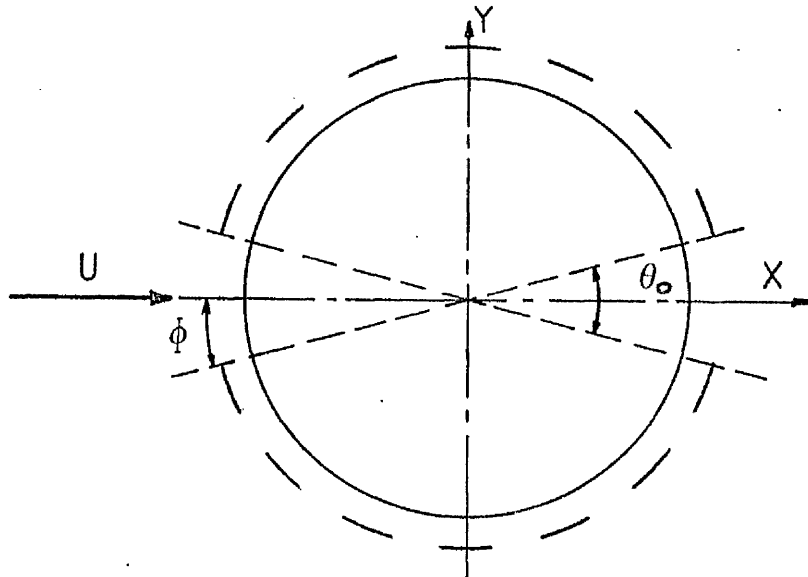
Diagram 7: Cross-sectional view of the partially slatted
device placed around a circular cylinder.
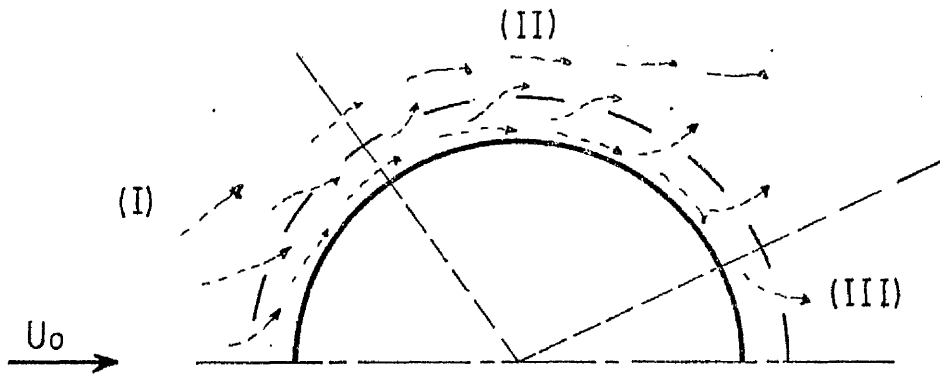
Diagram 8 : General flow pattern around a circular
cylinder fitted with a slat device.

17

CHAPTER 3

STATISTICAL ANALYSIS OF DATA

3.1 Introduction

In this chapter we shall present an outline of the basic statistical functions which are used in turbulence flow measurements, as required in the present investigation. We shall restrict our discussion to either single measurement records or to two simultaneous measurement records.

In general, four types of statistical functions are used to describe the basic properties of wake flows:

1. Mean square values

2. Probability density functions

3. Correlation functions and

4. Power spectral density functions.

The mean square values and probability density functions usually describe the amplitude characteristics of a measurement record, while the correlation functions and power spectral density functions usually describe the time and frequency dependent properties of a measurement record.

However, in the present study, because of restrictions imposed by the equipment used, it is not possible to find the probability density functions of the measured data. So the discussion will be concentrated on functions (1), (3) and (4) only. These functions will be briefly analysed below.

3.2 General Considerations

The origin of axes is taken at the centre of the models (Diag. 9); X is measured downstream in the direction of the free-stream velocity, Z is measured along the axis of the model, which is perpendicular to the free-stream velocity, and Y is measured

19

in the direction perpendicular to (XZ); that is, Y = 0 is the centre plane of the wake.

The velocity vector U at a given point in the flow field has usually non-zero values in all three orthogonal directions (X.Y.Z) and one can consequently select to record any one of the three velocity components U_i. However. the velocity field $U(X,Y,Z,t)$ of the investigated flow is usually a function of both space and time. This presents problems with subsequent analysis, and in order to proceed further we have to assume that the data recorded from measurements in this flow field is stationary. This means that the mean values and autocorrelation functions of measured data are independent of the time of measurement. The validity of this assumption regarding data from the present investigation is discussed later on.

For a stationary type of data, it follows that we can separate the velocity vector into a time-mean and a fluctuating component. so that

$$U(X,Y,Z,t) = \bar{U}(X,Y,Z) + u'(X,Y,Z,t)$$

or in tensor notation

$$U_i = \bar{U}_i + u'_i$$

where

i   represents the X, Y and Z directions.

We shall, for the rest of this dissertation, denote mean values by bars (e.g. $\bar{U}$, $\bar{V}$, $\bar{W}$) over the quantity concerned and. the fluctuating component by dashes (e.g. u', v', w').

20

3.3 Single Record Measurements

Let $\{x_n\}$; $n = 1, 2, \ldots, N$ be the data values of a single time history record $x(t)$ taken at the points $t_n = t_o + nh$; $n = 1, 2, \ldots, N$. The starting point t_o is arbitary and for stationary data it does not enter into the formulae. These points (or data values) are a distance h apart which is determined by the data logging frequency. that is

$$h = \frac{1}{f_s}$$

and N denotes the sample size of the measured record. In equation form, the original data values are

$$x_n = x(t_o + nh) \qquad n = 1, 2, 3, \ldots N.$$

It should perhaps be mentioned at this point that the measured record x_n can be any one of the velocity components along the three orthogonal axes of the flow field. Using this record, we can evaluate the following statistical quantities.

3.3.1. Mean Square Values (Mean values and Variances)

The general intensity of any random data may be described in rudimentary terms by a mean square value. In equation form, the mean square value for a sample time history $x(t)$ is given by

$$\overline{x^2} = \frac{1}{N} \sum_{n=1}^{N} (x_n)^2$$

However, it is often desirable to separate the data in terms of a static and a dynamic or fluctuating component. The static component may be described by a mean value, which is simply the arithmetical average of all values, i.e.

$$\overline{x} = \frac{1}{N} \sum_{n=1}^{N} x_n$$

The dynamic or fluctuating component may be described by a

21

variance, which is simply the mean square value about the mean, i.e.

$$\overline{x'^2} = \frac{1}{N} \sum_{n=1}^{N} (x_n - \bar{x})^2$$

The positive square root of the variance is called the standard deviation and is given by

$$\sqrt{\overline{x'^2}} = \left[\sum_{n=1}^{N} \frac{(x_n - \bar{x})^2}{(N-1)} \right]^{1/2}$$

The term (N-1) is used only to penalise a small sample size.

The relative (or local) turbulence intensity component of the investigated velocity component, which is a measure of the magnitude of the turbulence fluctuations, is defined by

$$Tu(x) = \frac{\sqrt{\overline{x'^2}}}{\bar{x}}$$

However, if the mean free-stream velocity (U_o) is known and the X-axis of the co-ordinate system has been selected parallel to it, then it is conventional to define the turbulence intensity of a fluctuating component by

$$Tu(x) = \frac{\sqrt{\overline{x'^2}}}{U_o}$$

In the present investigation, only the later definition of turbulence intensity is used.

3.3.2. Auto-correlation functions

The auto-correlation function describes the general dependence of the values of the data record at one time on the values at another time.

For N data values $\{x_n\}$, n = 1,2, ... N, from a record which is stationary with $\bar{x} = 0$, the estimated auto-correlation function at the displacement rh may be obtained by taking the product of the values at x_n and x_{n+rh} and averaging over the total number

22

of values N (Diag.10).
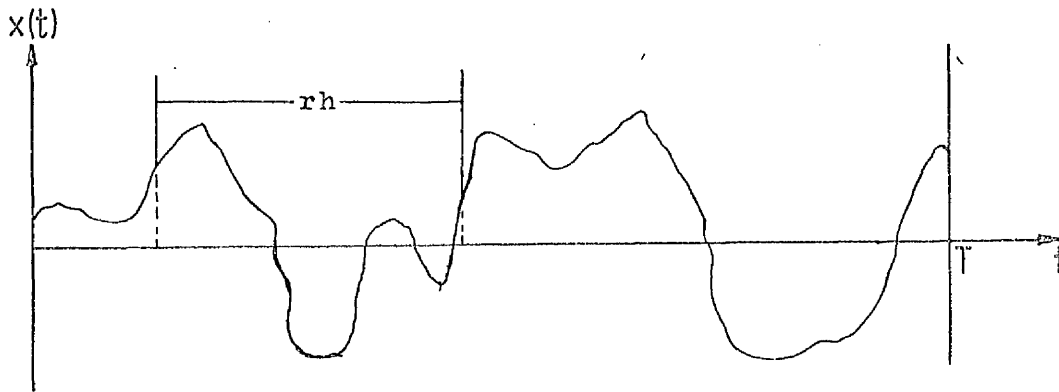
Diagram 10: Auto-correlation function measurement.

It is given by

$$R_x(rh) = \frac{1}{N-r} \sum_{N=1}^{N-r} (x_y \cdot x_{y+r}) \qquad r = 0,1,2,\ldots m$$

where

    r is the lag number

    m is the maximum lag number and,

    rh is the total (time) displacement

It is however convenient to normalize the auto-correlation function by dividing it, for large values of N, by the variance of the data values. The normalized auto-correlation function is called the auto-correlation coefficient ρ_x, and in equation form is given by

$$\rho_x = \frac{R_x(rh)}{\overline{x'^2}}$$

It can be shown theoretically (cf ref. 21) that ρ_x will always take values between plus and minus one, that is

$$-1 \leqslant \rho_x \leqslant 1$$

The principal application of an auto-correlation function or coefficient of a measured data, is to establish the influence of values of one time over values at a future time. Because

23

periodic data will have an autocorrelation coefficient which persists over all time displacements, as opposed to random data which diminishes to zero for large time displacements, the autocorrelation coefficient can clearly provide a powerful tool for detecting periodic data which might be "masked" by a random background.

3.3.3 Power Spectral Density Functions

The power spectral density function for stationary data describes the general frequency composition of the data in terms of the spectral density of its mean square value. It is given by

$$G_x(f) = \lim_{\Delta f \to 0} \lim_{T \to \infty} \frac{1}{T} \int_0^T \overline{x'^2}(t, f, \Delta f) \, dt$$

where

T is the total sample time (T = Nh)
f is the frequency of the data, and
Δf is the frequency resolution of the data.

An important property of the power spectral density function, is its Fourier-transform relationship with the autocorrelation function in the form of

$$G_x(f) = 2 \int_{-\infty}^{\infty} R_x(\tau) e^{-j2\pi f\tau} \, d\tau = 4 \int_0^{\infty} R_x(\tau) \cos 2\pi f\tau \, d\tau \qquad \ldots(3.1)$$

or conversely

$$R_x(\tau) = \int_0^{\infty} G_x(f) \cos 2\pi f\tau \, df \qquad \ldots(3.1a)$$

where

τ is the time lag between data values ($\tau = rh$).

In terms of the autocorrelation coefficient, the power spectral density function is given by

$$G_x(f) = 4\overline{x'^2} \int_0^{\infty} \rho_x(\tau) \cos 2\pi f\tau \, df$$

Before the advent of Fast Fourier Transforms for use on digital computers, equation (3.1a) was extensively used for the determination of the auto-correlation function and/or coefficient, since the evaluation of the power spectral density function can easily be determined using analog techniques (cf ref. 21). However, in the present time, the determination of power spectral density functions is done by means of direct Fourier transformation of the original data record. For a stationary record $x(t)$, the finite Fourier transform over the Kth record of length T is given by

$$X_k(f,T) = \int_o^T x_k(t)e^{-j2\pi f\tau} \, d\tau$$

and the power spectral density function is then defined by

$$G_x(f) = \lim_{T \to \infty} \frac{2}{T} E\left[\mid X_k(f,T) \mid^2 \right]$$

where

$K = 1,2,3, \ldots$, and

E is called the expected value opertor denoting an average operation over the index K.

The principal application of a power spectral density function is to establish the frequency composition of the measured data, which in turn, bears important relationships with the basic characteristics of the physical system involved.

3.4 Two Record Measurements

Consider two time history records $x(t)$ and $y(t)$, which are stationary and exist only for

$$t_o < t < t_o + T_r$$

where t_o is arbitrary and may be zero. The respective sample values for $x(t)$ and $y(t)$, assuming a sampling time interval

$$h = \frac{1}{2f_c}$$

are given by

$$x_n = x(t_o + nh)$$

$$y_n = y(t_o + nh)$$

where

$$n = 1,2,3 \ldots, N$$

and

$$Tr = Nh$$

From the measurement of these quantities, the following statistical functions are evaluated.

3.4.1. Cross-Correlation Functions

The cross-correlation function for two sets of stationary data describes the general dependence of the values of one set of data on the other with respect to the time and/or space. An estimate for the cross-correlation function for the values of $x(t)$ and $y(t)$ at a displacement rh, as shown in Diag.11, may be obtained by taking the average of the total number of values over the difference of the total number of values minus the lag value.
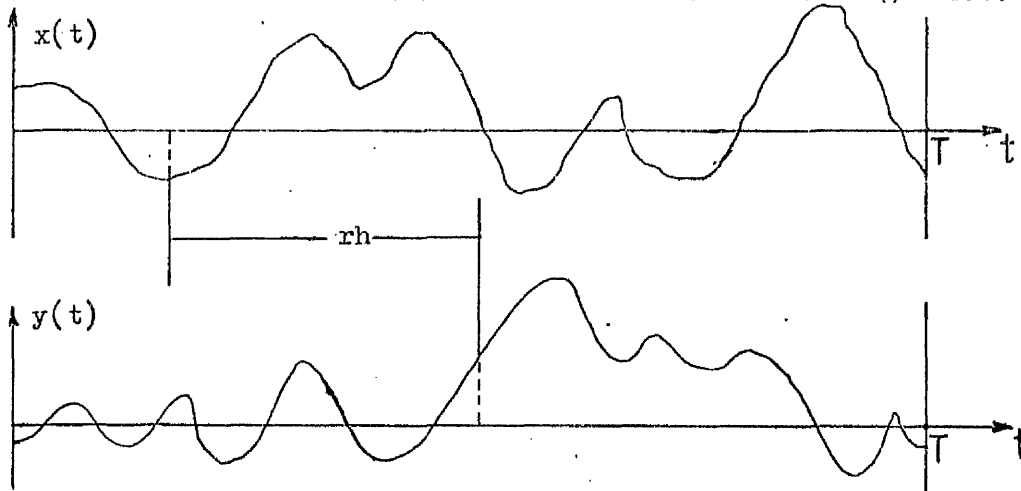
Diagram 11: Cross-correlation function measurement.
The relevant expressions are

$$R_{xy}(rh) = \frac{1}{N-r} \sum_{N=1}^{N-r} x_n\, y_{n+r}$$

26

and

$$R_{yx}(rh) = \frac{1}{N-r} \sum_{N=1}^{N-r} x_{n+r}\, y_n$$

These functions are always real-valued, which may be positive or negative. and have the property that

$$R_{xy}(-rh) = R_{yx}(rh)$$

The sample cross-correlation function $R_{xy}(rh)$ usually is normalized to have values between plus and minus one by dividing them by the product of

$$\sqrt{\overline{x'^2}} \cdot \sqrt{\overline{y'^2}}$$

This defines a sample cross-correlation coefficient in the form of

$$\rho_{xy}(rh) = \frac{Rxy(rh)}{\sqrt{\overline{x'^2}}\sqrt{\overline{y'^2}}} \qquad r=0,1,2,\ldots\ldots m$$

and which is theoretically satisfied by

$$-1 \leqslant \rho_{xy}(rh) \leqslant 1$$

A similar formula exists for $\rho_{yx}(rh)$.

Two types of information can be obtained from these functions. Firstly, for isotropic turbulence

$$R_{xy}(rh=o) = 0$$

and the value of $R_{xy}(o)$ is therefore a measure of anistropy of the flow. Secondly, the cross-correlation curve can be used to provide information about the phase relationship between the two fluctuating quantities x(t) and y(t).

3.4.2. Cross-Spectral Density Functions

The cross-spectral density function for a pair of fluctuating signals x(t) and y(t) is the Fourier transform of the cross-correlation function (equn. 2.9). Because the cross-correlation function is not an even function, the cross-spectral

27

density function $G_{xy}(f)$ is generally a complex number, such that

$$G_{xy}(f) = 2\int_{-\infty}^{\infty} R_{xy}(\tau)\, e^{-j2\pi f\tau}\, d\tau = C_{xy}(f) - jQ_{xy}(f)$$

with $\tau = rh$

and where the real part, $C_{xy}(f)$ is called the co-spectral density function and the imaginary part, $Q_{xy}(f)$ is called the quadrature spectral density function.

In direct frequency terms, the co-spectral density function can be thought of as the average product of x_y and y_{y+r} within a narrow frequency interval between f and $f + \Delta f$ divided by the frequency interval Δf. In terms of the cross-correlation function, is given by

$$C_{xy}(f) = 2\int_{-\infty}^{\infty} R_{xy}(\tau)\, \cos 2\pi f(\tau)\, d\tau$$

The quadrature spectral density function is the same as the co-spectral density function except that either $x(t)$ or $y(t)$, but not both, is shifted in time (or values) sufficiently to produce a 90° degree phase shift at frequency f. That is,

$$Q_{xy}(f) = 2\int_{-\infty}^{\infty} R_{xy}(\tau)\, \sin 2\pi f\tau\, d\tau$$

It is convenient to express the cross-spectral density function in complex polar notation, such that

$$G_{xy}(f) = \left| G_{xy(f)} \right| e^{-j\theta xy(f)}$$

where the magnitude $G_{xy}(f)$ and the phase angle $\theta_{xy}(f)$ are related to $C_{xy}(f)$ and $Q_{xy}(f)$ by

$$\left| G_{xy}(f) \right| = \sqrt{C_{xy}^2(f) + Q_{xy}^2(f)}$$

and

$$\theta_{xy}(f) = \tan^{-1}\left[\frac{Q_{xy}(f)}{C_{xy}(f)} \right]$$

By interchanging $x(t)$ and $y(t)$, one finds that

28

$$C_{xy}(f) = C_{yx}(f) \qquad \text{and} \qquad Q_{xy}(f) = -Q_{yx}(f)$$

Hence, the following relationships apply

$$G_{yx}(f) = G_{xy}^*(f)$$

or

$$G_{yx}(f) = G_{xy}(-f)$$

where $G_{xy}^*(f)$ denotes the complex conjugate of $G_{xy}(f)$

In some cases, it is usual to normalize the cross-spectral density magnitude $G_{xy}(f)$ by dividing it by $G_x(f)$ and $G_y(f)$, so that

$$\gamma_{xy}^2(f) = \frac{\left|G_{xy}(f)\right|^2}{G_x(f) \cdot G_y(f)}$$

where

$\gamma_{xy}^2(f)$ is called the squared coherence function, and theoretically it should satisfy the relationship

$$0 < \gamma_{xy}^2(f) < 1 \quad \text{for all } f$$

Cross-spectral density function measurements have many applications. They are used for the measurement of frequency response functions and the measurement of time delays τ as a function of frequency in the form of

$$\tau = \frac{\theta xy(f)}{2\pi f}$$

which is not available directly from the correlation function measurements.

3.4.3. Vortex Convection Velocity and Vortex Longitudinal Spacing

Vortex convection velocity is defined as the velocity with which vortices in a vortex wake are transported downstream relative to the body.

Vortex longitudinal spacing is defined as the distance in

29

the direction of the mean flow between the centres of two consequatively shed vortices of a vortex wake. The vortex convection velocity and the vortex longitudinal spacing are related by

$$U_r = f . a_v \quad - - - - -(1)$$

where

U_r is the vortex convection velocity,

f is the frequency of vortex shedding from one side of the body, and

a_v is the vortex longitudinal spacing.

The method used for the calculation of U_r and a_v is the one introduced by Simmons (20) (see also Chapter 5). Only a brief theoretical description of the above method will therefore be presented here.

The wavelength $\lambda(f)$ of a velocity perturbation at the shedding frequency travelling between two hot-wires, is given by

$$\lambda(f) = 2\pi l_o / \theta_{rs}(f) .$$

where

l_o is the hot wire spacing in the direction of the mean flow and

$\theta_{rs}(f)$ is the phase difference (angle) between the signals of the two sensors in the flow as a function of the frequency f. If the squared coherence between the signals from the two sensors is high (i.e. close to unity) and the perturbation at the shedding frequency is solely due to the passage of the vortices, then $\lambda(f)$ is a measure of the vortex longitudinal spacing a_v. Under these same conditions, the phase speed $C(f)$ at the shedding frequency, which is given by

$$C(f) = \frac{2\pi l_o f}{\theta_{rs}(f)}$$

30

can correspondingly be taken as a measure of the vortex convection velocity U_r (from [equn. (1)].

For the calculation of the phase angle $\theta_{rs}(f)$ and squared coherence $\gamma^2(f)$ refer to section 3.4.2.

3.5. Discussion

In the previous sections we have discussed the statistical approach used for analysing the measured data of this investigations. This approach is based on the assumption that the measured data record is stationary. The main reason for making this assumption is that data can be collected at arbitrary random times and sampled periodically thereafter without introducing too many errors. Furthermore, the statistical properties computed for each of a sequence of relatively short time intervals will not significantly vary from one time to the next. Here the word significantly means that variations are greater than would be expected due to statistical sampling variations. So every effort is usually made in practice to design experiments that will produce stationary data, because the necessary analysis procedures for non-stationary data are substantially more difficult.

The parameters used in order to establish the stationarity of a measured data record are the sample mean value and the mean square value of that record. In this work, two non-parametric tests are carried out on these two parameters, namely

i.   The Run test, and
ii. The Trent test.

Details regarding these tests and how they may be applied can be found in Reference 21.

The results from both tests, for randomly selected data records from the present investigation, are presented in Table 1. As it can be observed from this table, all selected records satisfy the requirements for stationarity set by the Trent test, but the results from the Run test are not that conclusive. Although the mean square values of the data records tested, satisfy the requirements for stationarity set by the Run test the mean values of the same data records do not always satisfy them. However, since three out of four conditions for stationarity are fully met and the fourth is only partially satisfied, the principle of stationarity regarding the whole set of measured records is acceptable in the present investigation.

In the statistical approach for the analsysis of data from turbulent wake flow investigations, all parameters involved, (e.g. autocorrelations, cross-spectral density functions, etc), integrate over all the flow processes which occur in the flow. As the flow processes are not strictly repetitive and considerable deformations occur within the flow, it is not possible from such measurements to evaluate the separate significant flow processes involved and their spatial and temporal developments. Consequently, time mean statistical measurements cannot identify the physical nature and occurence of those flow processes which give the largest contributions (in space and time) to the various fluctuating quantities.

Position of Measurement		RUN TEST		TRENT TEST	
X/D	Y/D	Mean Values	Mean Sqare Values	Mean Values	Mean Sqare Values
3.0	0.00	61	54	2469	2445
	0.53	76	55	2525	2525
	1.20	75	48	2350	2450
4.5	0.00	70	44	2518	2230
	0.53	71	55	2509	2640
	1.20	72	45	2460	2085
6.0	0.00	71	51	2529	2343
	0.53	65	48	2356	2129
	1.20	69	50	2463	2462
Range of values for acceptance		40 – 61		2145 – 2804	

TABLE 1: Results from tests for stationarity carried out on records of u′-velocity component as recorded behind model (I).
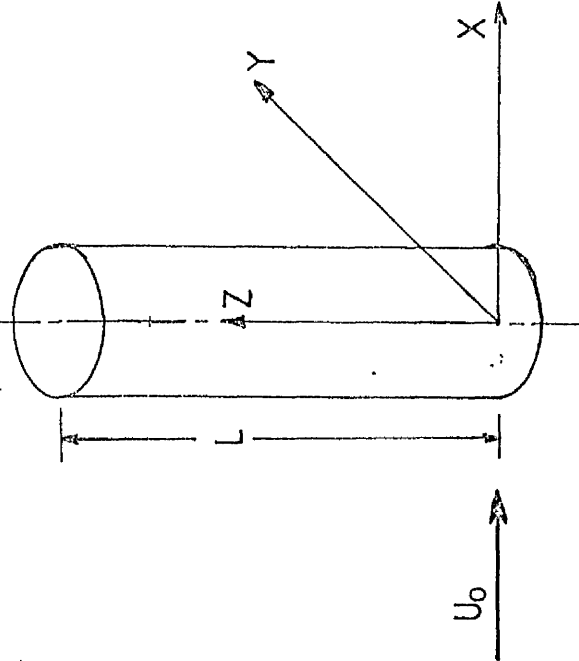
Diagram 9: Circular cylinder and co-ordinate axis.

CHAPTER 4

HOT-WIRE ANEMOMETRY

4.1 Introduction

Hot-wire anemometry has been widely employed for measuring
instantaneous flow velocity.   Thermal anemometry can be traced
back to the last two decades of the ninteenth century (Serr 1888;
Webber 1894; Oberbeck 1895) and has since undergone vigorous
development.

The principle of this technique is based on the convective
heat-transfer from an electrically heated element to the
surrounding fluid.   The amount of heat transfer depends on the
temperature difference and the geometry of the sensor as well as
on the flow velocity and other physical properties of the fluid.
Assuming that only one of the fluid parameters (e.g. velocity or
temperature) varies during a test, then the heat-transfer from
the sensing element can be interpreted as a direct measure of the
parameter in question.   Should more than one parameter vary,
there are techniques for differentiating between the effect of
each one.   However, in this discussion only changes due to flow
velocity are of interest, whereas changes in other parameters of
the flow are assumed to have negligible effect.

4.2. Basic Physics of Hot-wires

The analysis of forced convective heat transfer from a
heated body to the surrounding fluid is highly complex.   To make
the solution tractable, a variety of assumptions have to be made
depending on the prevailing conditions.   The case is further
complicated when applying the analysis to hot-wire sensors
as they are subject to natural convection at low flow velocities and to heat
conduction taking place in the probe supports and substrates.
However some knowledge of the physics of heat transfer is

35

necessary in order to assess the reliability of the hot-wire calibration.

Heat transfer from a hot-wire is usually expressed as a dimensionless quantity called Nusselt number. The Nusselt number is equal to the rate of heat transfer to the fluid per unit area $Q/1$. divided by the product of the thermal conductivity of the fluid and the temperature gradient $(T_w - T_o)$, that is

$$N_u = \frac{Q}{1 \cdot K_f (T_w - T_o)} \quad \text{---- (4.1)}$$

At low speeds (M <0.4) and moderate fluid densities, the Nusselt number may be expressed as a function of the Reynolds number, the Prandtl number and the angle of inclination of the sensing element to the mean direction of the fluid stream. In the following analysis the Reynolds number will be taken to be a function of the effective velocity of the flow seen by the hot-wire and which in practice is not equal to the mean flow velocity.

The Prandtl number in practice indicates a property ratio of the fluid and is equal to

$$P_r = \frac{C_p \mu_f}{K_f} \quad \text{---- (4.2)}$$

For gases at moderate temperatures, this quantity is very nearly constant, being about 0.7 for air under standard atmospheric conditions. In liquids it varies considerably with temperatures because the viscosity is a strong function of temperature. Since in this discussion we are dealing with air only (P_r constant), its effects on the Nusselt number need not be considered explicitly in the analysis.

The variation of Nusselt number with Reynolds number has provided the main analytical information for hot-wire anemometry in gases and this has been explored by many researchers. The first to do so was King[22] who in 1914 arrived at a solution for the heat transfer from an infinite cylinder in an incompressible flow, which can be expressed as

$$N_u = a + b R_e^{0.5} \qquad ----(4.3)$$

where
a and b are constants

More recent work (Collis & Williams (23), Bruun (24)) has shown that an exponent 0.45 gives a better correlation in the Reynolds number range usually operated in hot-wire anemometry.

As the expression given by equation (4.3) has been found to be of little value to the analysis of hot-wire anemometry, its modification is necessary. The heat transfer Q for a hot-wire can be expressed as

$$Q = \frac{E^2}{R} \qquad ---- (4.4)$$

where
E is the voltage through the hot-wire and

R is the electrical resistance of the hot-wire,

and the Reynolds number as

$$R_e = \frac{\rho U_{eff} d}{\mu} \qquad ----4.5)$$

Substituting equations (4.4) and (4.5) into equation (4.3) and rearranging it yields

$$E^2 = aRlK_f(T_n - T_o) + blk_f R(T_n - T_o) \left(\frac{\rho U_{eff} d}{\mu}\right)^{0.5} \qquad ----(4.6)$$

If the temperature gradient $(T_w - T_o)$ remains constant, then equation (4.6) can be reduced to

37

$$E^2 = A + B U_{eff}^{0.5} \qquad \text{----(4.7)}$$

where

A and B are constants.

Equation (4.7) is known in hot-wire anemometry as King's law. A more general expression of equation (4.7) takes the form of

$$E^2 = A + B U_{eff}^n \qquad \text{----(4.8)}$$

with index n having values of 0.45-0.5. Several more analytical expressions have been suggested by various investigations. all of which give varying degrees of accuracy in the subsequent linearization. A comprehensive collection is given in Reference 29.

4.3. Effective Velocity U_{eff} in Turbulent Flow

4.3.1. Single Normal Hot-wire

For a single hot-wire probe having its hot-wire placed perpendicular to the mean flow direction in the XZ plane as shown in diagram 12,
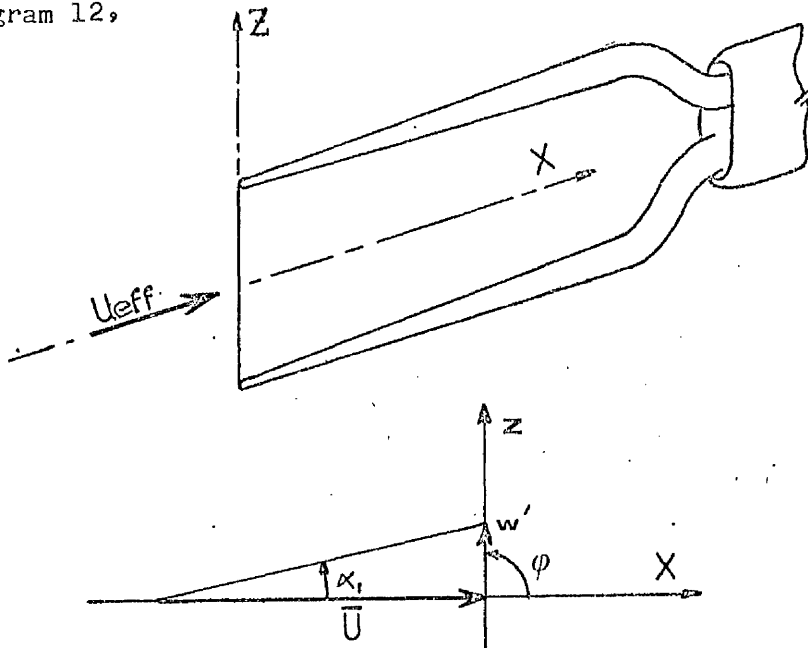
Diagram 12: Schematic of a single hot-wire probe and its associated flow field.

the effective cooling velocity U_{eff} can be equated to

$$U_{eff} = \sqrt{(\bar{U} + u')^2 + w'^2 + v'^2} \; \sin(\varphi - \alpha_1) \quad \text{------------(4.9)}$$

Series expansion of the square root terms yields

$$\left[(\bar{U} + u')^2 + w'^2 + v'^2\right]^{1/2} = \bar{U}\left[1 + \frac{u'}{\bar{U}} + \frac{v'^2 + w'^2}{2\bar{U}^2} - \frac{u'v'^2 + u'w'^2}{2\bar{U}^3} + \cdots\right] \text{------(4.10)}$$

Series expansion of $\sin(\varphi - \alpha_1)$ after the substitution for

$$\varphi = \frac{\pi}{2} \quad \text{and} \quad \alpha_1 = \arctan \frac{w'}{\bar{U}}$$

yields

$$\sin(\varphi - \alpha_1) = \left[1 - \frac{w'^2}{2\bar{U}^2} + \frac{w'^4}{24\bar{U}^4} - \cdots\cdots\right] \quad \text{------------(4.11)}$$

Substitution of equations (4.10) and (4.11) into equation (4.9)

leads to

$$U_{eff} = \bar{U}\left[1 + \frac{u'}{\bar{U}} + \frac{v'^2}{2\bar{U}^2} - \frac{u'v'^2}{2\bar{U}^3} - \frac{u'w'^2}{\bar{U}^3} - \frac{u'^2 v'^2}{4\bar{U}^4} - \frac{u'^2 w'^2}{4\bar{U}^4} - \frac{v'^2 w'^2}{2\bar{U}^4} - \frac{u'^4}{8\bar{U}^4} - \frac{v'^4}{8\bar{U}^4}\right] (4.12)$$

For time mean velocity measurements, equn. (4.12) is time

averaged, yielding to

$$\bar{U}_{eff} = \bar{U}\left[1 + \frac{\overline{v'^2}}{2\bar{U}^2} - \frac{\overline{u'v'^2}}{2\bar{U}^3} - \frac{\overline{u'w'^2}}{\bar{U}^3}\right] \quad \text{------------(4.13)}$$

For fluctuating velocity measurements, the time averaged equn.

(4.13) is subtracted from equn. (4.12) yielding

$$U'_{eff} = U_{eff} - \bar{U}_{eff} = \bar{U}\left[\frac{u'}{\bar{U}} + \frac{v'^2 - \overline{v'^2}}{2\bar{U}^2} - \frac{uv'^2 - \overline{uv'^2}}{2\bar{U}^3} - \frac{uw'^2 - \overline{uw'^2}}{\bar{U}^3} - \cdots\right] (4.14)$$

From equations (4.12), (4.13) and (4.14) it will be seen that in

a turbulent flow it is normal to have

$$\bar{U}_{eff} \neq \bar{U} \quad \text{and} \quad U'_{eff} \neq u'$$

even if all terms of 3rd and higher orders are disregarded.

4.3.2. Slanting a hot-wire relative to U_{eff}

39

If the hot-wire of a probe is making an angle θ to the XY plane of flow, as in Diag. 13,
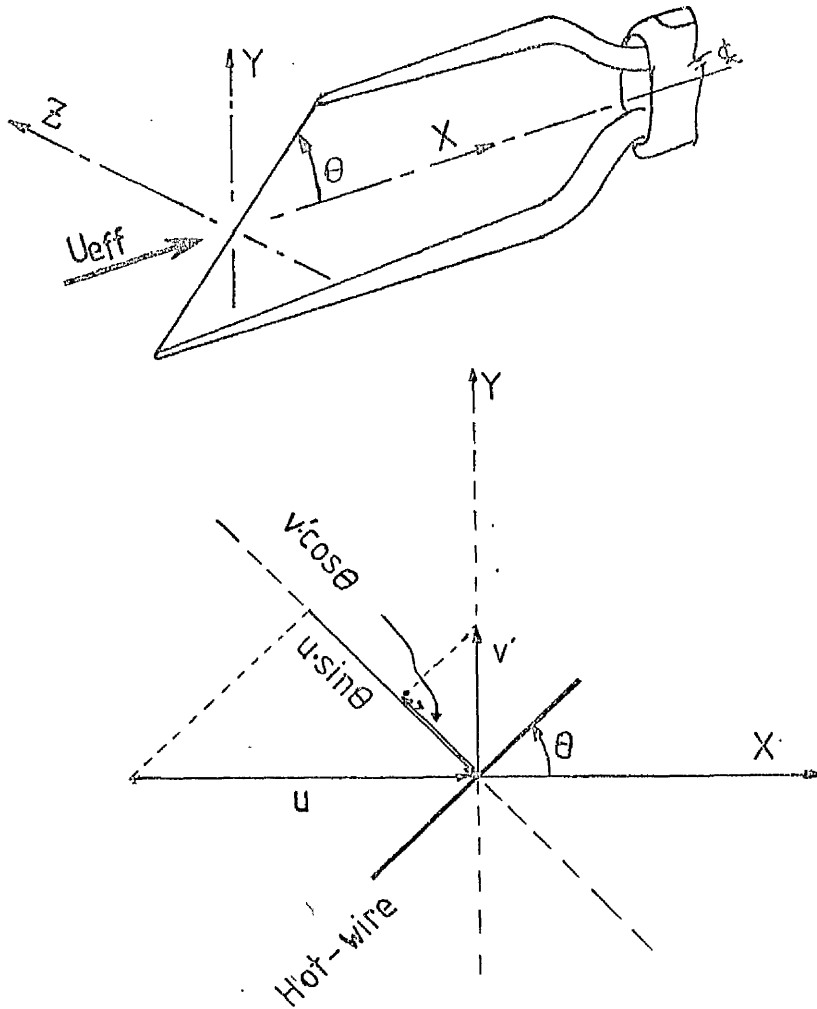
Diagram 13: Schematic of a Hot-Wire probe slanted relative to U_{eff} and its associated flow field.

the normal component of the effective velocity is expressed by

$$U_{eff} = \sqrt{\left[(\bar{U} + u').\sin\theta - v'\cos\theta\right]^2 + w'^2} \quad \text{-----(4.15)}$$

Series expansion of the terms inside the square root yields

$$U_{eff} = \bar{U}\sin\theta\left[1 + \frac{u'}{\bar{U}} - \frac{v'}{\bar{U}}\cot\theta + \frac{w'^2}{2\bar{U}^2\sin^2\theta} - \frac{3u'v'^2}{2\bar{U}^3}\cot^3\theta + \right.$$

$$\left. + \frac{3u'^2v'}{2\bar{U}^3}\cot\theta - \frac{u'w'^2}{2\bar{U}^3\sin^2\theta} + \frac{w'^2v'}{2\bar{U}^3}\frac{\cot\theta}{\sin^2\theta} - \dots \right] \quad \text{--(4.16)}$$

40

For mean velocity measurements, equn. (4.16) is time averaged.
with 3rd or higher order terms ommitted yielding

$$\overline{U}_{eff} = \overline{U}\sin\theta\left[1 + \frac{\overline{w'^2}}{2\overline{U}^2\sin\theta}\right] \quad \text{------------(4.17)}$$

For fluctuating velocity measurements, equn. (4.17) is taken away
from equn. (4.16) yielding to

$$U'_{eff} = U_{eff} - \overline{U}_{eff} = \overline{U}\sin\theta\left[\frac{u'}{\overline{U}} - \frac{v'}{\overline{U}}\cot\theta + \frac{w'^2 - \overline{w'^2}}{2\overline{U}^2\sin\theta}\right] \quad \text{----(4.18)}$$

Equations (4.17) and (4.18) are giving the relationship between

U_{eff}, U, u', v', w' and θ only for the case of the hot-wire being
slanted relative to the XY plane. However, similar expressions

can be derived for the case of a hot-wire being slanted to

another plane.

4.4. Measurement of Turbulent Fluctuations

For measurements in turbulent flow fields with Turbulence

Intensity levels of Tu < 0.20 certain simplifying assumptions can

be made which give rise to little error in the final result. It

is assumed that the flow field can adequately be described by

means of U, u', v' and w' velocities, and that all 3rd or higher

order terms in equations (4.12) and (4.16) can be neglected.
(i.e. u' << 1, v' << 1, w' << 1)

The flow velocities can thus be calculated using equns. (4.13)

and (4.14) for a single hot-wire normal to the flow, and equns.

(4.7) and (4.18) for a cross-slanted hot-wire probe.

41

Choosing the values of angle θ and φ to be

$$\varphi = \frac{\pi}{2} \qquad \text{(single, normal to the flow, hot-wire)}$$

and

$$\left.\begin{array}{l} \theta = \dfrac{\pi}{4} \\[2mm] \theta = \dfrac{3\pi}{4} \end{array}\right\} \quad \text{(Cross-Slanted hot-wire probe)},$$

Equations (4.12) and (4.16) yield

$$U_{eff}(\frac{\pi}{2}) = \bar{U} + u' + \frac{v'^2}{2\bar{U}} \qquad \text{------------(4.20a)}$$

$$U_{eff}(\frac{\pi}{4}) = k\left[\bar{U} + u' + \frac{w'^2}{\bar{U}} - v'\right] \text{------(4.20b)}$$

and

$$U_{eff}(\frac{3\pi}{4}) = k\left[\bar{U} + u' + \frac{w'^2}{\bar{U}} + v'\right] \text{----(4.20c)}$$

where

$$k = \sin\theta = \cos\theta = \frac{\sqrt{2}}{2}$$

for $\quad \theta = \dfrac{\pi}{4} = \dfrac{3\pi}{4}$

For mean flow velocity measurements, time averaging of equns. (4.20a, b. and c) yields.

$$\bar{U}_{eff}(\frac{\pi}{2}) = \bar{U} + \frac{\overline{v'^2}}{2\bar{U}} \qquad \text{---------------(4.21)}$$

and

$$U_{eff}(\frac{\pi}{4}) = U_{eff}(\frac{3\pi}{4}) = k\left[\bar{U} + \frac{\overline{w'^2}}{\bar{U}}\right] \text{-------(4.22)}$$

For fluctuating velocity measurements, the time averaged equations (4.21) and (4.22) are taken away from equations (4.20a, b, and c), yielding to

42

$$U'_{eff}(\tfrac{\pi}{2}) = u' + \frac{v'^2 - \overline{v'^2}}{2\overline{U}} \simeq u' + \frac{v'^2}{2\overline{U}} \quad \text{---} \quad (4.23)$$

$$U'_{eff}(\tfrac{\pi}{4}) = k\left[u' - v' + \frac{w'^2 - \overline{w'^2}}{\overline{U}}\right] \quad \text{----------} \quad (4.24)$$

and

$$U'_{eff}(\tfrac{3\pi}{4}) = k\left[u' + v' + \frac{w'^2 - \overline{w'^2}}{\overline{U}}\right] \quad \text{----------} \quad (4.25)$$

If linearization of the anemometer's signal is used (see section 4.5) and the measuring chain is assumed to have this transfer function

$$\overline{E} - E_o = SU_{eff}$$

where

S is a general transfer function,

then the general signal-to-velocity relationship would be obtained from

$$\overline{E}(\varphi) - E_o = S\, U_{eff}(\varphi) \quad \text{------------} \quad (4.26)$$

Applying this relationship to equations (4.21) through to (4.25) yields two possible sets of results:

(a) for time-averaged signals

$$\overline{E}(\tfrac{\pi}{2}) - E_o = S\left[\overline{U} + \frac{\overline{v'^2}}{2\overline{U}}\right] \quad \text{--------} \quad (4.27)$$

$$\overline{E}(\tfrac{\pi}{4}) - E_o = \overline{E}(\tfrac{3\pi}{4}) - E_o = kS\left[\overline{U} + \frac{\overline{w'^2}}{\overline{U}}\right] \text{---} \quad (4.28)$$

(b) for fluctuating signals

$$E'(\tfrac{\pi}{2}) = S\left[u' + \frac{v'^2 - \overline{v'^2}}{2\overline{U}}\right] \quad \text{------------} \quad (4.29)$$

43

$$E'\left(\frac{\pi}{4}\right) = kS\left[u' - v' + \frac{w'^2 - \overline{w'^2}}{\overline{U}}\right] \quad \text{---------(4.30)}$$

and

$$E'\left(\frac{3\pi}{4}\right) = kS\left[u' + v' + \frac{w'^2 - \overline{w'^2}}{\overline{U}}\right] \quad \text{----------(4.31)}$$

Since $\frac{w'}{U} << 1$ has been assumed, it is reasonable to discard the terms containing $(w'^2 - \overline{w'^2})$ and $\overline{w'^2}$. Thus the equations (4.27) — (4.31) are reduced to:

(a) For a single hot-wire probe normal to the flow

$$\overline{U} + \frac{\overline{v'^2}}{2\overline{U}} \approx \overline{U} = \frac{1}{S}\left[\overline{E}\left(\frac{\pi}{2}\right) - E_o\right] \quad \text{----------(4.32)}$$

$$u' + \frac{v'^2}{2\overline{U}} = \frac{1}{S}\left[E'\left(\frac{\pi}{2}\right)\right] \quad \text{---------(4.33)}$$

(b) For a Cross-slanted hot-wire probe

$$\overline{U} = \frac{1}{kS}\left[\overline{E}\left(\frac{\pi}{4}\right) - E_o\right] = \frac{1}{kS}\left[\overline{E}\left(\frac{3\pi}{4}\right) - E_o\right] \text{-----(4.34)}$$

$$u' = \frac{1}{2kS}\left[E'\left(\frac{3\pi}{4}\right) + E'\left(\frac{\pi}{4}\right)\right] \quad \text{-------------(4.35)}$$

and

$$v' = \frac{1}{2kS}\left[E'\left(\frac{3\pi}{4}\right) - E'\left(\frac{\pi}{4}\right)\right] \quad \text{---------------(4.36)}$$

The above expressions were based on the assumption that all hot-wire probes were placed in the XY-reference plane. The result was that measurements were obtained of U, u´, v´ and tolerably, u´v´.

4.5. Calibration and Linearization

For the purpose of carrying out calibration of the hot-wire anemometer, a low turbulence flow of known mean velocity is required in which the probe is positioned in the same attitude as

44

it would be used in actual operations.

The calibration consists of simultaneous measurements of the mean flow velocity Ueff and voltage output E from the anemometer. Using these two parameters, graphs of either $(\bar{E} - E_0)$ or $(\bar{E}^2 - E_0^2)$ versus the mean velocity of flow are constructed, where E_0 is the voltage output from the anemometer at zero flow velocity. Thus, the calibration constants in an assumed Velocity-Voltage relationship can be determined. A typical calibration curve obtained in the present experiments is shown in Diag 14. However, as it can be seen from this figure, the relationship between the anemometer's voltage output and velocity of flow, for the velocity range considered, is not linear. This is because the amount of heat transmitted by a heated body to the surrounding fluid is not a linear function of the velocity of the fluid medium.

Such a non-linear curve is generally permissable for measurements in flows having a low degree of Turbulence Intensity (Tu < 10%). However, where higher degrees of Turbulence Intensity do exist, or, where two or more hot-wires are used for simultaneous measurements, then it becomes necessary to linearize the Voltage-Velocity relationship. The purpose is to avoid any non-linear distortions of the signals and to ensure a reasonable operation.

For linearization purposes, the general relationship between Voltage and Velocity is assumed to be given by

$$E = F(U) \qquad\qquad ---- (4.37)$$

where

F (U) describes a general function of U, the mean flow velocity.

In order to obtain a linear relationship, it is convenient to invert equn. (4.37) as

$$U = F^{-1}(E) \qquad ---- (4.38)$$

If the inverted function $F^{-1}(E)$ is made to give the following relationship between the input voltage Ein and the linearized output voltage Eout in the form

$$Eout = C_2 F^{-1}(E_{in}) \qquad ---- (4.39)$$

it then follows from equn. (4.38) that

$$Eout = C_2 U \qquad ---- (4.40)$$

thus resulting in a linear Voltage-Velocity relationship. It should be noted that Ein is in fact E referred to earlier.

In the present investigation, an approximation for the inverted function $F^{-1}(Ein)$ which was proposed by Froebel (25) is used. Froebel proposed that the function $F^{-1}(Ein)$ be approximated to a polynomial series of the form

$$F^{-1}(Ein) = F^{-1}(\bar{E}-E_o) = k1(\bar{E}-E_o) + k2(\bar{E}-E_o)^2 + k3(\bar{E}-E_o)^4 \quad ---- (4.41)$$

so that equn. (4.38) becomes

$$U = k1(\bar{E}-E_o) + k2(\bar{E}-E_o)^2 + k3(\bar{E}-E_o)^4 \quad ----------- (4.41a)$$

where

k1, k2, k3 are calibration constants,

and the general equation (4.37) be expressed in the form

$$(\bar{E} - E_o) = C_2 F(U) \qquad ---- (4.42)$$

where

C_2 is another calibration constant.

This function [equn. (4.41)] gives a smooth continuous approximation of the general function

$$(\bar{E} - E_0) = F(U)$$

over a specified velocity range.

The values of constants k1, k2 and k3 are determined by specifying that equation (3.41a) should satisfy the unlinear relationship $F(V) = \bar{E} - E_0$ at three different values of mean flow velocity. This in fact yields three simultaneous equations the solutions of which give the corresponding values of k1, k2 and k3. Having determined the constants, it then follows from equation (4.42) that the ratio $(\bar{E} - E_0) / C_2$ for any hot-wire probe of a given type will be equal to the function $F(U)$. Adjusting the input signal to the equation (3.41) to the value $(\bar{E} - E_0)/C_2$ will therefore ensure a linear output signal. A typical linearized relationship from this investigation is presented in Diag. 15 This should be compared with its non-linear equivalent, presented in Diag.14, and the advantages of the linear relationship are obvious.

The linearization was carried out on the digital data and at the same time with the calculation of the velocity components.
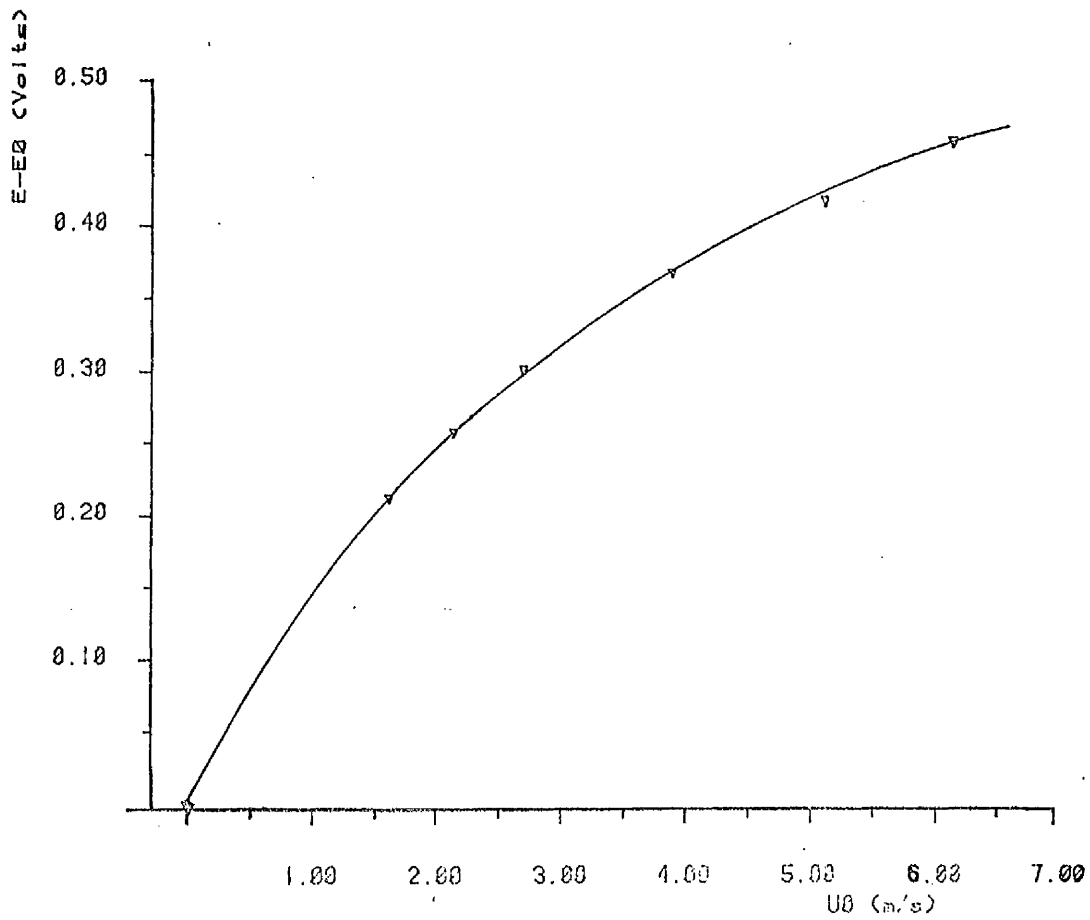
DIAGRAM 14.: Typical non-linear calibration curve of a
hot-wire output.
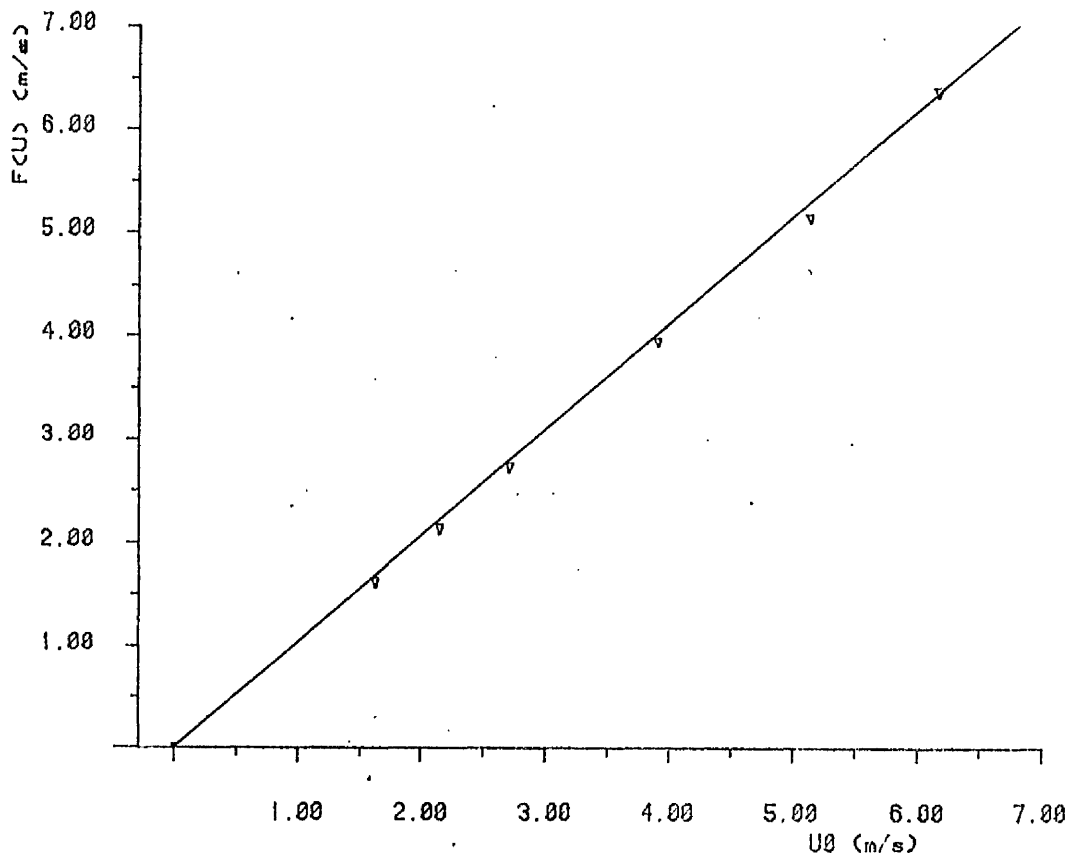
DIAGRAM 15: Typical linearised curve of a hot-wire output.

CHAPTER 5

EXPERIMENTAL INVESTIGATION

49

5.1. Introduction

The flow in the wake of a bluff body is essentially dominated by the generation and shedding of vortices resulting from boundary layer separation. The wake thus produced is periodic in which the flow field is unsteady and fluctuant. The shedding of vortices is related to Strouthal and Reynolds numbers. For bluff bodies with sharp edges. it is generally believed that the Strouhal number for vortex shedding is not greatly affected by the Reynolds number. This is not so with bluff bodies with very rounded surfaces, such as circular cylinders. For such bodies, the Strouthal number for vortex shedding is greatly affected by variations in the Reynolds number. However. for convenience of geometrical configuration and for practical reasons, the wake flow behind circular cylinders as bluff bodies has been much more extensively studied than any other bluff section. Although it is not the intention of the present work to try to add further understanding to the flow phenomena of such bodies, circular cylinders are nevertheless used solely for the purpose of carrying out an investigation into the mechanism with which the slat device exerts its influence on the effect of vortex excitation. For this purpose. observations of the flow characteristics in the wake of a plain circular cylinder and of a circular cylinder. fitted with the slat device can be used for comparative assessment of any fundamental changes rendered (to the wake flow) by the presence of the slat device.

Though analytical models for the wake flow are useful in the attendant studies, and many such models for circular cylinders

have been proposed (e.g. Von Karman (2), Roshko (26), Gerrard (6), etc), basic experimental contributions are indispensible as the flow characteristics in the wake of a complicated geometrical section, such as that of the slatted model, are hardly calculable from the first principles.

The experimental arrangement and test procedures as well as data aquisition for the present experimental investigation will be described in the following sections.

5.2. Experimental Considerations

Since the flow field in the wake of a bluff body is generally three dimensional and unsteady, it requires many measurement points at short time intervals in order to reveal its structure. As mentioned in Chapter 2, the flow conditions at a given point in the wake can be described by three orthogonal mean velocities and their corresponding fluctuating components; to measure them all at probably many thousands of points over a reasonable time period is quite impracticable, for data handling alone. Thus it is desirable to restrict the number of measurement positions and to select only those important velocity components in order to avoid collecting a huge data load unnecessarily. The choice made is explained below.

5.2.1. Velocity components to be measured

The mean and fluctuating velocity components of the wake flow are to be measured using a constant temperature anemometer (C.T.A.) system. The C.T.A. will be used in conjunction with either a single or cross-slanted hot-wire probe. The use of a single hot-wire probe permits measurements to be made of one mean

51

velocity and one fluctuating velocity component. The use of a cross-slanted hot-wire probe permits the measurement of one mean velocity and two fluctuating velocity components.

The considerations, as to which mean velocity and fluctuating velocity components are of importance, are based on

(a) The time-mean velocity field which has a strong undirectional preference along the X-direction, and

(b) The geometry of the models. In the present investigation, the fluctuating velocity component in the Z-direction (i.e. w') is likely to be small compared to those in the other two axese (i.e. u' and v').

With these considerations in view, the velocity components to be measured are the mean velocity in the X-axis, U, and the fluctuating velocity components along the X- and Y- axes, u' and v' respectively.

Hence

(a) The single hot-wire probe is used to measure the mean velocity component, U, and the fluctuating velocity component u' and

(b) The cross-slanted hot-wire probe to measure the mean velocity component U, and the fluctuating velocity components u' and v'.

Because of the amount of data needed to be analysed, the use of a high speed digital computer became apparent. In this respect, the PDP 11/45 digital computer has been made available for this work. Although it is not the most suitable computer to use because of its limited processing capacity (192K RAM memory),

its availability to the writer makes it a suitable choice. Furthermore, its ability to convert analog signals into digital data brought another advantage in its use. However, its use brought restrictions on the amount of data that could be handled at any time. After an initial investigation, the maximum amount of data that could adequately be analysed was found was found to be 10.000 values. However, the recording or conversion time for the machine requires some explanation since we are originally dealing with analog signals.

The conversion time is a function of the rate at which an analog signal is converted to digital data, and, the number of digital data values required, that is

$$Tr = \frac{N}{f_s}$$

where

T_r is the conversion time

N is the total number of digital data,

f_s is the rate (frequency) with which a number of analog signals are converted to digital values.

The rate of conversion or sampling frequency, f_s, is a function of the highest frequency content of the analog signal. This relationship, known as the Niquist criterion, is expressed as

$$f_s = 2f_c$$

where

f_c is the maximum cut-off frequency of the Low-Pass filter used to limit the frequency content of the analog signal.

In the present investigation, f_c was set to 125 Hz, giving

53

$$f_s = 250 \text{ Hz}.$$

Therefore, the conversion time was found to be

$$Tr = \frac{10,000}{250} = 40 \text{ sec}$$

This value was considered as satisfactory for the effects of non-stationarily of the wake flow to be reduced to acceptable levels (cf reference 21).

5.2.2. Position of measurements

(a) Across the wake flow (transverse along the Y-axis)

After considering existing information regarding the wake flow (cf. reference 8), it was concluded that the region in the wake that is likely to bring about effects of oscillatory behaviour of the bluff body is the near wake right behind the body to a few diameters distance away. In order to avoid unnecessary interferences which may exist in the local vicinity of the body and which may obscure measurements for comparitive study of the effects between the proposed models, the positions for the sensing probe to be set in the wake have been decided at 3.0, 4.5 and 6.0 diameters downstream of the model's central axis (i.e. not closer than three diameters).

Choosing the position of measurements to be carried out across the wake, the need for as many points was restricted by the time available and ability for the measured data to be processed.

Assuming that the wake flow is symmetrical about the XZ-plane, measurements were taken at eleven positions across half the wake width in the Y-direction, from the centre-line of the wake to 1.33 diameters away from it. The upper limit was set by

54

the phyiscal dimensions of the equipment used. The distance between two adjacent measuring points was taken as 0.13D.

(b) Along the wake flow (transverse along the X-axis)

Measurements of mean flow velocity and u'-fluctuant flow velocity are made using two single hot-wire probes normal to the mean flow direction, as shown in Diag.16 .

Eight positions of measurement, along the X-axis, were chosen between X/D = 3.0 and X/D = 5.1 and measured with respect to the position of the forward probe. The spacing between two consequative measurements was thus 0.3D. The upper limit (i.e. X/D = 5.1) of the position of measurement was set by the physical dimensions of the probe holder.

In choosing the lateral position of measurement as well as the vertical spacing of the probes, the following requirements had to be taken into consideration.

1. The need for high spatial resolution between successive measurements,

2. The need for the squared coherence between the two signals from the probes to be high, and

3. The need to keep the errors in the measurement of the distance and phase angle between the probes small.

Requirements (1) and (2) call for the two hot-wires to be as close as possible to each other, while requirement (3) calls for the hot-wires to be sufficiently far apart. Furthermore, requirement (2) calls for both hot-wires to be placed as close as possible to the path of vortex centres. A simple way of finding the approximate position of the path of a vortex centre is to

observe the position of maximum intensity from the turbulence intensity graphs (19). From these graphs, the path of the vortex centres along the Y-direction, was found to be at Y = 0.60D, (on average for all three models used).

The distance of separation between the probes was chosen to be 0.6D along the X-axis and 0.1D along the Z-axis (20).

The vertical position (i.e. the Z-direction) of the sensing probe for both sets of measurements was set at 3.5 diameters above the base of the model.

5.3. Experimental Apparatus

(a) Wind Tunnel

Two different wind tunnels were used in the investigations.
(i). An open-jet wind tunnel made in Germany, having a "working" section of 0.65 m length and 0.30 m diameter. It offers a velocity range from 0.6 m/s to 12.6 + 0.3 m/s with a longitudinal component of turbulence intensity of about 1.6% at the position of 0.21 m downstream from the front nozzle of tunnel.
(ii). A low speed, low turbulence intensity single return close-circuit wind tunnel. It has a rectangular shaped working section, having the following dimensions:

Length	1.70 m
Width	1.15 m
Height	0.84 m

It operates up to a maximum velocity, in the working section, of 30 + 0.3 m/s. The longitudinal turbulence intensity component of the flow is 0.4%, while the lateral one is 0.6%, both components measured at the position of centre axes of the working section.

The open-jet tunnel was used during the early stages, owing

56

to it being conveniently accommodated in a separate room and not being under constant demand by undergraduate laboratory work. However, subsequent analysis of data taken indicated severe distortion of the wake flow field. This was found to be due to the blockage effect of the model and subsequent spillage of the jet flow.

Subsequently, all further investigations were carried out in the close-circuit wind tunnel. Measurement of the free stream velocity was by means of a digital pressure micromanometer.

(b) Constant temperature anemometer system (C.T.A.)

The C.T.A. system used is a DISA, type 56C00 multichannel system, consisting of three C.T.A. units, three signal conditioning units and one Mean Value unit.

Each C.T.A. unit consists of a 56C01 compensating unit and a 56C16 C.T.A. bridge. The whole C.T.A. unit is designed for use with standard DISA wire probes.

For measurements of flow velocity, the unbalance of the bridge, caused by changes in the flow velocity field at the probe position, is corrected via a feedback amplifier system. The voltage needed to balance the bridge is amplified and available via a BNC connector at the rear of the unit.

The signal conditioning units are DISA type 56N20. They are used for filtering and amplification of fluctuating signals before they are available to other equipment. The block diagram in Diagram 17, shows the set-up of a C.T.A. unit and a signal conditioning unit.

The Mean Value unit is DISA, type 56N22. It is used to

57

measure the D.C. component of the output voltages from the C.T.A. units. Because of its great accuracy of measurement, it is mainly used for the calibration and balancing of the C.T.A. bridge.

(c) Hot-wire Probes

In general, a probe for a C.T.A. system consists of the following components:

> Sensor element,
> Sensor support,
> Probe body, and
> Electrical connections.

In the probes used, the sensor element is a thin cylindrical wire made of platinum-plated tungsten wire of 5 um diameter and 1.25 mm length. The wire is suspended between two stainless steel prongs, to which it is spot-welded.

In the present investigation, two different types of probe configurations are used:

(i) Single-sensor probe

This is a DISA, type 55P11, miniature wire probe. It consists of a single straight wire sensor element placed perpendicular to the probe axis.

(ii) Dual-sensor probe

This is a DISA, type 55P61, miniature X-array probe. It consists of two cross-slanted wire sensing elements, set at 45° and 135° degree angles to the probe axis.

(d) Computational system for data processing

The computer system used for the analysis of measured data is a PDP 11/45 digital computer and its associated accessories. The processing unit has a 192K bytes RAM memory. Its associated

58

accessories include a two disc storage system (80 M bytes of
storage capacity), a magnetic reel tape system, low speed
terminals, a printer and two digital plotters.

The analog-to-digital convertor with its associated signal
conditioning units are used in paralled with the PDP 11/45.   The
A-to-D convertor is able to convert the input analog data at a
rate of between 5 Hz and up to a maximum of 2.5 KHz.

The operating language of the PDP 11/45 is FORTRAN IV.
version 2.5.

5.4. Test Models

Three different types of models are used in this
investigation. They include a plain circular cylinder (Model I),
a plain circular cylinder whose periphery is completely
surrounded with slats (Model II) and a plain circular cylinder
whose periphery is partially surrounded by slats (Model .III).
These models were chosen because they are the same ones used by
Wong (13,14) in his investigations into the suppression of
vortex-induced vibrations and buffeting.   A photograph   of
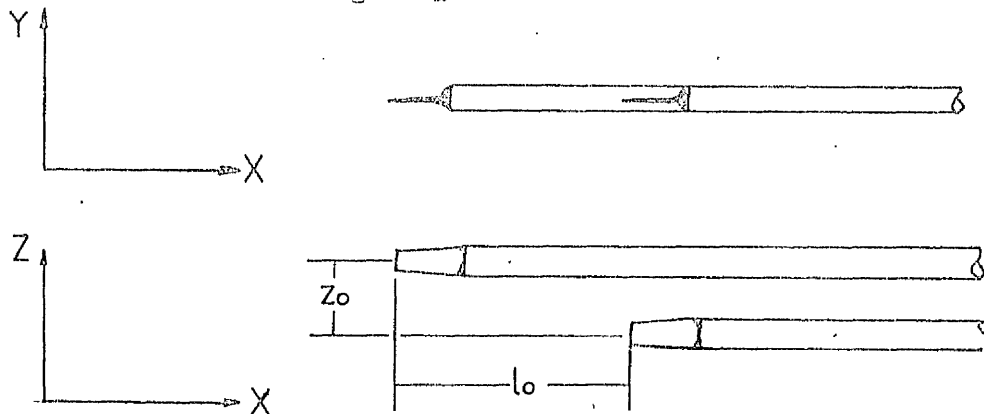each model is shown in Diagram 18.

Diagram 16:Plan and elevation of probe configuration.

Model (I) is made of circular polyvinylcloride tube of 0.075m outside diameter. Both ends of the tube are closed using wooden plugs. Two types of this model are used: one which is 0.84 m long. i.e. having a length-to-diameter ratio of 11.2 and thus fully spanning the working section of the wind tunnel. and a second of 0.75 m long. i.e. having a length-to-diameter ratio of 10. thus having one of its ends free in the stream flow. The former model is used for the study of the free-end effects (see chapter 6) while the later one is the one used for the investigations on the effects of the slat device upon the wake flow.

In models (II) and (III). the slat device consists essentially of a number of rectangular shaped slats disposed around model (I) [L/D 10] and placed longitudinally along its length. They are kept at a distance from the body surface by rings or formers. Regular openings or slots are formed between the slats through which fluid flow can take place. The slats are made of wood 0.8 mm thick. The three geometrical parameters adopted to describe the slat device. namely, the open area ratio α, the non-dimensional width of the slats β, and the non-dimensional gap distance between the slats and the adjacent body surface γ. have the same values that Wong(13) found for best results in suppressing vortex-induced oscillations.

In model (III), the angle θ of the front and rear openings is also having the value that Wong (14) found to give the best suppression characteristics for the device, because it allows for the maximum inlet of flow under the positive frontal pressure.

5.5. Experimental Set-up

The wind tunnel used in this investigation has already been described in Section 4.2.

The movement of the sensing probe along the X- and Y-axis is controlled by a traversing mechanism system placed inside the wind tunnel's test section. The system was carefully levelled on all principal axes using the cross-hair of a microscope eye-piece, and fastened to the wind tunnel floor using heavy duty stick-on tape as a precautionary measure, for the whole unit is heavy enough to withstand the flow pressure by itself. For the velocity measurements across the wake, the traversing mechanism (Diag. 19.) allowed the movement of the probe along the Y-axis direction to be controlled from the outside of the wind tunnel using the same arrangement of stepper motor-sweep drive unit as before. The position of the probes along the Y-axis was set using the lead screw and remained the same throughout the measurements. The relative accuracy of probe positioning was 0.01 mm and 0.2 mm along the X- and Y-axis respectively.

Special care was taken in positioning and aligning the hot-wire probe itself with respect to all three major axes. This was carried out using the cross-hair of a microscope eye-piece and fine wire makeshift plum-lines. The fine wires were hung from the ceiling of the test section at exactly the centre line position, one in front of the probe and one at the rear of it. By aligning the cross-hair of the eye-piece to the fine wires, the hot-wires of the probe were positioned and aligned along the centre line of the wind tunnel.

The models were mounted inside the wind tunnel and secured

through a nut-bolt-nut arrangement (Diagram 20) and precautions were taken to avoid any vibration that might occur during vortex shedding.

5.6. Experimental Procedure

(i) Calibration of the C.T.A.

The first step taken in the calibration procedure is to balance the C.T.A.'s bridge. If two C.T.A.'s are used, each bridge has to be balanced individually. The voltage output from each C.T.A. unit, when balanced, was recorded for 50 seconds on an analog tape recorder. Then, the wind tunnel was started up and run at a speed corresponding to a flow velocity of 0.60 m/s. This speed was chosen as the minimum acceptable for the hot-wire measurements without the need for the heat transfer from the probe to the flow through natural convection to be taken into consideration. The wind tunnel was allowed to run for approximately 10 minutes in order to attain steady state flow conditions. The voltage output from the C.T.A. unit was then recorded and the flow velocity noted down.

The above procedure was repeated for a further seven flow velocities and up to a maximum of 6.4 m/s.

These recordings were then transferred to the PDP 11/45 computer which computed the mean value of the voltage at each flow velocity. Thus, the non-linear relationship between the voltage output and the mean flow velocity was obtained (Diag. 14).

However, what is required is a linearized relationship between the voltage output and mean flow velocity, for reasons

already described in Section 4.5. A linear relationship is obtained from the solution of equations 4.41a and 4.42. This requires the calculation of the constants, that is. K1, K2 and K3 and C2 which appear in these equations. Once calculated, the constants K1, K2 and K3 remain the same for all further measurements made with the same type of probe. The constant C2, however, has to be recalculated with every new measurement.

The constants K1. K2 and K3 are obtained from the solution of equation 4.41a at three different flow velocities, say at 0.6 m/s, 3.3 m/s and 6.4 m/s.

The correct value of constant C2 is usually determined by the specification of a fixed linear output voltage at a given flow velocity, say at 6.4 m/s.

This calibration procedure is very simple to use once the initial calculation of constants K1, K2 and K3 has been carried out, as it requires the calibration at one flow velocity (i.e. calculation of C2) each time a new set of measurements is initiated.

(ii) Turbulence Measurements

Initially, each C.T.A. bridge was balanced individually and the voltage output from each C.T.A. unit was recorded for 50 seconds on the analog tape recorder. The wind tunnel was started and run at a speed corresponding to a mean flow velocity of 6.2 m/s. It was then allowed to run at this speed for 10 minutes so that steady state flow conditions could be attained. Then, the mean and fluctuating voltages from one C.T.A. unit and both signal conditioning units were recorded and the corresponding

63

position and the mean free-stream flow velocity noted down. The probe was moved to a new position of measurement, along the Y-axis or X-axis in the case of single probe measurements, and new recordings of the mean and fluctuating voltage were taken. This procedure was repeated for all measurement positions along the axis of measurement.

Having taken measurements for all positions along the axis of measurement, the wind tunnel was stopped and either the probe was moved to a new position along the X-axis (in the case of along the Y-axis measurements), or, a different model was placed inside the tunnel (in the case of along the X-direction measurements). Also, before a new set of measurements was initiated, the probe sensing wires were cleaned using pure acetone and the C.T.A. bridge was re-balanced. Then, the wind tunnel was started and the procedure described above repeated for every position along the axis of measurement.

5.7. Data aquisition and processing

A schematic of the instrumentation used for the data aquisition a processing of signals from a cross-slanted hot-wire probe is shown in Diagram 21.

The electric signal from the two hot-wires is aquired through two constant temperature anemometers and their corresponding signal conditioning units. The output voltage taken directly from one of the C.T.A.'s provided the mean $\bar{E}_0$ and $\bar{E}$. The output from the signal conditioning units provided the fluctuating voltage signals $E'(\pi/4)$ and $E'(3\pi/4)$. For practical considerations, the frequency content of the fluctuating signals

64.

has to be limited. The limits in this investigation were set by considering the frequency of the vortex street behind the plain cylinder. For R_e = 3.05 X 10^4, the working Reynolds number of the investigation, the Strouhal number for a plain cylinder is about 0.2. Thus. the Strouhal vortex-shedding frequency may be obtained from

$$ f_s = \frac{U_o S_t}{D} $$

For this investigation, the shedding frequency f_s is found to be approximately 16 Hertz. So the filters on the signal conditioning units were set so as to allow fluctuating signals in the frequency range between 1 Hz and 125 Hz.

The signals from one C.T.A. and both signal conditioning units were recorded on a four channel analog tape recorder (Data Aquisition Ltd, type DA 1432-4). Since only three channels were used at any one time, the fourth channel was used for low frequency noise compensation on the recorded signal. The magnetic tapes used for the recording of signals are Maxwell. type DA 90 commercial cassette tapes. All signals were recorded using the Frequency Modulation (F.M.) technique. The recorded data was subsequently transferred through a second set of signal conditioning units and the Analog-to-Digital convertor to the PDP 11/45 computer. The digitized signals (12-bits) were stored on 1200 feet magnetic reel tapes.

Further analysis of the digitized signals involved the calculation of the parameters already mentioed in Sections 3.2 and 3.3.

The plotting of the results is carried out using a Tektronix

type 4662, digital plotter in parallel with the PDP 11/45. Flow chart diagrams of the programs used in the analysis of single and joint data records are given in Diagram 22.

5.8. Discussion

So far, two important assumptions regarding the wake flow have been made. One, regarding the state of the flow, is assumed that the flow is two dimensional, that is the fluctuating velocity component along the Z-axis as well as the mean velocity components along the Y- and Z-axis are negligible. However, in real situations of wake flow this may not be true. Two dimensional flow can only exist around infinitely long (two dimensional) bodies. The models used have a finite length (L/D = 10) and therefore all the velocity components can exist.

The second assumption made is that the wake flow is symmetrical along the XZ-plane of reference. Many investigators (cf reference 27) have found that this is not the case. In real situations of wake flow because of the alternative way the vortices are shed the wake flow "wobbles" periodically in time and space, and near the body, is far from symmetrical. However although the wake flow may "wobble", it does this with a given periodicity and so if measurements are made, say at a point A, which is at a distance B from the geometric Y-axis, for long enough, its properties (such as mean velocity) will be exactly the same as its mirror image point on the other side of the axis. This in most practical investigations has been proved, and because of the amount data reduction it offers has been used extensively (cf references 18, 35).

Regarding the method used for the recording of the analog signal, it can be said that it is one of the best available for this purpose. The frequency modulation technique for signal recording used in conjunction with low frequency noise compensation. permits the recording of low frequency signals to be made with a signal-to-noise ratio for the tape recorder used of approximately 42 db. Also, the use of signal conditioning units just before the A-to-D convectors, rejected any high frequency modulation of the analog signal present due to internal electronic noise of the tape recorder.

However, whereas every possible precaution is taken in order to eliminate sources of experimental error, there are errors present which are unavoidable. We may consider some possible errors in measurements introduced by the following sources.

(i) The tunnel flow velocity can only be maintained to within + 0.1 m/s,

(ii) The variation of ambient temperature during the test runs which had to be conducted over a period of several days.

(iii) The positioning of the probe, with reference to any linear or angular datum, can not be absolutely accurate.

(iv) Steady state conditions can not be fully maintained during a test run,

(v) The analog signal could not be wholly retained after digitization,

(vi) The assumption that $w' \sim 0$ used in the calculation of U (mean velocity) and u' (fluctuating velocity) may not be entirely justified.

(vii) Errors as high as 2% (cf. ref. 28) can be introduced

67

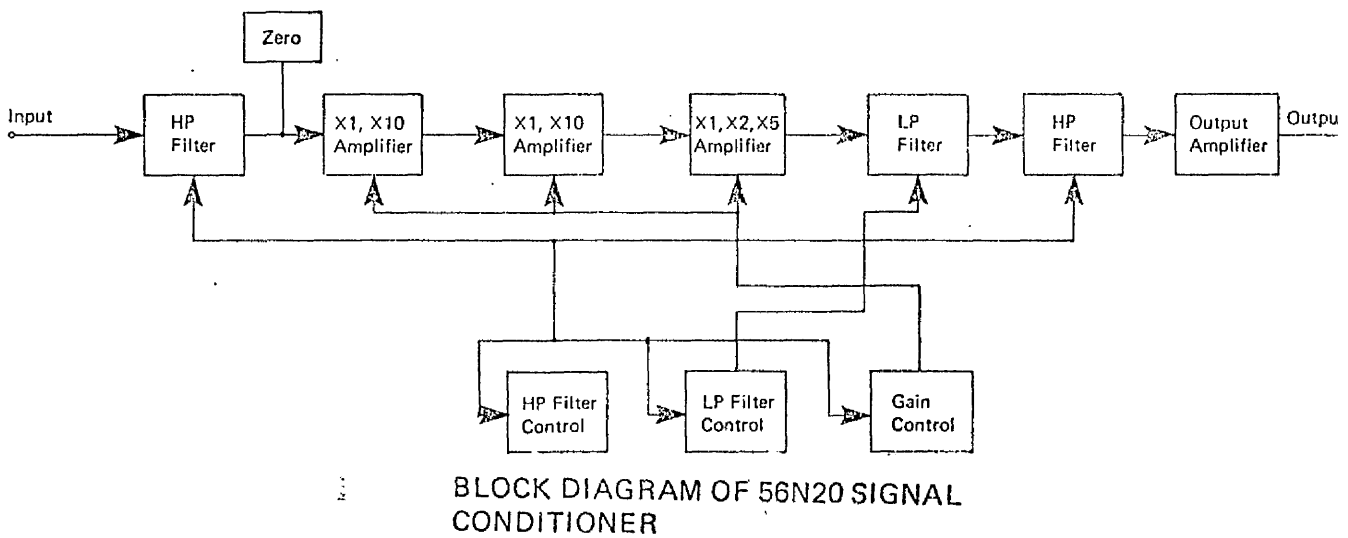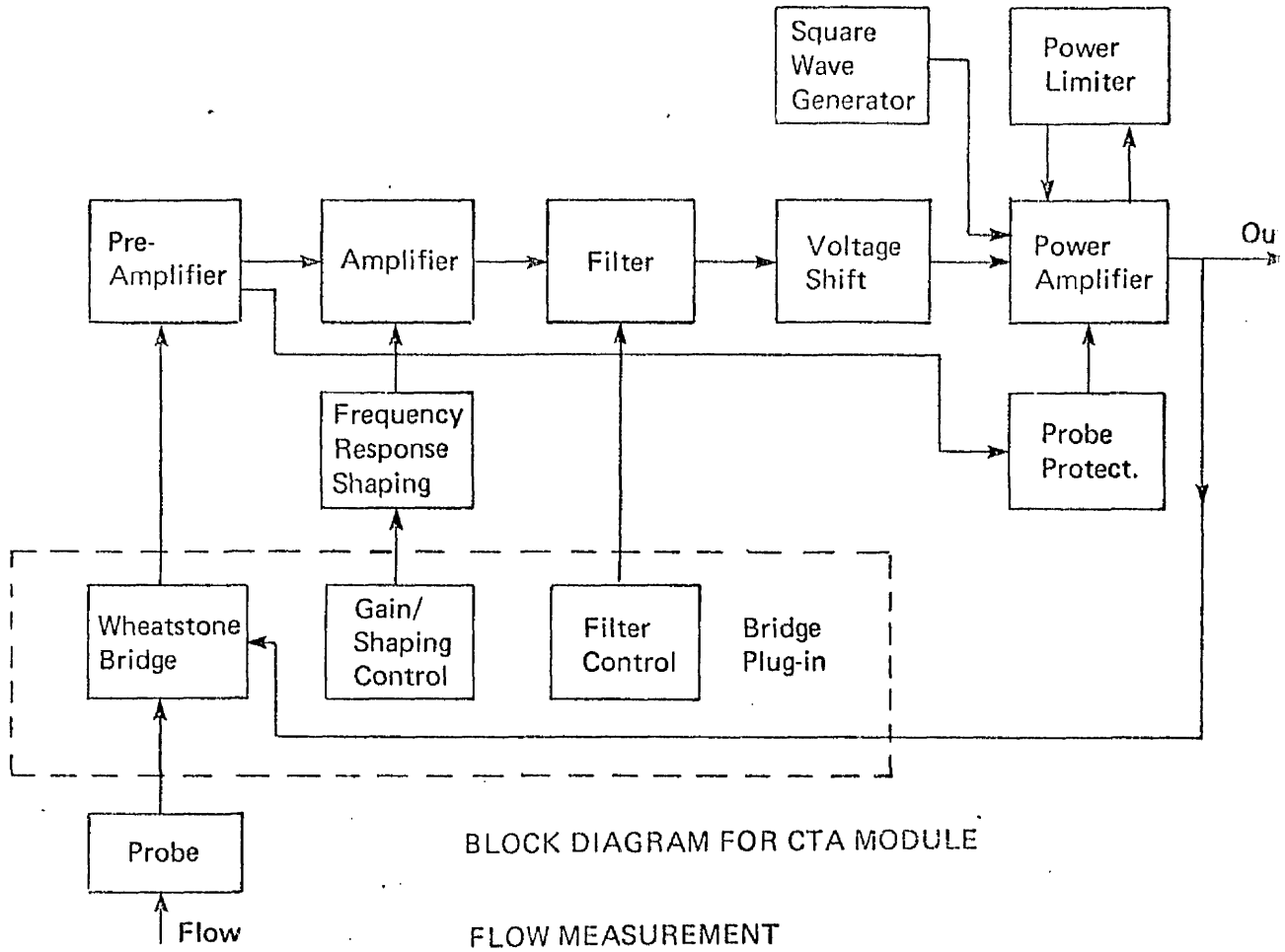through the process of Voltage-Velocity linearization.

BLOCK DIAGRAM FOR CTA MODULE

FLOW MEASUREMENT

BLOCK DIAGRAM OF 56N20 SIGNAL CONDITIONER

Diagram 17: Block diagrams for a Costant Temperature Anemometer and a Signal Conditioning unit.

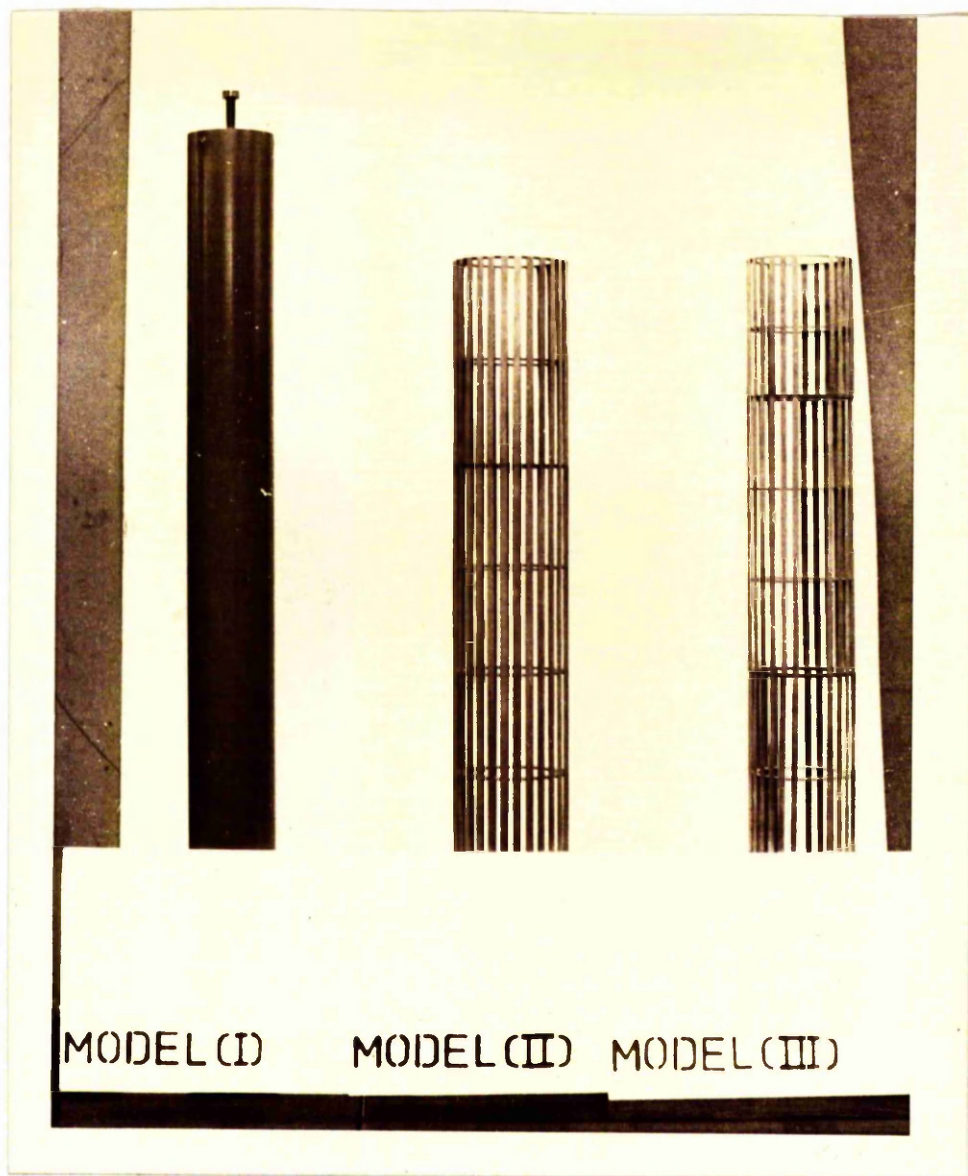MODEL(I)   MODEL(II) MODEL(III)

Diagram 18: Photograph of the the models used in the
            present investigation. Models (II) and
            (III) are shown without the plain circular
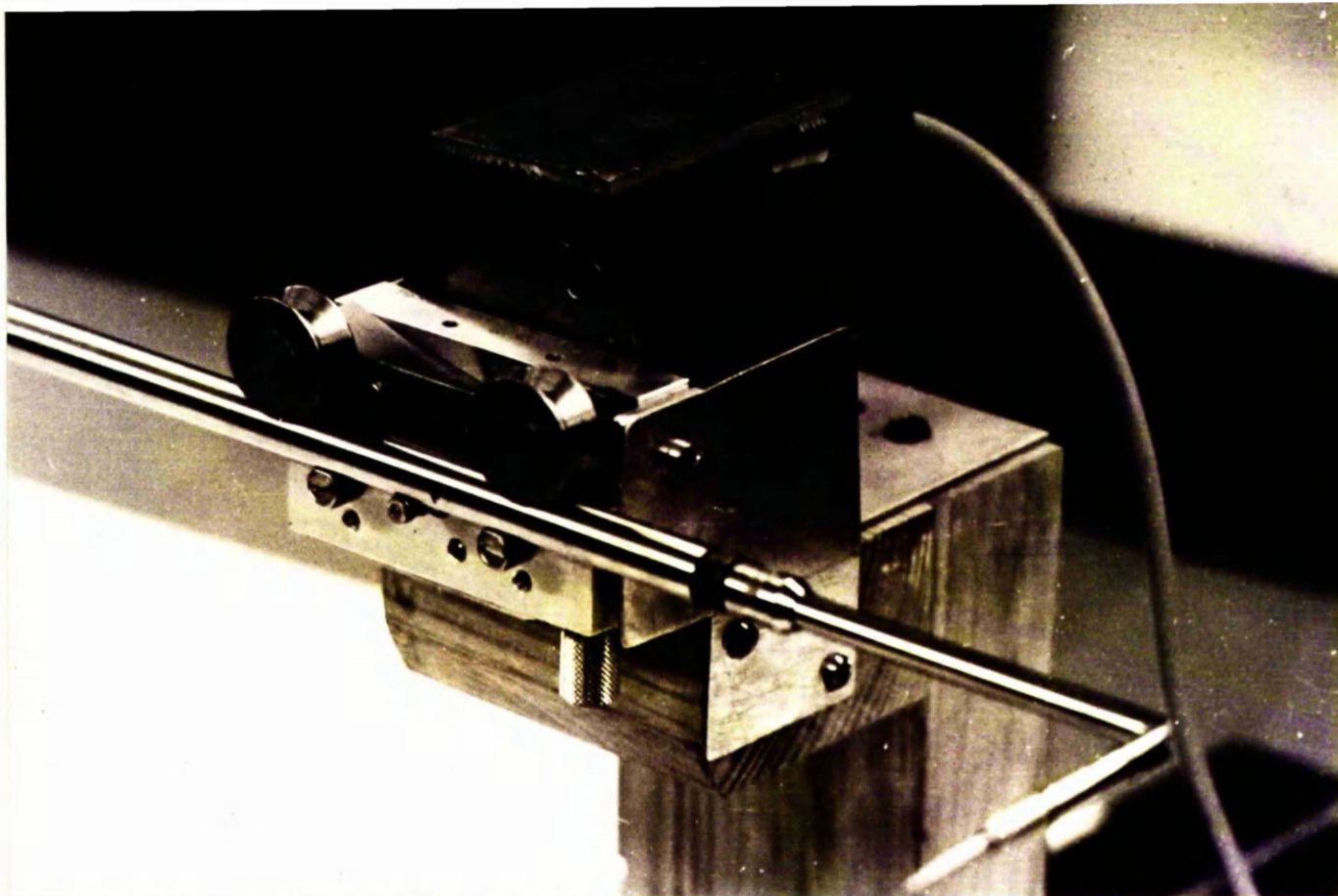   cylinder.

Diagram 19: Photograph showing the Traversing Mechanism
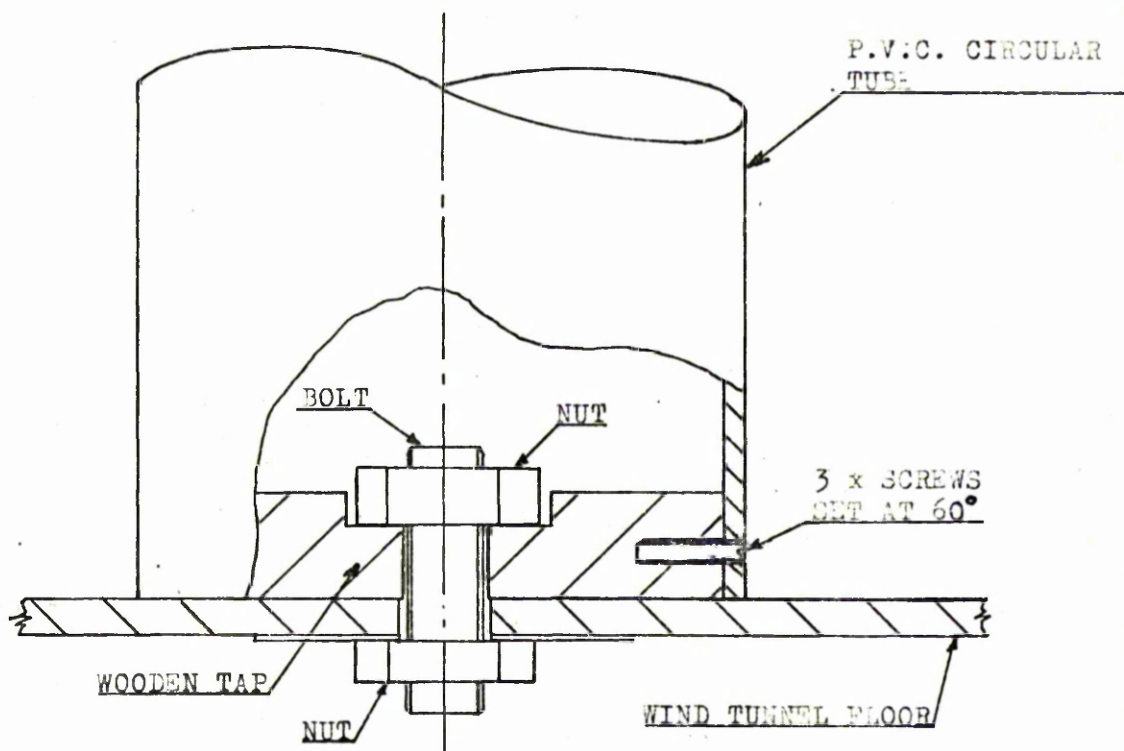and the way it was mounted.

Diagram 20: Cross-sectional view of a model showing
the mounting arrangement when placed inside
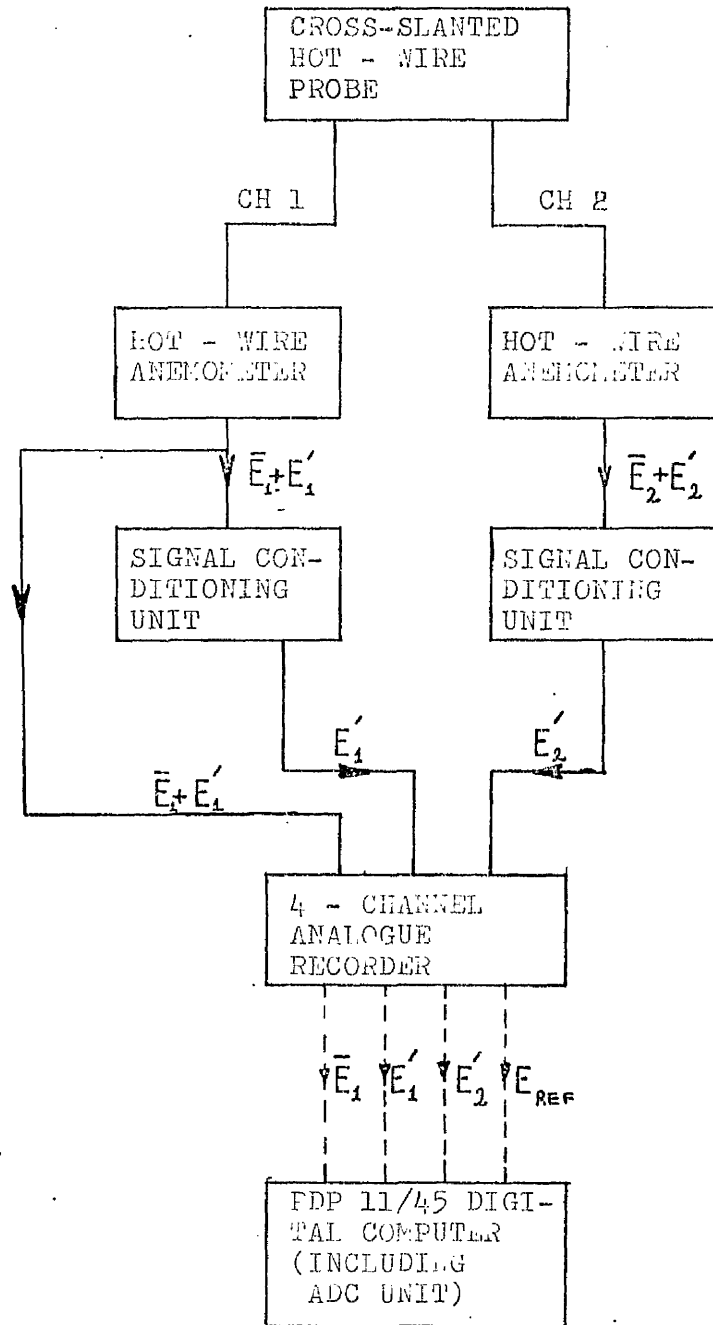the wind tunnel.

CROSS-SLANTED
HOT - WIRE
PROBE

CH 1

CH 2

HOT - WIRE
ANEMOMETER

HOT - WIRE
ANEMOMETER

$\bar{E}_1 + E_1'$

$\bar{E}_2 + E_2'$

SIGNAL CON-
DITIONING
UNIT

SIGNAL CON-
DITIONING
UNIT

E_1'

E_2'

$\bar{E}_1 + E_1'$

4 - CHANNEL
ANALOGUE
RECORDER

$\bar{E}_1$ E_1' E_2' E_{REF}

PDP 11/45 DIGI-
TAL COMPUTER
(INCLUDING
ADC UNIT)

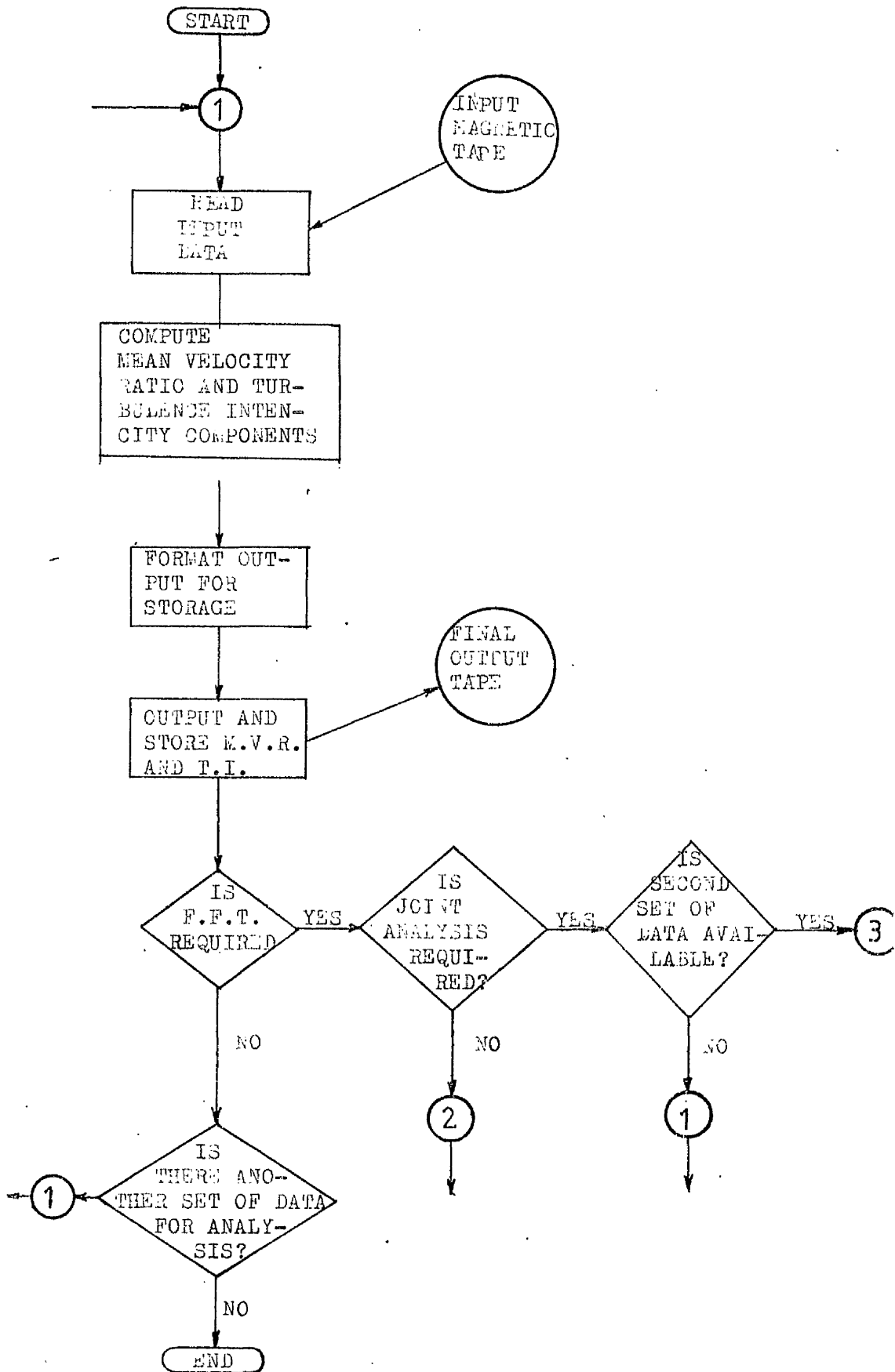Diagram 21 : Schematic of instrumentation system for
stationary Cross-Slanted hot-wire probe.

71

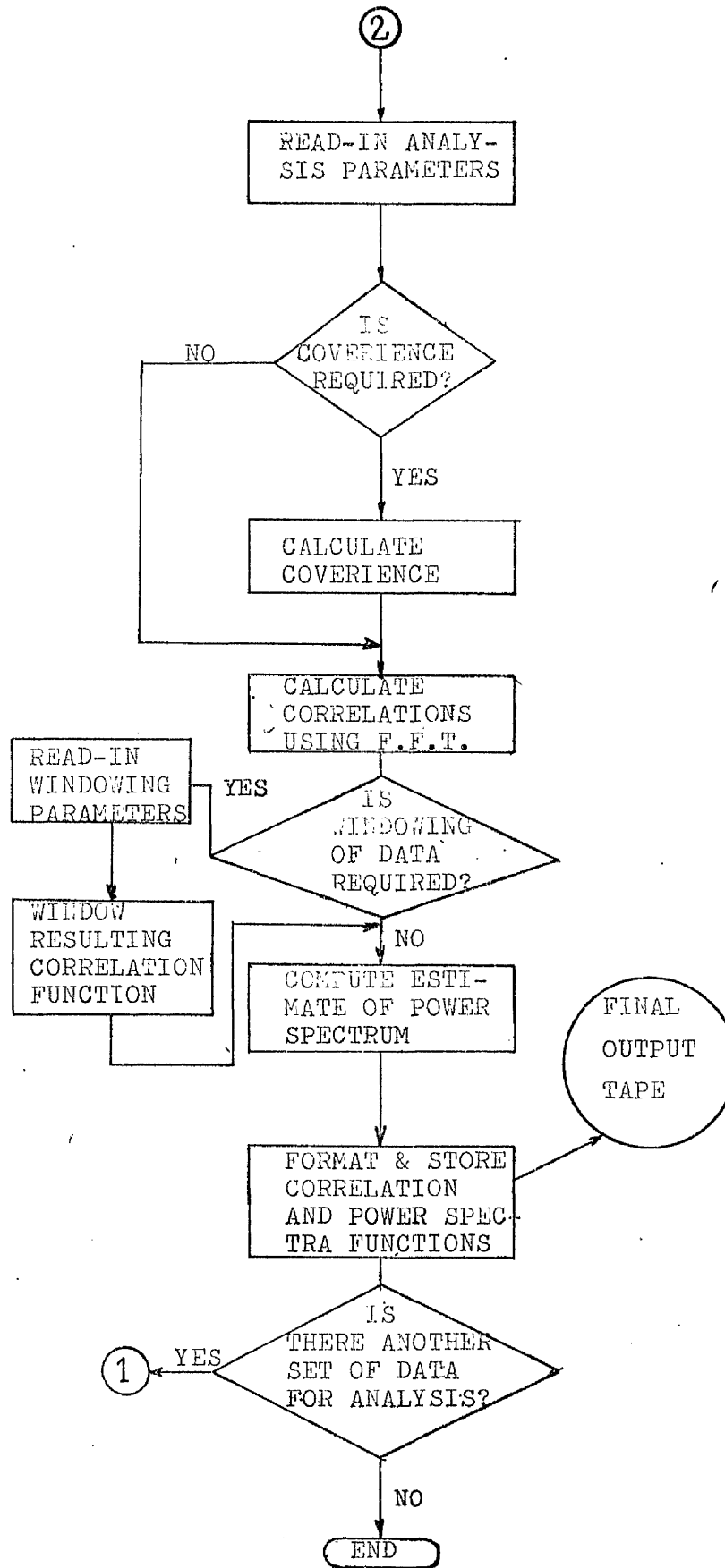Diagram 22: Digital computer flow charts for analysis of single or joint records.
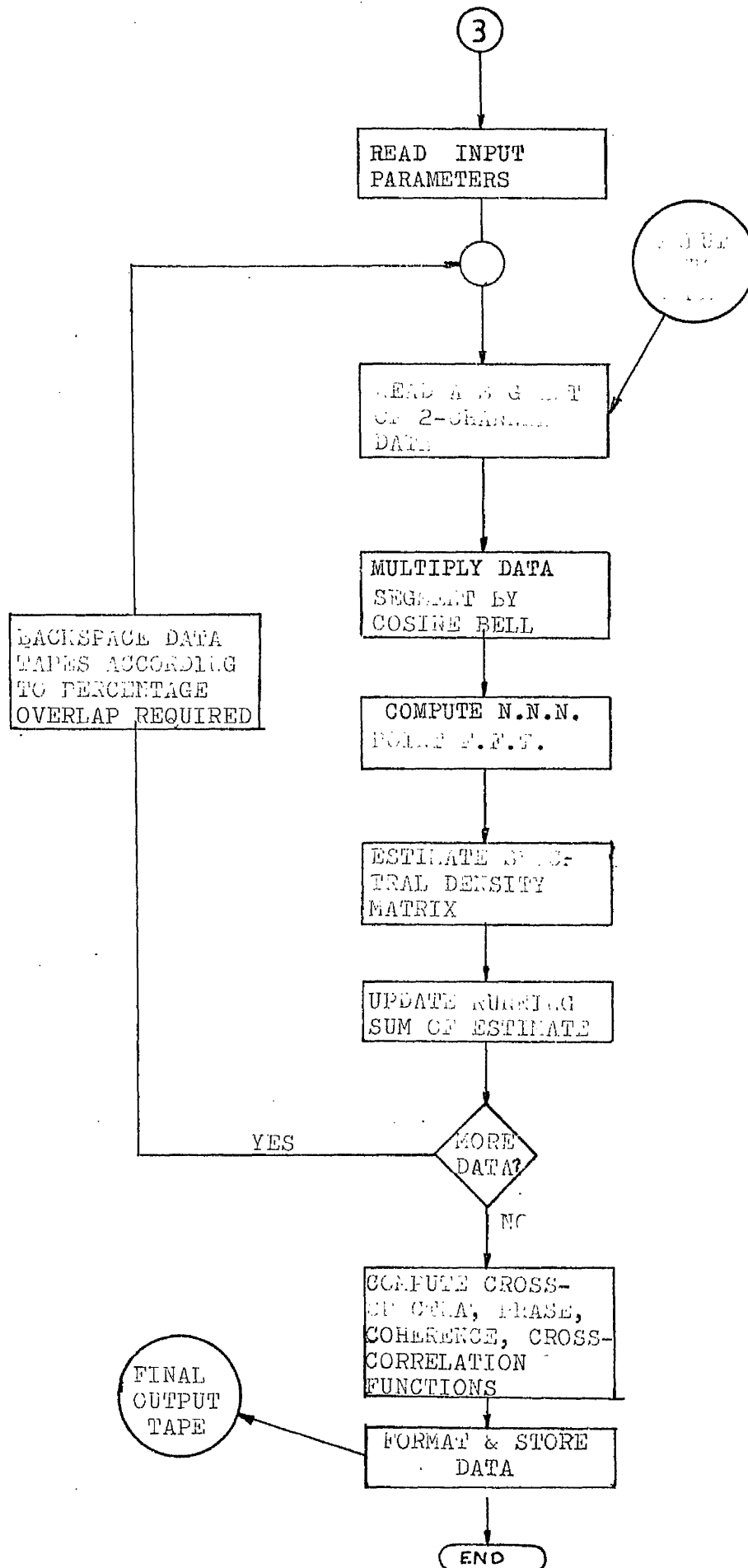
Diagram 22: (Continued)

(3)

READ INPUT
PARAMETERS

READ A SEGMENT
OF 2-CHANNEL
DATA

MULTIPLY DATA
SEGMENT BY
COSINE BELL

BACKSPACE DATA
TAPES ACCORDING
TO PERCENTAGE
OVERLAP REQUIRED

COMPUTE N.N.N.
POINT F.F.T.

ESTIMATE SPEC-
TRAL DENSITY
MATRIX

UPDATE RUNNING
SUM OF ESTIMATE

YES — MORE DATA?

NO

COMPUTE CROSS-
SPECTRA, PHASE,
COHERENCE, CROSS-
CORRELATION
FUNCTIONS

FINAL
OUTPUT
TAPE

FORMAT & STORE
DATA

END

Diagram 22: (Continued)

74

CHAPTER 6

PRESENTATION OF RESULTS

6.1 Introduction

In this chapter, the results obtained from measurements of mean flow velocity and fluctuant velocities in the near wake of each model used, will be presented.

The measured velocities are presented without any blockage corrections. This is partly because there is no reliable correction formulae available for the wake flow of a bluff body, and partly because the necessary correction factor may appear to be very small according to Richter and Naudascher (30) (the correction factor is extremely small if $D/H < 0.1$). Also the effects of the model's free-end upon the wake flow, at the positions where measurements were to be made, was examined by studying the flow behind a 2-D and a 3-D plain circular cylinder. The results indicated that the use of a three-dimensional model in the present investigation, when measurements are taken near the base and not too near the free-end, is not totally unreasonable. The power spectra, shown in the subsequent sections of this chapter, are part of the results computed in the frequency range between 0Hz and 125 Hz, with a frequency resolution of 0.49 Hz.

For the purposes of discussion, in some cases only those results taken at selected locations normal to the mean flow direction will be represented in detail. Furthermore, because of the large volume of data aquired from measurements involving various flow parameters and positions, it may be helpful to give a plan showing how these results are to be presented. This may also be of help in the subsequent discussion when comparison of results between the models are to be made.

6.2. Plan for presenting the results

In introducing the plan, we shall use the following symbols:

(I) :   Plain circular cylindrical model

(II) :   Fully slatted model

(III):   Partially slatted model.

For comparison purposes, the results are grouped in three parts.

a) Part α - Present measurements compared with existing results

Model Measurement	Present Investigation	Bloor & Gerrard(19)	Roshko(18)
	(I)	(I)	(I)
Mean Velocity Ratio	✓	✓	—
Wake Energy	✓	—	✓

Figure (α -1)

b)   Part β - Across the wake measurements (transverse along the Y-direction)

Symbol	Description
A	Mean Velocity Ratio
Tu(u)	Turbulence intensity of u'-velocity
Tu(v)	Turbulence intensity of v'-velocity
Guu	Power Spectra of u'-velocity
Gvv	Power Spectra of v'-velocity
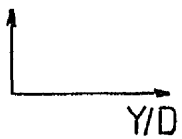
X/D = 3.0	
Model Measurement	(I) (II) (III)
A Tu(u') Tu(v')	Y/D
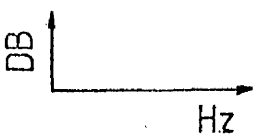
Figure (β -1)

Power Spectra Guu at X/D=3.0	
Model Y/D	(I) (II) (III)
0.00 0.53 1.20	DB ... Hz

Figure (β -2)

Power Spectra Gvv at X/D=3.0			
Model	(I)	(II)	(III)
Y/D	DB ↑		
0.00			
0.53			
1.20	→ Hz		

Figure ($\beta - 3$)

X/D=4.5			
Model	(I)	(II)	(III)
Measurement	↑		
A			
Tu(u')			
Tu(v')	→ Y/D		

Figure ($\beta - 4$)

Power Spectra Guu at X/D=4.5			
Model	(I)	(II)	(III)
Y/D	DB ↑		
0.00			
0.53			
1.20	→ Hz		

Figure ($\beta - 5$)

Power Spectra Gvv at X/D=4.5			
Model	(I)	(II)	(III)
Y/D	DB ↑		
0.00			
0.53			
1.20	→ Hz		

Figure ($\beta - 6$)

X/D=6.0			
Model	(I)	(II)	(III)
Measurement	↑		
A			
Tu(u')			
Tu(v')	→ Y/D		

Figure ($\beta - 7$)

Power Spectra Guu at X/D=6.0			
Model	(I)	(II)	(III)
Y/D	DB ↑		
0.00			
0.53			
1.20	→ Hz		

Figure ($\beta - 8$)

Power Spectra Gvv at X/D=6.0			
Model	(I)	(II)	(III)
Y/D	DB ↑		
0.00			
0.53			
1.20	→ Hz		

Figure ($\beta - 9$)

c)   Part γ - Along the wake measurements (longitudinal, along the X-direction)

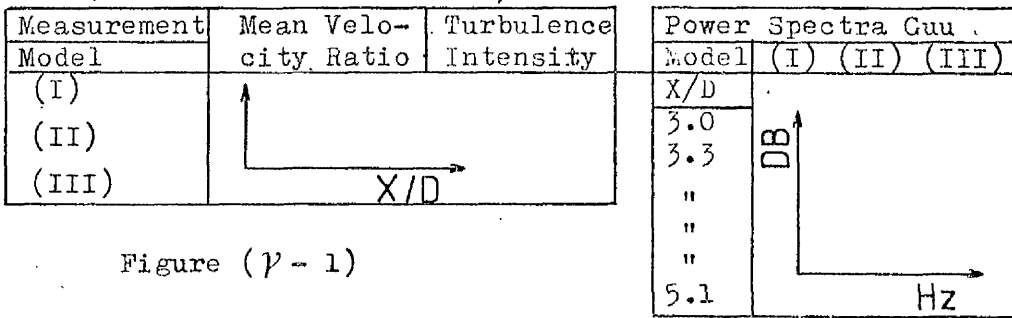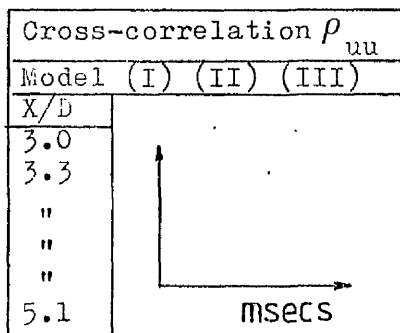| Symbol	Description
Guu	Power Spectra Function
ρ_{uu}	Cross-correlation coefficient
θ	Phase angle
γ_{uu}	Squared coherence
Ur	Vortex convection velocity
a_V	Vortex longitudinal spacing

Figure (γ - 1)
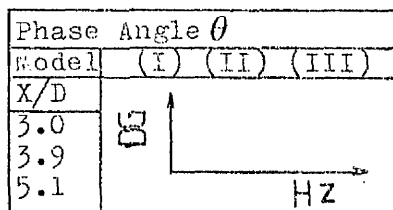

Figure (γ - 2)

Figure (γ - 3).

Figure (γ - 4)
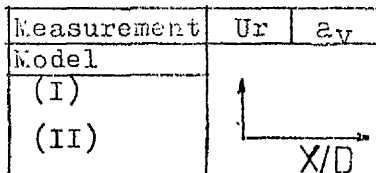

Figure (γ - 5)

Figure (γ - 6)

79
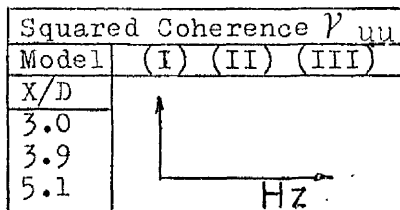
6.3. Part α -Present measurements compared with existing results

In Fig (α-1), results due to Bloor & Gerrard and Roshko, obtained from references (19) and (18) respectively, are compared with present measurements. Despite the differences in the test Re between the various investigations and the way models were mounted in the tunnel (i.e. both 2-D and 3-D), the trends remain similar in all cases.

Further comparisons of various wake parameters are given in Table 2. These show that results obtained from present work are in good agreement with those obtained by other investigators (19,31,32,33). Thus the methods used in this investigation are considered satifactory.

6.4. Part β - Across the wake measurements

6.4.1. Position of measurement at X/D = 3.0

Figure (β-1) shows respectively the mean velocity ratio and turbulence intensity components. Examination of the mean velocity ratio plots indicates that the mean velocity distribution behind all three models can be divided into three flow regions.

In flow region 1, 0 < Y/D < 0.40, the mean velocity recovery for models (II) and (III) is considerably less than that of model (I). This suggests, for the case of models (II) and (III), the presence of a slow moving flow of high static pressure.

In flow region 2, 0.40 < Y/D < 0.93, a strong mean velocity recovery is taking place, especially for models (II) and (III). The steep gradient of the plots (i.e. $d(U/U_\alpha)/dY$) is an indication of the presence of a strong shear layer. In the case

of model (I), a mean velocity recovery also exists, but the gradient is not so steep. Nevertheless, the trend shown by the respective graphs is similar for all models.

In flow region 3, 0.93 < Y/D < 1.33, the mean velocity ratio, for all three models, have reached values close to unity. The flatten shape of the curves with respect to the lateral distance from the wake central line has taken place. The components of turbulence intensity associated with the plain cylinder have a "smooth" peak at Y/D ≃ 0.53, with v′-velocity component being greater than that of u′-velocity component. This may be attributed to the oscillatory behaviour of the wake that has been observed to occur behind a plain cylinder.

The turbulence intensity for the slatted devices show a distinct peak, the maximum of which centres around Y/D = 0.7. This peak is thought to be a result of the presence of a strong shear layer rather than due to vortex shedding, as it would be further discussed in this section. While the intensity of the u′-velocity is higher than that of v′-velocity, in contrast to that with the plain circular model, the absolute magnitude of both intensities is considerably smaller than those of model (I).

Figure (β-2) shows respectively the power spectra of the u′-velocity component at three selected lateral positions in the wake flow. Two distinct peaks are observed in the spectra of model (I) at Y/D = 0.00. The first peak occurs at 15.2 Hz (i.e. near the Strouthal number for a 2-D model) and the second at twice that frequency, i.e. 30.4 Hz. The presence of a second peak in the spectra taken at the wake axis has been observed by other investigators as well (18,34). A plausible explanation put

forward by some of them is that a probe placed in the wake centre is subjected to disturbances from vortices shed from both sides of the body, and hence, the occurrence of a double frequency peak. The intensity of the first spectral peak attains its maximum at Y/D = 0.53 and then decreases as evidently shown by the plot at Y/D = 1.20, while the intensity of the second peak decreases rapidly from the wake centre and disappears around Y/D = 0.4 (results at this point not shown).

The power spectra plots for the slatted models show no signs of periodic content up to Y/D ≅ 1.0. This suggests that the flow is turbulent with no periodicity of any significance contained in it. The spectra at Y/D = 1.20 of the fully slatted model (II) show a single peak at 12.2 Hz, but of very small intensity. This further suggests that the process of vortex formation may have started, but due to the low intensity of the vortices at this position, their effect on the body is negligible. The spectra for the partially slatted model (III) show a complex frequency content, but prominent isolated peaks that could be associated with a single frequency component are not apparent. Visual inspection of the hot-wire signals indicated low level velocity fluctuations with periodic components of varying frequency being present only intermittently.

Figure (β-3) shows the frequency power spectra of v′- velocity component at various locations in the Y′-direction. With model (I), a distinct spectral peak at 15.2 Hz is observed at all three positions considered. Its intensity is generally higher than that of the u′-velocity component and has its maximum

82

value at the centre of the wake (i.e. Y/D = 0.00) and then decreases with increasing distance along the Y-direction. No double frequency peak has been observed. The high intensity of the v'-velocity power spectra is further evidence of the effect of the oscillatory behaviour of the wake.

In the case of the slatted models (i.e. models (II) and (III)) any significant sign of spectral peaks did not occur until further outboard from Y/D = 0.00. In general, the intensity of these peaks is considerably lower than those corresponding to the plain circular model, which suggests that the wake flow behind the slatted models is rather steady and the effects of any vortices upon the body are very small.

6.4.2. Position of measurement at X/D = 4.5

Figure (β-4) shows respectively the mean velocity ratio and turbulence intensity components at various positions along the Y-direction

The mean velocity ratio plots indicate that the three flow regions observed behind each model at X/D = 3.0 are not so distinct, especially with model (I). The mean velocity in the wake of model (I) increases uniformly along the Y-direction and in general, its values are higher than they were at X/D = 3.0, while in the case of the slatted models, the mean velocity is higher near the wake centre (i.e. Y/D < 0.8) and lower further away from it.

The turbulence intensity of the u'-velocity in the wake of model (I) shows a broad peak at Y/D = 0.53 with its maximum being approximately equal to that observed at X/D = 3.0. However, no

83

distinct peak is observed in the turbulence intensity of the v'-velocity of model (I) which has its maximum intensity occurring at the centre of the wake and decreasing rapidly with increasing distance along the Y-axis. The sharp peak observed in both turbulence intensity plots of the slatted models at X/D = 3.0 is still evident at this position although here the peak is broader and of higher intensity. The widening of the intensity peaks observed at this position for all three models may be attributed to the wake being broadened at this position. Since the sharpness of the intensity peaks in the wake of the slatted models was thought to be due to the presence of a strong shear layer, the broadening of these peaks at X/D = 4.5 suggests that the strength of that shear layer has began to wane.

Figures (β-5) and (β-6) show respectively the power spectra of the u'-velocity and v'-velocity components at various positions along the Y-direction.

The power spectra plots of both velocity components of model (I) show a distinct spectral peak at 15.2 Hz at all positions of measurement. The intensity of the u'-velocity spectral peak attains its maximum at Y/D = 0.53, while that of v'-velocity attains its maximum intensity at the wake centre and then decreases with increasing distance along the Y-direction. In general . the intensity of the v'-velocity spectral peak is higher than that of the u'-velocity.

The power spectra in the wake of the fully slatted model (II) are somewhat different from those at X/D = 3.0. At this position (i.e. X/D = 4.5) a distinct spectral peak at 12.2 Hz is observed in the spectra of both velocity components and at all

recording positions along the Y-direction. A second spectral peak of smaller intensity at 24.4 Hz is also observed but only at positions near the wake centre (i.e. Y/D < 0.4). The intensity of both spectral components attains its maximum at Y/D = 0.66 and is considerably smaller than that of the plain circular model. The presence of two distinct spectral peaks at the wake centre together with the single "narrow-band" frequency spectral peak observed at all other positions along the X-axis indicate the presence of a "vortex-street-like" wake flow behind model (II). However, the strength of the formed vortices - as indicated by the intensity of the spectral peaks - is quite low and consequently their effects upon the body cannot be of significance.

The power spectral plots for the partially slatted model show no sign of periodicity up to Y/D $\simeq$ 0.40. However, a distinct spectral peak of the "wide-band" frequency at 15.2 Hz is observed at Y/D$\simeq$0.53, the intensity of which is very small and attains its maximum value at Y/D = 0.8. The existance of such a spectral peak does not necessarily indicate a breakdown of the shear layer and thus the formation of vortices at a single frequency. What it does indicate is, that the formation of low intensity vortices has taken place intermittently over a range of frequencies, but the formed vortices are incoherent and thus their effects upon the body are still quite insignificant.

6.4.3.   Position of measurement at X/D = 6.0

Figure (β-7) shows the mean velocity ratio and turbulence intensity plots at various positions along the Y-axis.

The mean velocity behind all three models shows no major differences over that at X/D = 4.5, except that its magnitude is generally higher.

The turbulence intensity of the u'-velocity of model (I) is almost symmetrical about Y/D = 0.66 and its maximum is slightly lower (10%) than at X/D = 4.5. The turbulence intensity of the v'-velocity shows a small peak at Y/D = 0.4 from the wake centre. In general, its intensity is higher than it was at X/D = 4.5, as well as being higher than that of u'-velocity component at X/D = 6.0.

The turbulence intensity plots for the slatted models show no markded differences over those already observed at X/D = 4.5, except perhaps that the peaks are broader and of higher intensity, which is in contrast to those observed for the plain circular model.

The power spectral plots of the u'-velocity and v'-velocity components is shown in Figures (β-8) and (β-9).

A distinct spectral peak at 15.2 Hz is observed in the spectra of model (I) at all positions along the Y-direction. The intensities of both spectral components increase with distance from the wake centre, but are lower than those found at X/D = 4.5.

The power spectra of model (II) indicate a single distinct spectral peak at 12.2 Hz to be present at all positions along the Y-axis. The intensity of these spectra attain a maximum at Y/D = 0.66, which is higher than that found at X/D = 4.5. This suggests that the vortices formed upstream of X/D = 6.0 are still

growing in strength, in contrast to model (I) which is losing strength at this position. Also, because the intensity of the v'-velocity spectra is lower than that of the u'-velocity, the indications are that the wake of the fully slatted model is not as oscillatory as that of the plain circular model. despite its "vortex-street-like" pattern.

The power spectra for the partially slatted model show that the wake does not contain any periodic flow structures up to Y/D = 0.4. Beyond that position, a single spectral peak of "wide-band" frequency at 15Hz is observed at all positions along the Y-direction. The intensity of both spectral components has maximum values at Y/D = 0.66, and in general is higher than that at X/D = 4.5. This suggests that although the process of vortex formation may have started, it is still rather slow and fully coherent vortices of any significance do not appear until further downstream in the X-direction. Because of this, the wake flow of the partially slatted model (III) is very steady up to six diameters away from the body.

6.5. Part γ -Along the wake measurements (longitudinal along the X-direction)

The mean velocity ratio and turbulence intensity, at various positions along the X-axis, are shown in Figure (γ-1).

The mean velocity ratio plot for model (I) indicated that its value remains quite constant along the X-direction, (at least between X/D = 3.0 and X/D = 5.1), at about 0.83. A similar behaviour has been observed by Sonnervile (33), showing a mean value of around 0.79. In contrast, the mean velocity for the

fully slatted model increases linearly with X/D. Despite the high rate of increase, the mean velocity values for model (II) are considerably lower (up to 50%) compared to those of model (I). The mean velocity for model (III) shows a gentle increase with X/D and is observed also that the velocity recovery for this model is the lowest of all three models, being about 60% lower than of model (I) and 30% than that of model (II).

The turbulence intensity for the plain model (as shown in the figure above) decreases with increasing distance along the X-axis. This trend is in excellent agreement with existing results and observations (19,35). The turbulence intensity for the fully slatted model, however, increases almost linearly with no apparent trend of reaching maximum at least up to 6D away from the model. The turbulence intensity plot for model (III) show that this quantity varies slowly with respect to changes in position along the X-direction. Its absolute intensity is at least 25% lower (at X/D = 5.1) than that of the other two models and the trend indicates that the wake flow undergoes only small changes for the positions between X/D = 3.0 and X/D = 5.1. Although a similar behaviour has been observed in the measurements discussed in part (β), (compare figs. (β-1), (β-4), (β-7)), a direct comparison with those results is not possible. This is because the quantity analysed in part (β) is

$$u' + \frac{w'^2 - \overline{w'^2}}{\overline{U}} \qquad \text{------------- (Cross-Slanted probe)}$$

while in the present case is

$$u' + \frac{v'^2 - \overline{v'^2}}{2\overline{U}} \qquad \text{------------- (Single probe)}$$

88

. (refer also to section 4.4). .

Figure (γ-2) shows respectively the power spectra. A distinct spectral peak at 15.2 Hz is observed in the spectra of model (I) at all positions of measurement. and as expected, its intensity 'decreases with increasing distance along the X-direction away from the model. A second spectral peak at 30.2 Hz is also observed at some positions but its intensity is considerably lower (70%) than that at 15.2 Hz. The power spectra for model (II) show no spectral peaks of any significance for positions up to X/D = 3.6. However, a distinct spectral peak at 12.2 Hz is observed at X/D = 3.9. Although its intensity is small. its presence signifies that the process of vortex formation at a single frequency could have started. This is further supported by the spectra plots for the positions up to X/D = 5.1, which show that the intensity of the peak increases with increasing X/D values. Since the intensity of power spectra can be related to the strength of the formed vortices, it can thus be speculated that the formed vortices would continue to grow at least up to X/D = 6.0 (see also Figs (β-5) & (β-6).

The power spectra for the partially slatted model shows no spectral peaks of any significance at any frequency or position of measurement. The absence of such a peak implies that the wake flow is steady and completely turbulent at least up to six diameters behind the model. This is in good agreement with the results already discussed in section 6.4.4.

The cross-correlation functions for all three models and at various positions along the X-axis are shown in Figure (γ-3). The plots for model (I) show that the velocity signals are well

89

correlated at all positions up to X/D = 5.7 and since the maximum cross-correlation occurs at positive time delay (i.e. at 12 msecs). they indicate that the velocity fluctuations around the shedding frequency are moving in the streamwise direction and away from the model. No correlation between the two velocity signals is observed for the fully slatted model. for positions up to X/D = 3.6. The absence of any correlation is evidence of the non-existance of any coherent periodicity in the wake flow. The first observation of the existance of correlation is made at X/D = 3.9. Above this position. the correlation value between two signals increases with distance along the X-direction. This suggests that for positions beyond X/D = 3.9, the wake flow is increasingly becoming periodic. If the flow in the wake is of the "vortex-street-type" then it would be possible to compute the frequency of vortex formation by using the period measured between two successive peaks of the cross-correlation function. The measured period is 86 msecs. and by using the relationship

$$f = \frac{1}{T}$$

where

f is the frequency in Hz; and

T is the period in secs,

we get

$$f = \frac{1}{86 \times 10^{-3}} = 11.8 \text{ Hz}$$

This value is in good agreement with the value obtained from the frequency spectra (i.e. 12.2 Hz). and therefore the assumption made that the wake flow behing a fully slatted cylinder (for X/D > 3.9) is vortex-street-like is further

justified.

The cross-correlation plots for model (III) show no correlation whatsoever between the velocity signals at any position of measurement which further indicated the total absence of any periodicity in the wake at least up to X/D = 5.7 D. However, the velocity fluctuations are still moving in the spanwise direction and away from the model.

Figures (γ-4) and (γ-5) show the phase angle and squared coherence at selected positions along the X-axis. By definition (see section 3.4.2.), the squared coherence function can be a measure of the periodic nature of the wake. The more the periodic the flow structure of the wake is, the higher the values of squared coherence would be, (i.e. ~1), although the reverse argument is not always correct. Although limited information can be obtained directly from the plots, except perhaps to emphasize the high coherent wake flow of the plain circular model and the total absence of it in the wake flow of the partially slatted model, they are used for the calculation of the vortex convection velocity and longitudinal vortex spacing. In order to calculate these flow quantities it is necessary for the wake flow to be of high coherence (i.e. $\gamma^2 > 0.9$, see also chapter 4). This requirement is fulfilled with the plain circular model at all X/D positions, with the full slatted model at positions equal or greater than X = 4.2D and at no position at all along the X-axis by the partially slatted model. Therefore, Figure (γ-6) shows the vortex convection velocity and vortex longitudinal spacing for model (I) at all X/D positions and for

91

model (II) at positions X/D⩾4.2. The trend shown by the vortex velocity ratio plot behind model (I) is similar to that found by Bloor & Gerrard (19). Bearman (37) has shown that the vortex convection velocity can be related to two important geometric wake parameters, namely, the transverse and the spanwise distance between two consecutive vortices in the wake. He further showed that trends similar to that shown by the plot of model (I) can be identified with the "widening" of the wake, i.e. the ratio of the transverse distance between two vortices to the spanwise one between them is increasing as distance along the X-direction increases. However the trend shown by the vortex velocity ratio plot of model (II) is in contrast to that indicated by model (I). A trend as that shown by the plot of the vortex convection velocity behind model (II) suggests that the ratio of the transverse distance between two vortices to the spanwise one decreases as distance away the model increases, i.e. the wake is not as widd as that of model (I) for X/D positions up to at least 6.0. The plots however show that for larger X/D values (i.e. X/D⩾6.0), the geometric characteristics of the wake behind model (I) & (II) become similar.

The values of the vortex longitudinal spacing found behind model (I) are somewhat lower to those found by other investigators (31),(32), although they fall well within the range of values suggested by El Baroudi (38). Although the values of the vortex longitudinal-spacing found in the wake of model (II) fall within the range of values found in the wake of model (I), the trends shown by the two plots are different. This further reveals of how disimilar the wake flow between a plain circular model and a fully slated one is.

92

CHAPTER 7

GENERAL DISCUSSION AND CONCLUSIONS

7.1 General Discussion

In the present study we have investigated the wake flow of circular cylindrical models with or without the presence of a slat device. The objective of the investigation is to establish the influence of the slat system upon the wake flow, and thus shed some light on the flow mechanisms used by such a device to delay the formation of vortices in the flow. For the purpose of examining the differences in the flow behind the various models used, comparative measurements were made in the wake of a plain circular cylinder, a circular cylinder fitted with the fully slatted device, and a circular cylinder fitted with the partially slatted device, under identical flow conditions.

The measurements taken in the wake of a plain circular cylinder (model (I)), reveal the existance of a vortex-street-like flow aat all positions of the wake studied. The separated shear layers from each side of the body become unstable and roll-up into discreet vortices in the region between the rear of the model and $X/D = 3.0$, as power spectral analysis at $X = 3.0D$ (refer to Fig (γ-2)) indicated that the breakdown of the shear layers has already taken place. Thus the flow field becomes periodic and well correlated over relatively long distances along the X-direction (as observed from the cross-correlation function, Fig. (γ-3)), with almost all its associated energy being concentrated to a single frequency, i.e. the vortex shedding frequency. As the vortices grow, they tend to entrain fluid from the near wake region behind the body (i.e. $X < 3.0D$), and cause a low pressure field to be established. As these vortices drift downstream, the pressure field changes and this gives rise to fluctuating pressure forces acting upon the body, as will be seen

94

in the accompanying diagram 23.

The ways in which the slat devices modify the near wake flow are discussed below.

(a) Circular cylinder fitted with the fully slatted device.

The flow in the wake of a circular cylinder fitted with the fully slatted device can be divided into two flow regions along the X-direction. namely, a region where the free shear layers are distinct from one another and separated by a slow moving flow, (extending up to 3.6D behing the model) and another region extending beyond the first one, where the mixing of flow from the two shear layers and the slow moving flow has taken place, and the flow is periodic. These two regions have the respective flow characteristics.

Measurements of various flow quantities (such as mean velocity and turbulence intensity) at X = 3.0D show that the slow moving flow observed in region one. extends up to 0.4D in the Y-direction. This inner flow region is characterised by small local mean velocities which remain almost constant, and irregular fluctuating velocities of very small magnitude. Above this region and up to $Y \simeq 1.0D$, the flow is dominated by free shear layers which appear to be stable. A high mean velocity recovery is observed to take place and the magnitude of the irregular fluctuating velocities has increased considerably, attaining its maxima around $Y \simeq 0.7D$. Because the flow is fully turbulent, the wake at this X/D position is stable and non-oscillatory.

As distance along the X-direction increases away from the model, the position along the Y-direction where the slow moving

flow adjoins the free shear layers shifts towards the centre of the wake, so much so that at X/D = 4.5 the two flows are not distinct any more (refer to Fig (β-1)). The reason for this is that free shear layers are by their nature unstable, and as they move downstream the model would break down into discreet vortices. Power spectral analysis (refer to Fig (γ-2)), reveals that the first signs of periodicity in the wake (associated with shear layer break down) are apparent at a position around X = 3.6D. Vortices are flow regions of low pressure and therefore require fluid in order to grow. Part of this fluid is thought to be supplied by the slow moving flow region, through the process of entrainment (6). As the vortices grow, they continue to entrain fluid out of the slow moving flow region, with the result that at some position downstream the two flows become fully mixed. Present measurements indicate that this occurs at a position around X = 4.5D. For X/D positions further downstream, the vortices continue to grow, as indicated by the power spectral analysis and the flow becomes increasingly periodic and vortex-street-like. Thus the wake is unsteady and oscillatory. The frequency of vortex shedding in this wake region is found to be lower (by 20%) to that of the plain circular cylinder and the vortices do not attain intensities comparable to those of model (I) until X = 6.0D.

Summarising the above, it can be said that the presence of the fully slatted device effectively delays the formation of vortices in the wake by increasing the distance where free shear layer instability occurs further downstream of the body. Since, as already mentioned, vortices are low pressure flow regions,

their removal from the close quarter of the body infers that the pressure in the near wake would automatically have a higher value. This implies that the base pressure is also raised as compared with the case when the vortices are formed right at the rear of the body. This increase in the base pressure has been experimentally confirmed by Wong (14), who attributed this to the ejection of fluid in the base region i.e. to base bleed flow. However, the observed increase of base pressure is not thought to be the only flow mechansim which causes the delay of the vortex formation. The presence of stable free shear layers, as observed in Fig (χ-2), at positions close to X = 3.0D indicated the existance of a second flow mechanism which has acted in such a way that has resulted in the avoidance of the instability of those layers occurring near the body. It is well known that ejection of high energy flow into a separated shear layer acts a a stabilizing agent and delays its breakdown into discreet vortices. It is thought that this is what might be taking place near the body, with the high energy flow being supplied by the flow ejected through the side slats of the device. Wong (13), who was the first to postulate the existance of such flows, has called them "Counter-flows". Further indications about the existance of counter-flows near the body have been forthcoming from photographs of the near wake taken by Galbraith (36) in a smoke-tunnel.

A suggested flow pattern behind a fully slatted device is shown in Diag. 24.

Finally, if no detachment of vortices is taking place near

97

the body surface (i.e. they are formed somewhere downstream), it is likely that this would reduce the pressure fluctuations acting upon the rear part of the body. A reduction of surface fluctuating pressures is in effect a reduction of excitation. When the cause of excitation is reduced, the body is less likely to be subjected to strong vibratory forces. If vibration should still occur, the amplitude will certainly be reduced. The fully slatted device has indeed showed these characteristics..

(b) Circular cylinder fitted with the partially slatted device.

From the results previously discussed, it is evident that the wake behind a circular cylinder fitted with the partially slatted device contains no conherent periodic flow structures of any significance over a region of at least 6D behind the body. The flow is characterised by the presence of two distinct shear layers separated from each other by a region of slow moving flow. The wake appears steady and its characteristics change little along the X-direction as is indicated by the turbulence intensity and power spectral analysis (refer to Figs (γ-1) and (γ-2)). The same arguments may be applied to the causes of wake stability as those already given to the fully slatted device. However, the reason that the partially slatted device is more effective in delaying vortex formation is attributed to the increased amount of high energy fluid ejected in the rear of the body. This is made possible by the larger opening provided in the high pressure region at the frontal area of the body and the larger opening provided at the rear. How much of the increased amount of high energy flow is ejected through the side slats. as counter-flow,

and how much is ejected through the opening in the base, as base bleed, cannot be accurately assessed. However deductions regarding the relevant importance of the above can still be made by using results already obtained. These results suggest that the amount of flow ejected in the base region is considerably higher than that ejected through the side slots. Mixing of the shear layer flow with that from the increased slow moving flow region would result in the shear layers being of lesser strength and the flow in the wake (in general) being more "uniform" in comparison to that behind either model (I) or model (II) (refer to Figs. (γ-1) and (γ-2). Also because of the lesser strength of the free shear layers, the rate of mixing (entrainment?) with the base bleed flow would be lower. This, in conjunction with the increased amount of base bleed flow results in the wake remaining stable and non-oscillatory at longer X/D distances. Because of the limited X/D distance of measurements taken behind the body, the final configuration of the wake, i.e. if the wake becomes oscillatory or if it remains turbulent at all X/D positions, is not known. However, indications from the power spectra results (see Fig (β-9)), suggest that the wake might become periodic further downstream, but with the strength of the formed vortices being small (if compared with either of the models studied).

Summarizing, it can be said that the presence of the partially slatted device delays the formation of vortices to very long distances downstream due mainly to the increased amount of high energy fluid being ejected in the base region of the body.

A schematic representation of the wake behind a partially

99

slatted device is shown in Diagram 25.

With the formation of vortices occurring further downstream there is likely to be a considerable reduction of the pressure fluctuations. The absence of surface fluctuating pressures is in effect a removal of excitation from the body. When the cause of excitation is thus removed, the body is then free from the vibratory forces as it is no longer subject to the oscillatory agent produced by vortex shedding. This may underline the reasons behind the effectiveness of the partially slatted device in suppressing vortex induced oscillation.

7.2 Conclusions

An experimental investigation of the wake developed behind circular cylinders with or without slat devices at X/D positions from 3.0 to 6.0 leads to the following conclusions:

1.   Regular vortex shedding behind a plain circular cylinder has been found at all X/D positions and the wake is unstable and oscillatory at positions very close to the body.

2.   The wake behing a circular cylinder fitted with the fully slatted device may be classified into two flow regions:

(a)   A flow region extending up to X = 3.6D, in which the free shear layers are stable and separated by a slow moving flow. In general, the flow is turbulent and the wake is stable and non-oscillatory, and

(b)   A flow region beyond X = 3.6D, where the free shear layers have broken up into discreet vortices, the flow is periodic and the wake is unstable and oscillatory.

3.   The wake behind a circular cylinder fitted with the

partially slatted device is found to be stable and non-oscillatory, with no regular vortex shedding present at any X/D position.

Parameter / Source	a_v/D	St	U_r/U_o
KOKKALIS	3.4 - 4.0	0.185	0.65 - 0.75
(19)	——	——	0.73 - 0.83
(31)	4.27	0.187	0.80
(32)	4.10	——	0.82

TABLE 2: Comparison of various wake parameters
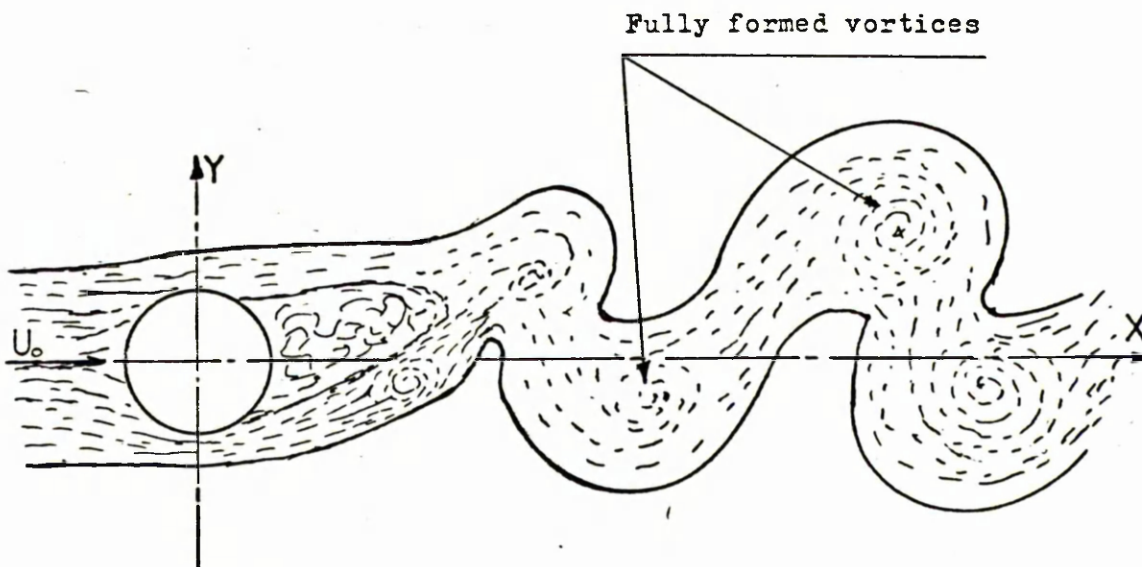
Diagram 23: Schematic of the wake flow behind a plain circular cylinder
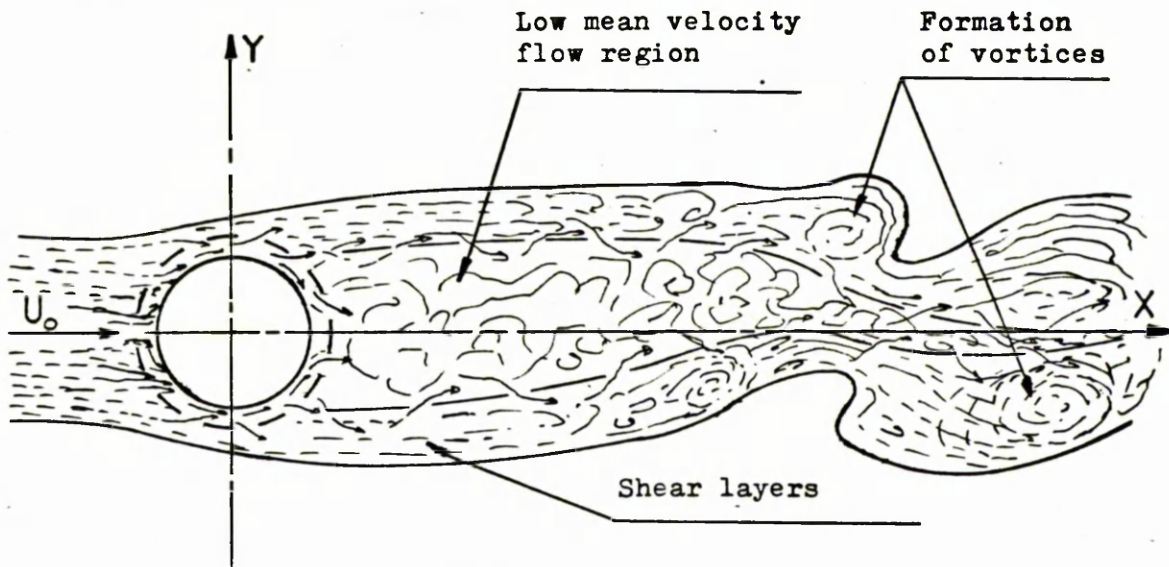
Diagram 24: Schematic of the wake flow behind a fully
slatted circular cylinder.
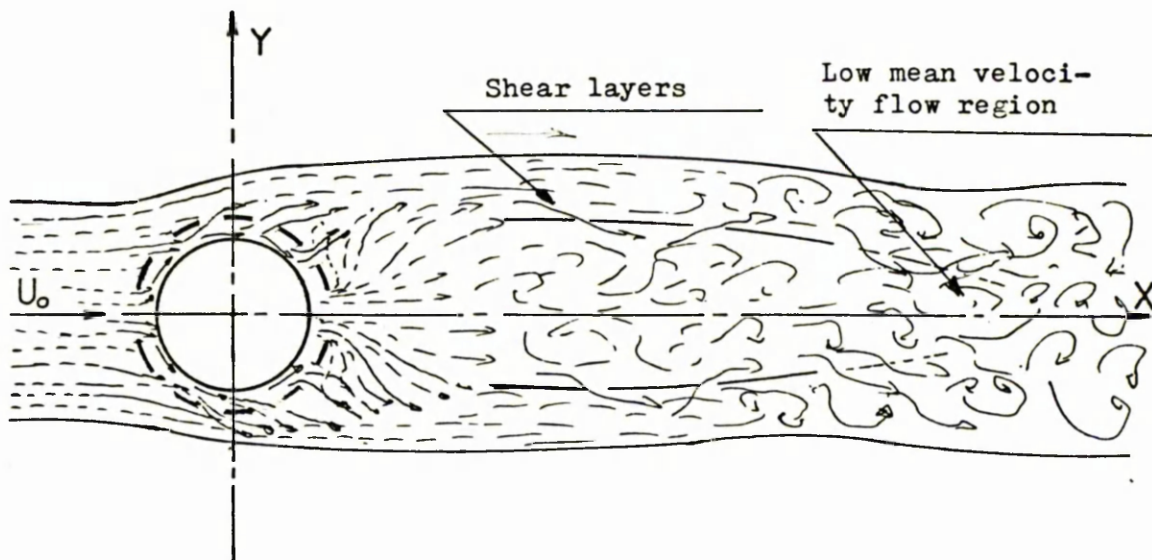
Diagram 25: Schematic of the wake flow behind a partially
slatted circular cylinder .
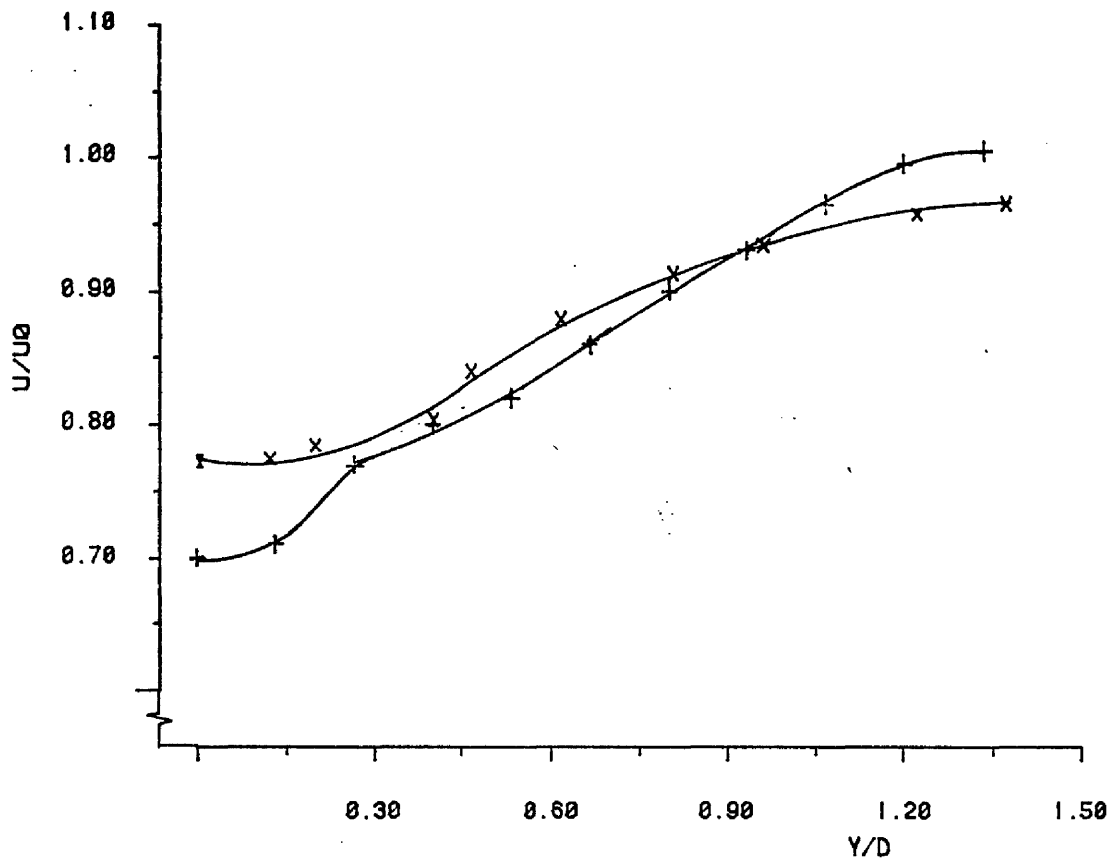
Distribution of mean velocity ratio transverse to the wake at X/D=6.0,*
+ - Kokkalis, ✕ - Bioor et al (Re=16,000).
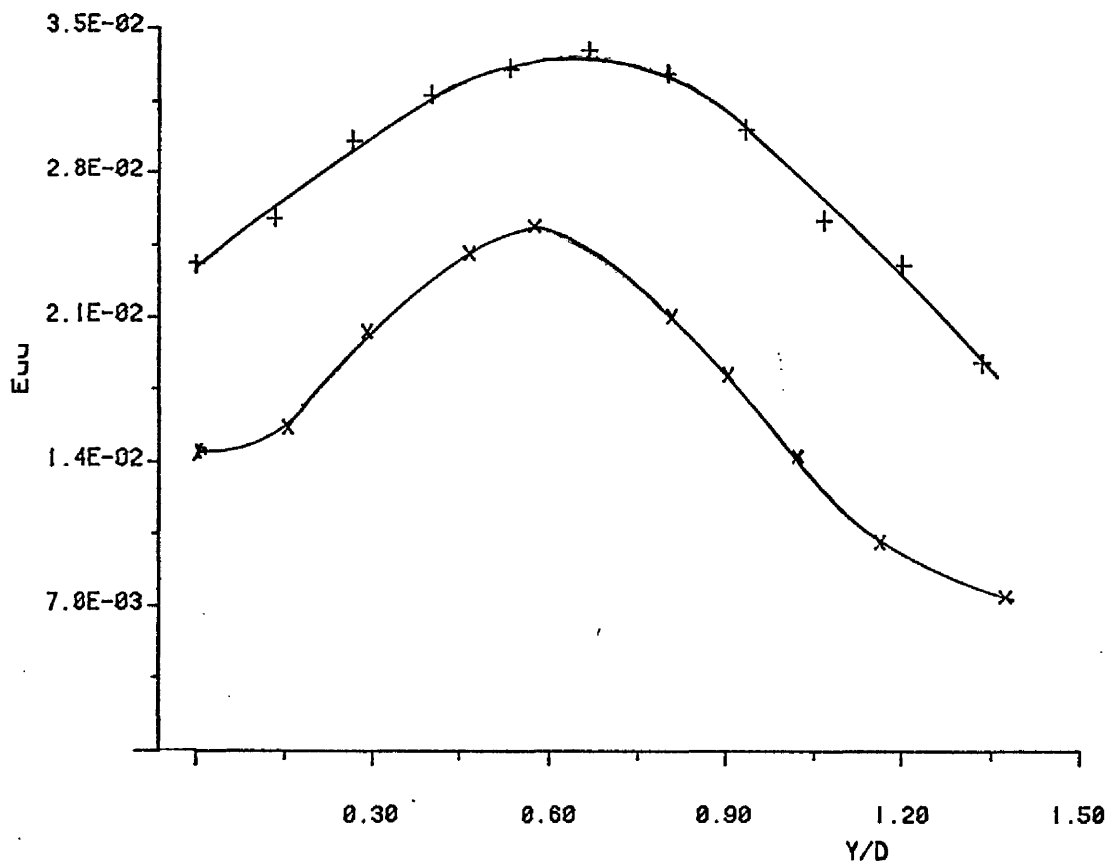
FIGURE (⍺-1): Distribution of wake energy transverse to the
wake at X/D=6.0 . + - Kokkalis, ✕ - Roshko (Re=500)

103

FIGURE (β-1): Distribution off Mean Velocity Ratio and Turbulence
Intensity transverse to the wake at X/D=3.0

	Model (I)	Model (II)	Model (III)
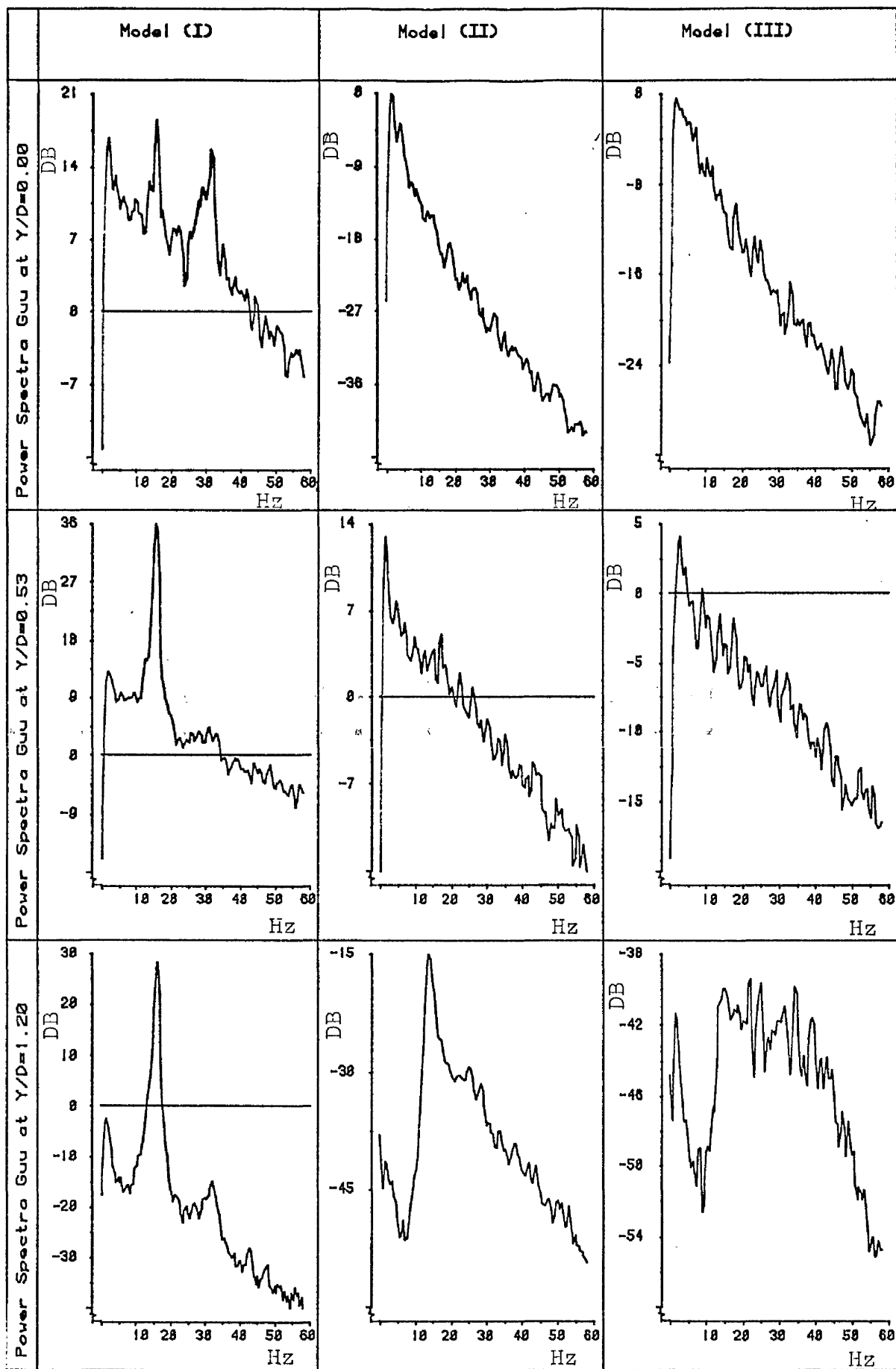
Figure (β-2): Distribution of Guu Power Spectra transverse to the wake at X/D=3.0 .
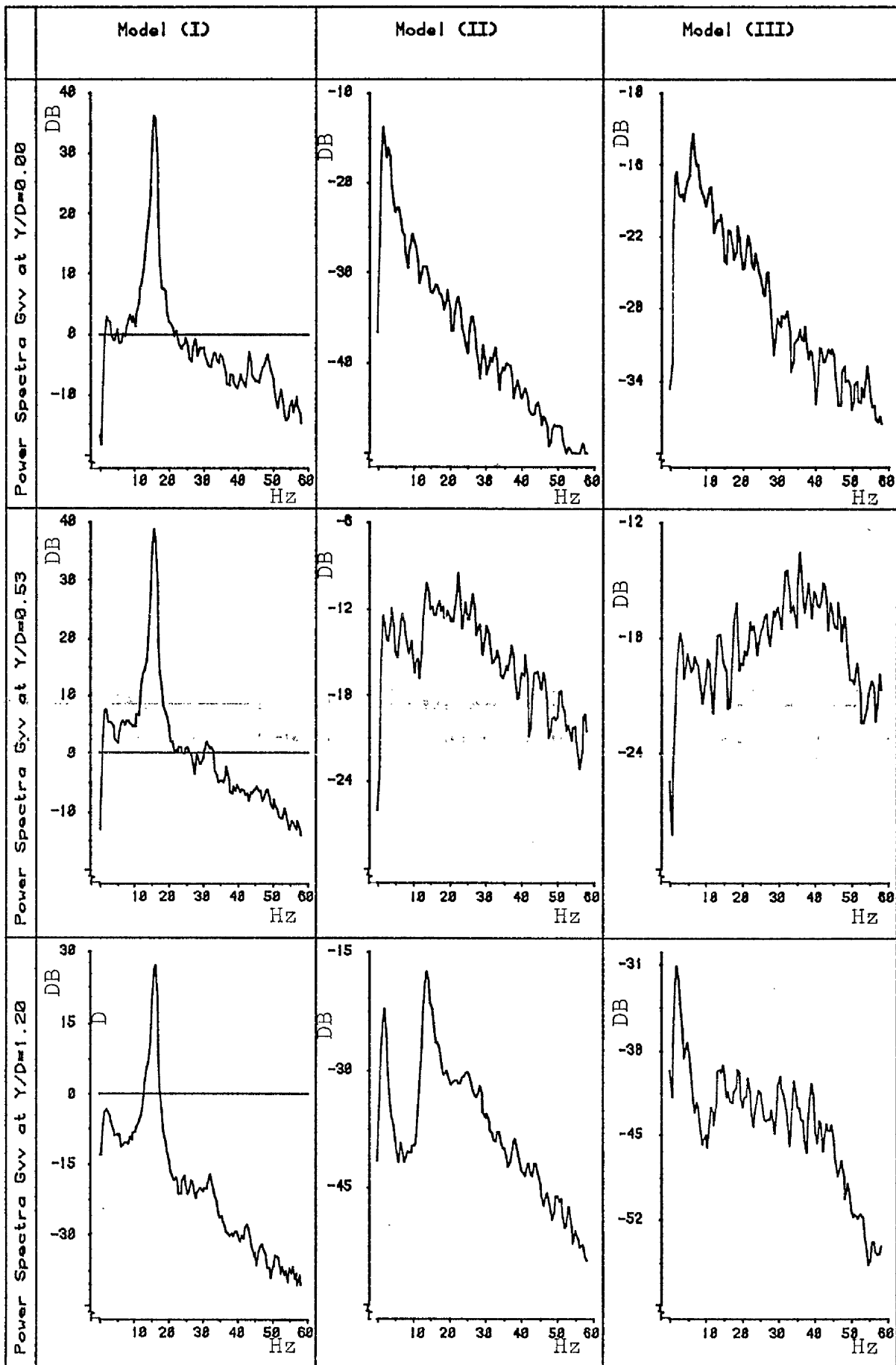
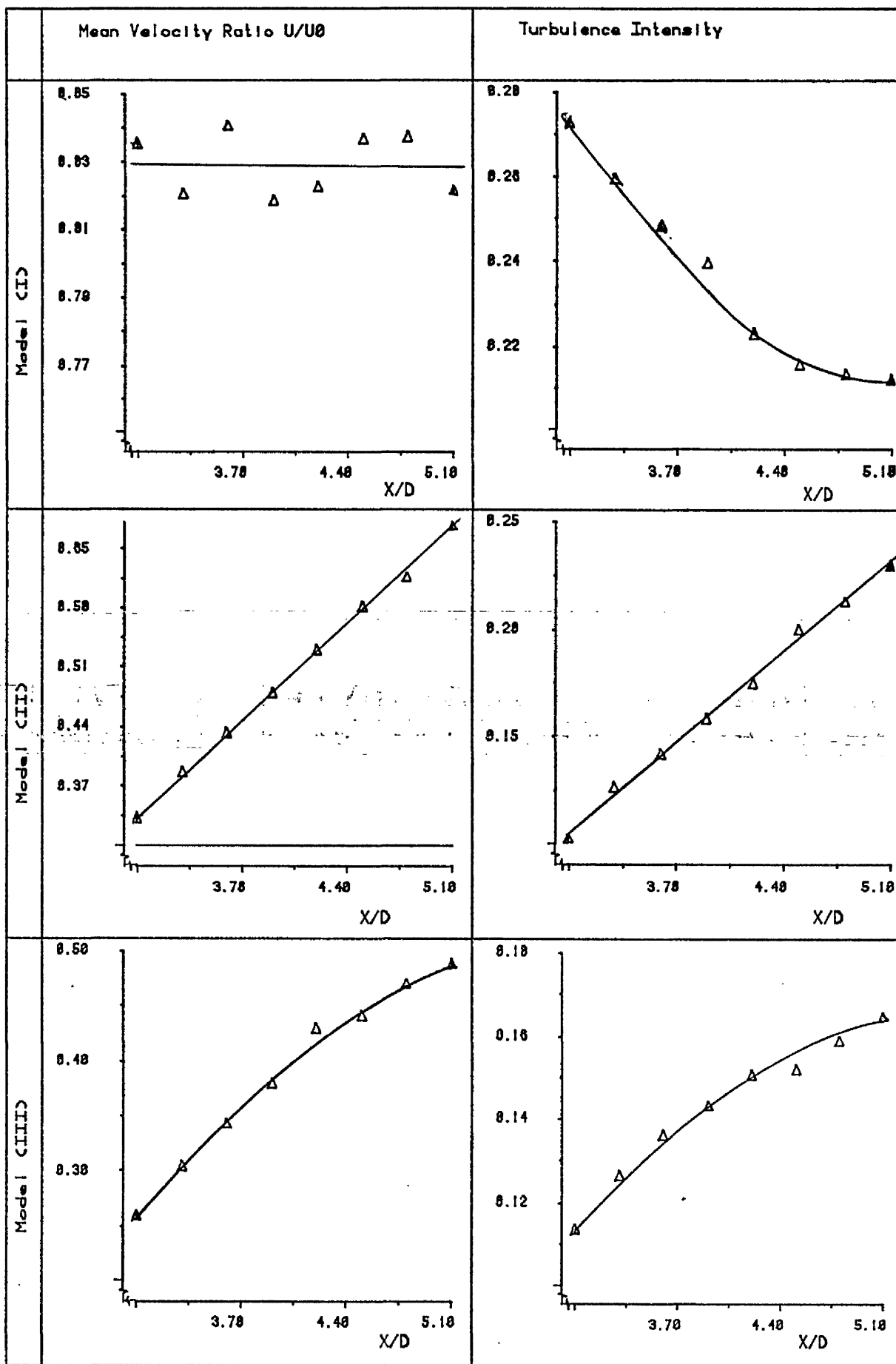Figure (β-3): Distribution of Gvv Power Spectra transverse to the wake at X/D=3.0 .

106
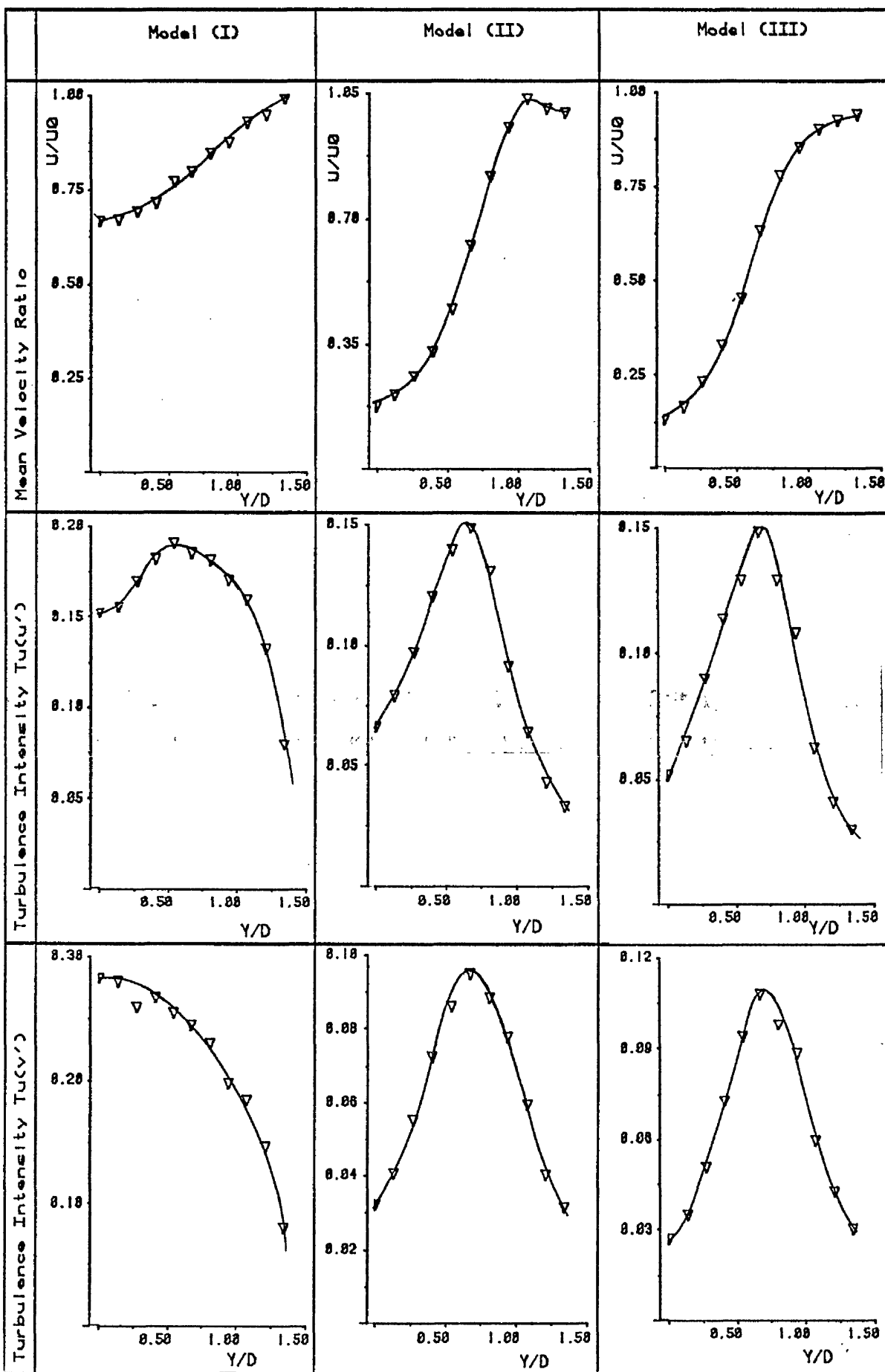
FIGURE (β-4) "Distribution of Mean Velocity Ratio and Turbulence Intencity transverse to the wake at X/D=4.5".

107
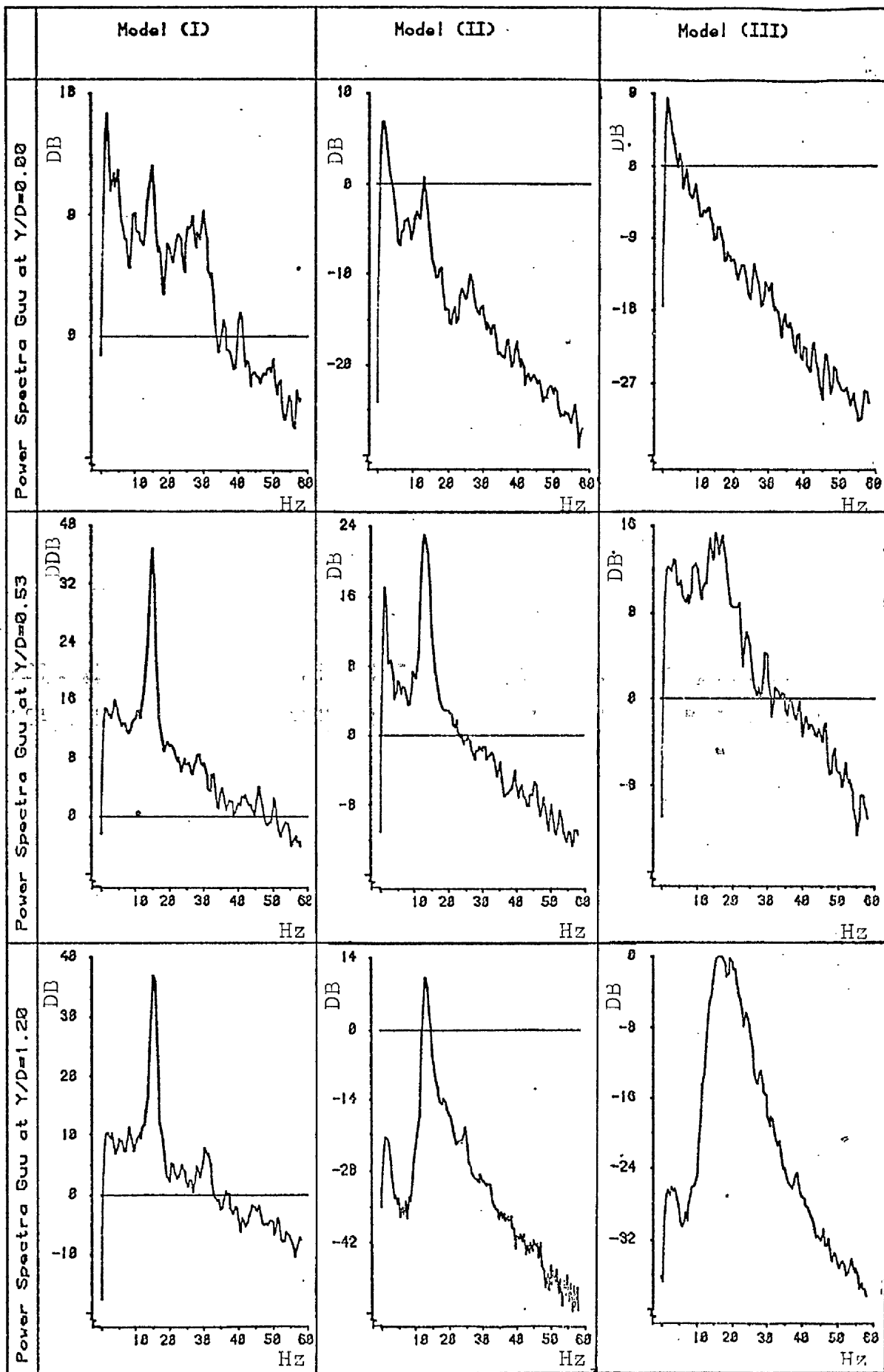
Figure (β-5): Distribution of Guu Power Spectra transverse to the wake at X/D=4.5 .

108

Figure (β-6): Distribution of Gvv Power Spectra transverse to the wake at X/D=4.5 .
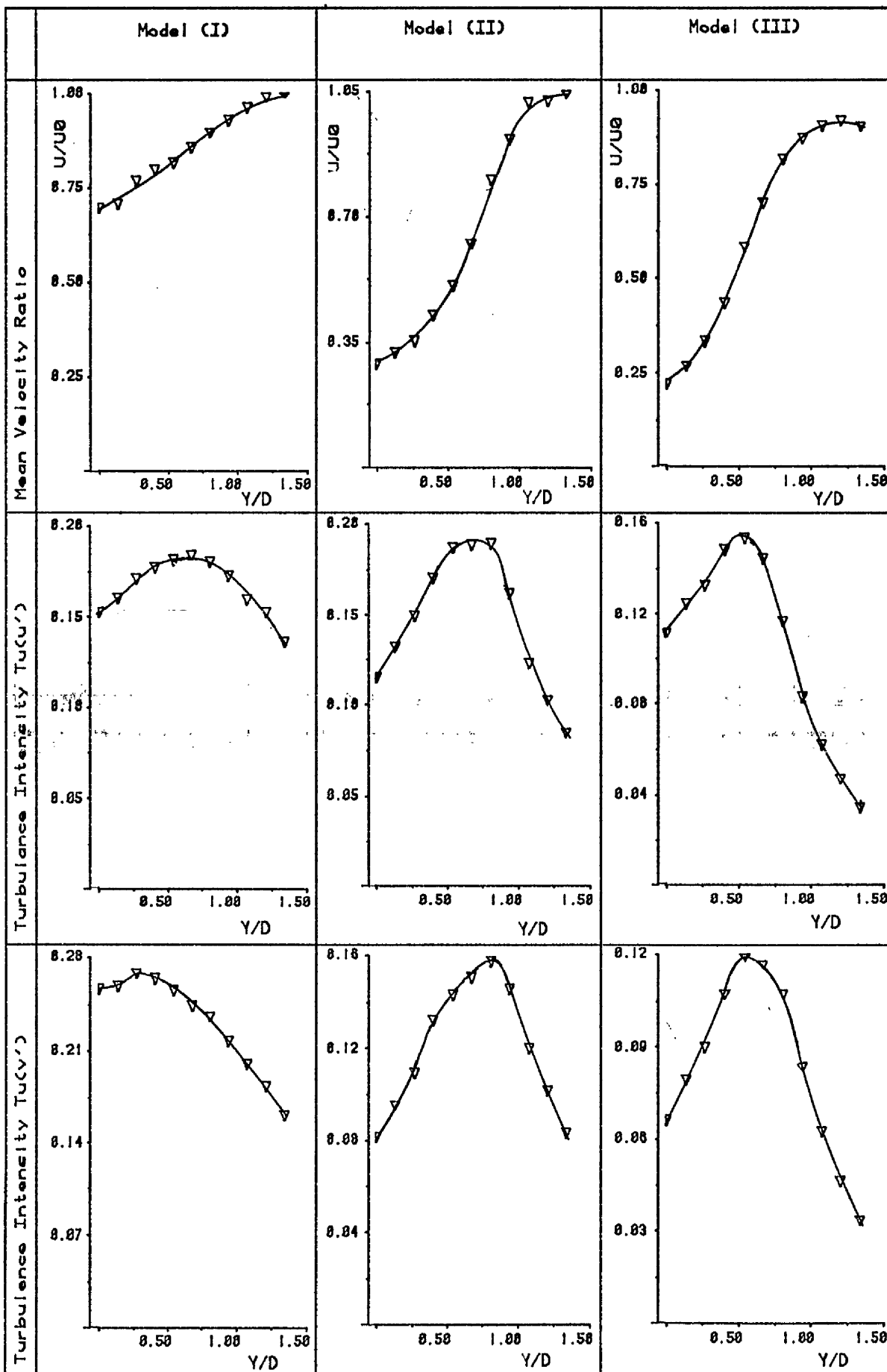
FIGURE (β -7): Distribution of Mean Velocity Ratio and
Turbulence Intencity transverse to the wake at X/D=6.0 .

110

Figure (β-8): Distribution of Guu Power Spectra transverse
to the wake at X/D=6.0 .

111
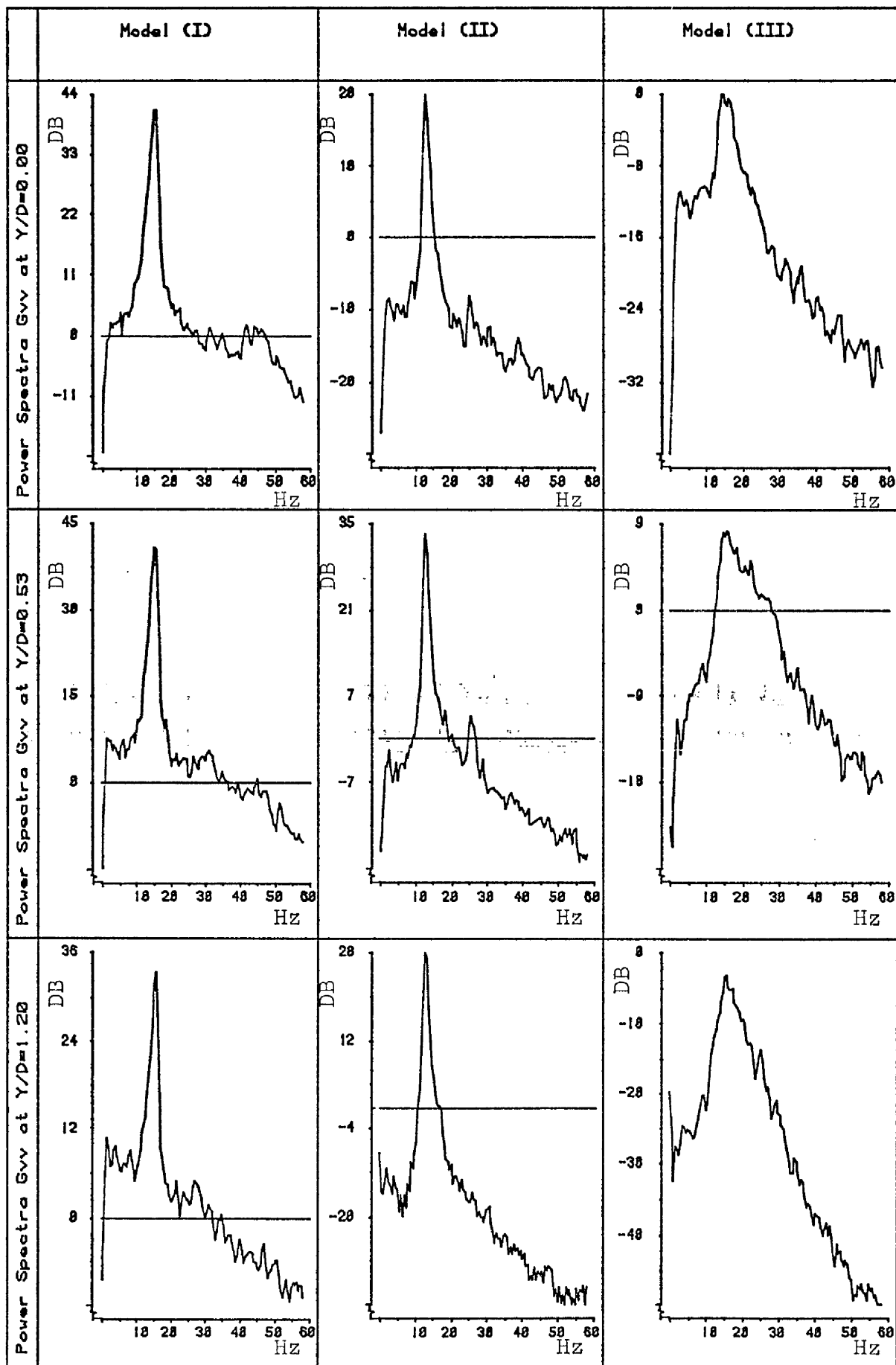
Figure (β-9): Distribution of Gvv Power Spectra transverse to the wake at X/D=6.0 .

FIGURE (γ-1) Distribution of Mean Velocity Ratio and Turbulence Intensity along the wake (Y/D=0.6).
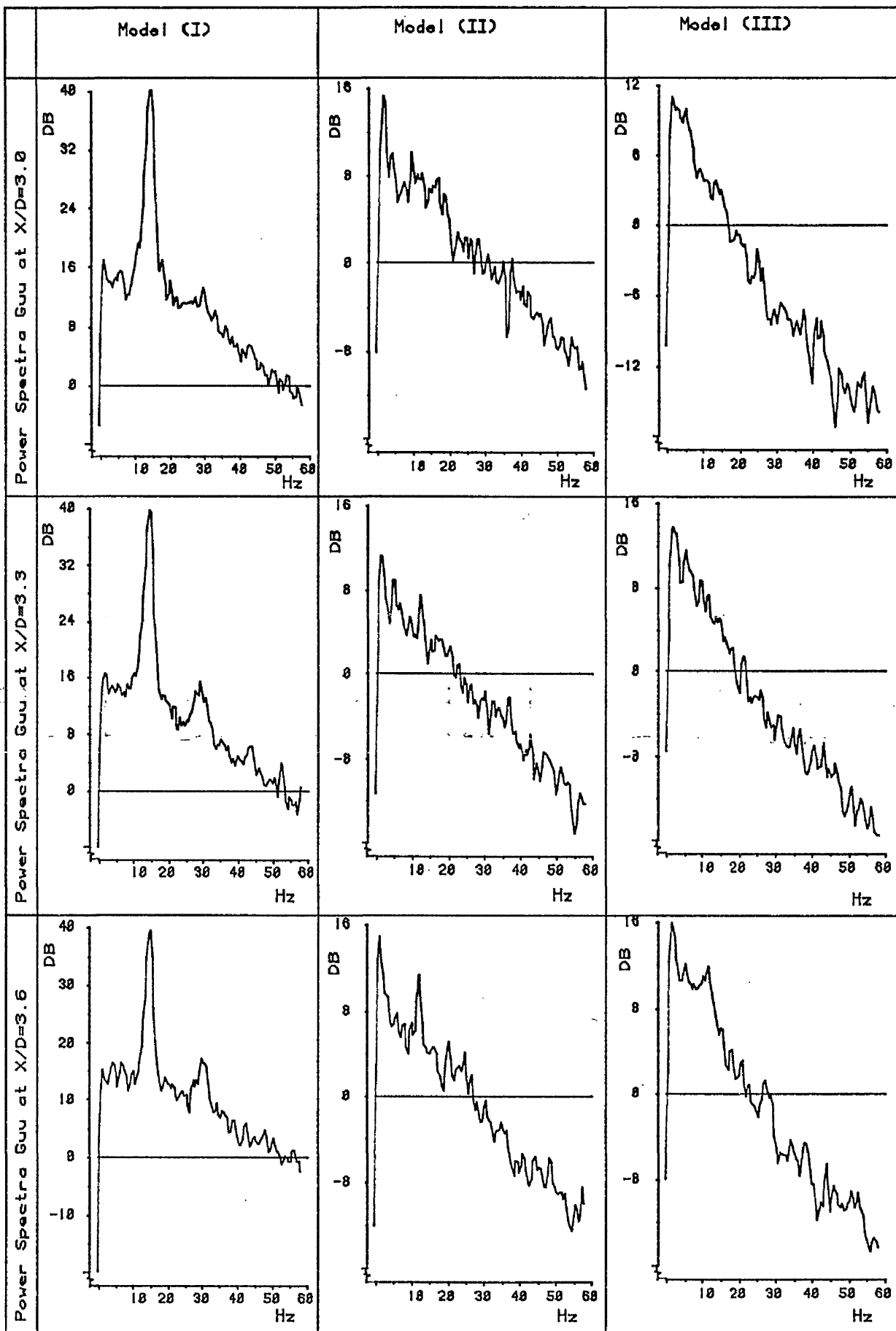
FIGURE (γ - 2): Distribution of Power Spectra along the wake axis and at Y/D=0.6 .
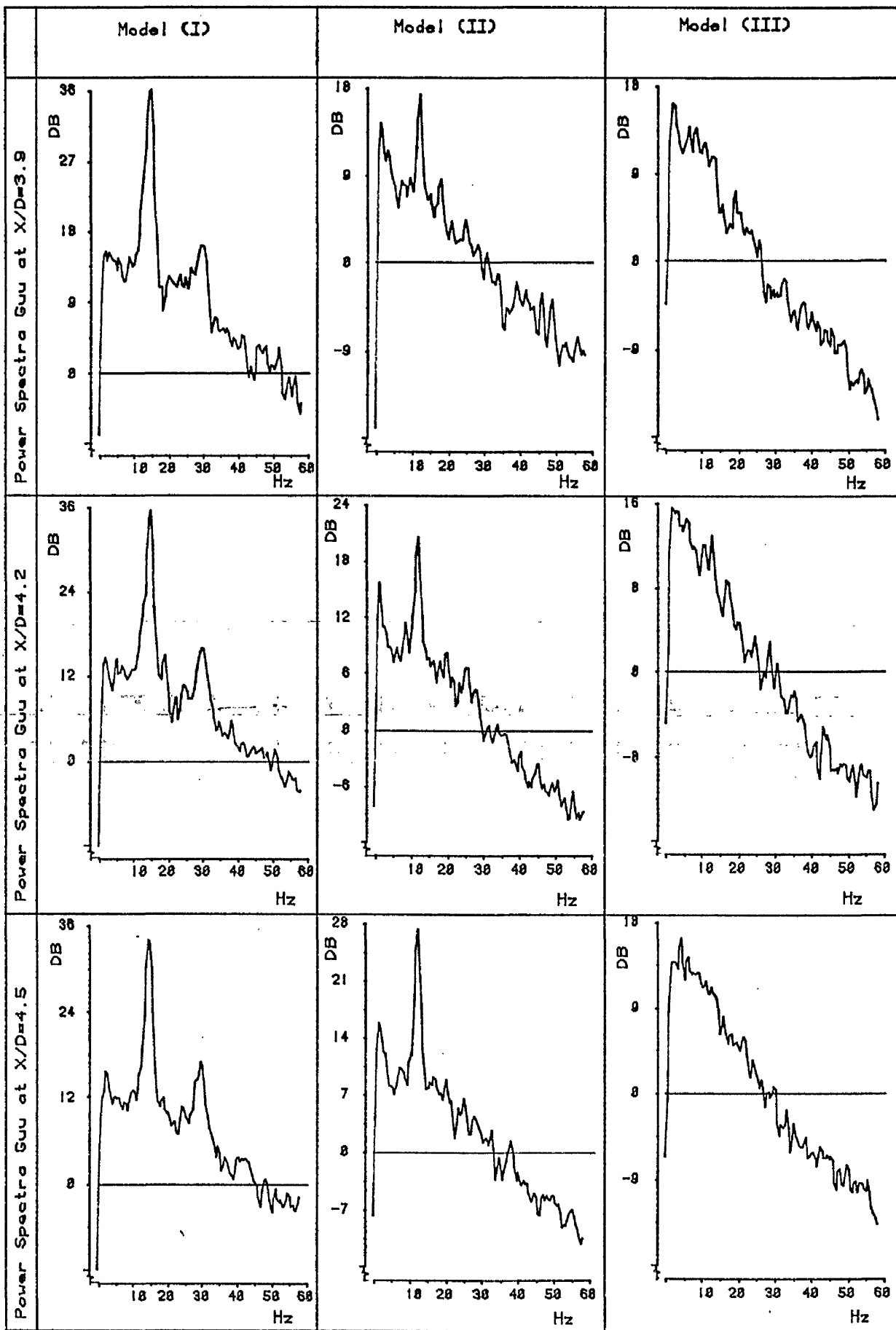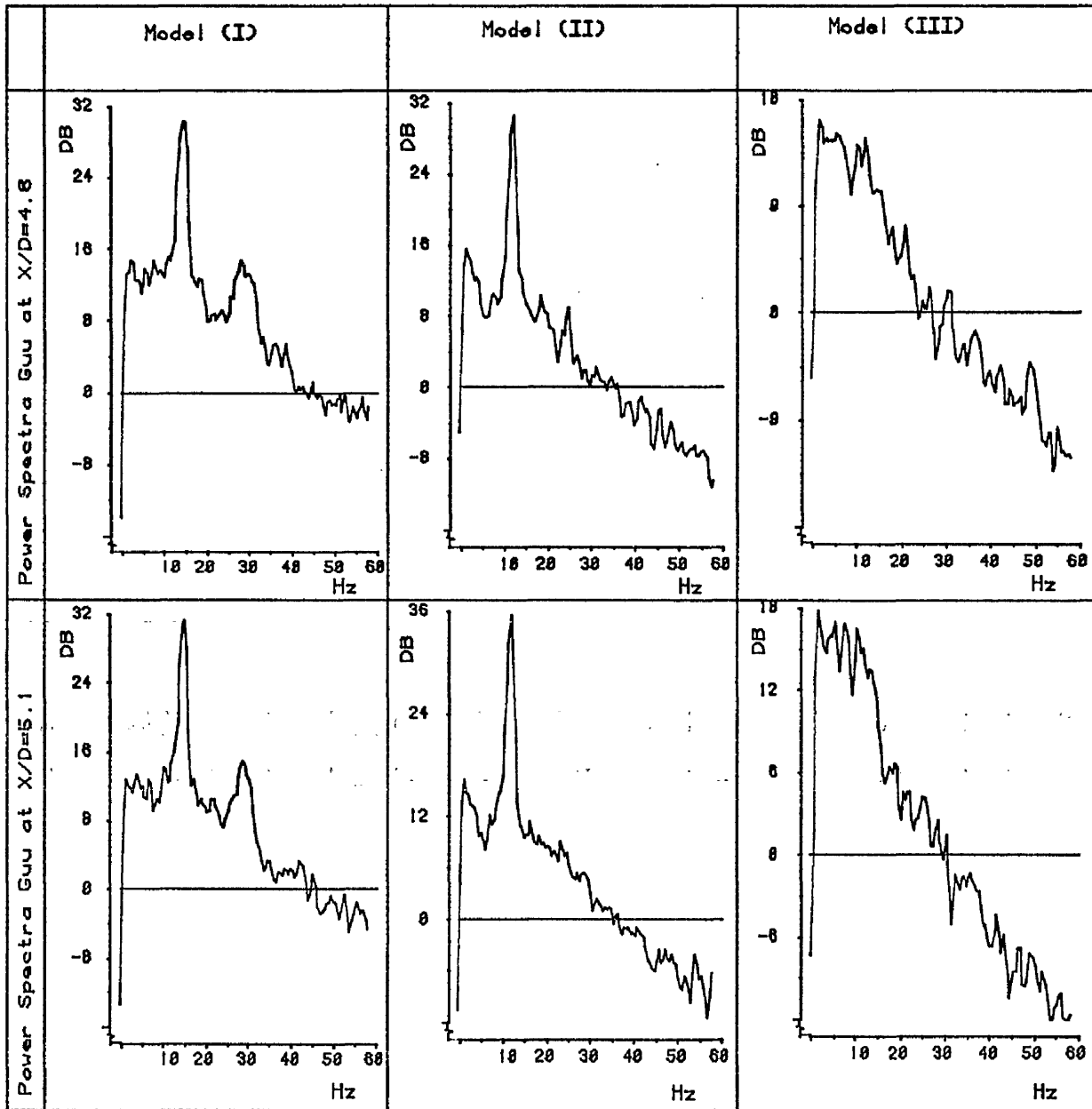
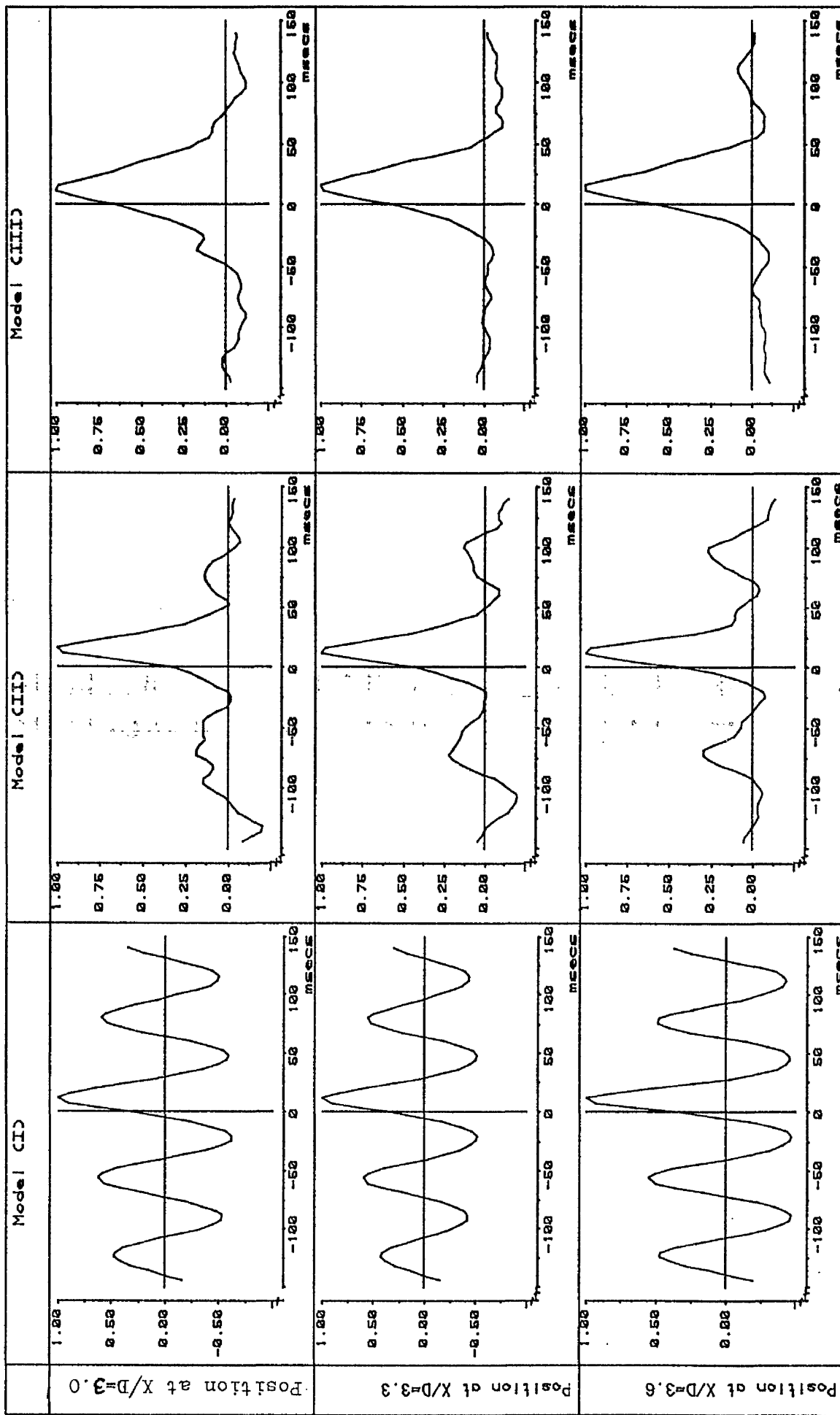FIGURE (γ - .2): (Continued)

FIGURE (γ-2): (Continued)

116

FIGURE $(\gamma$ -3): Cross-Correlation coefficient function at various positions along the wake .
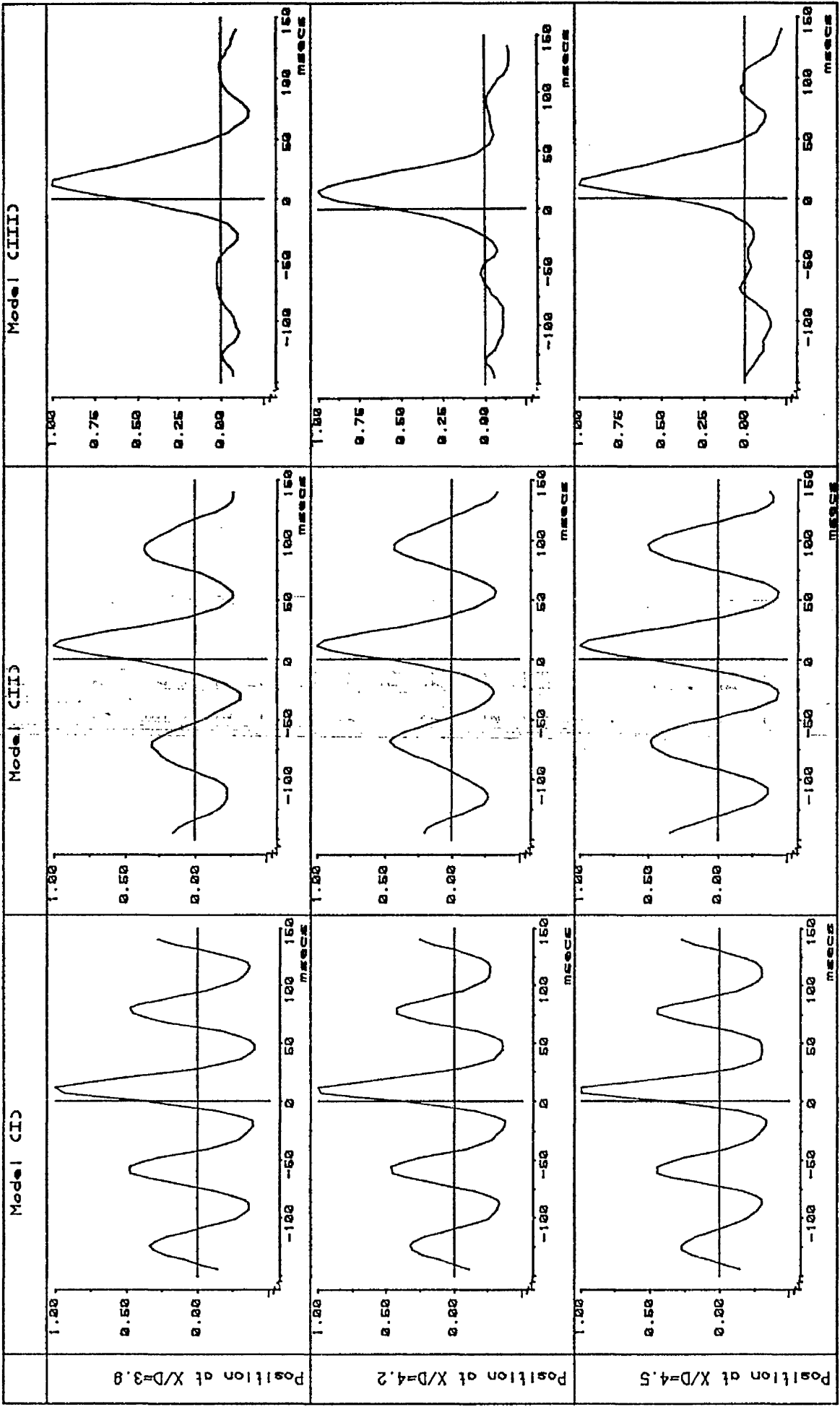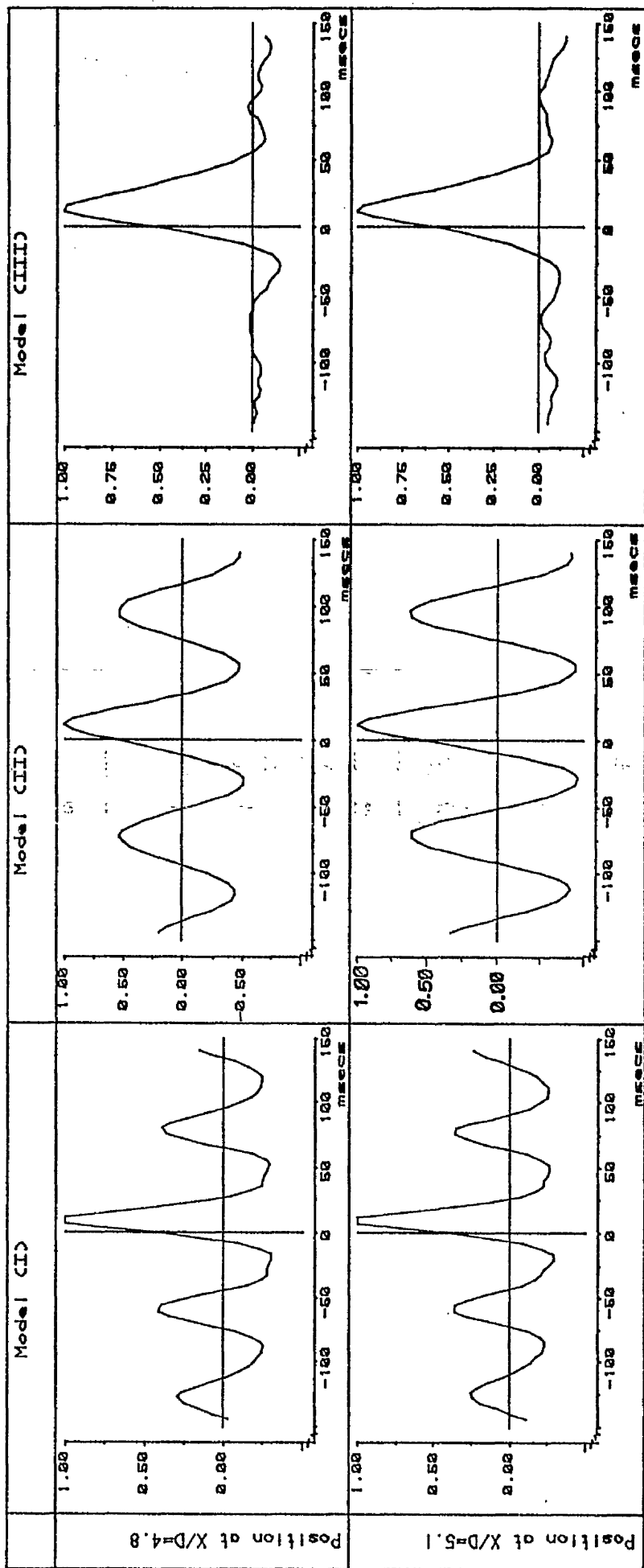
117

FIGURE (γ-3): (Continued)
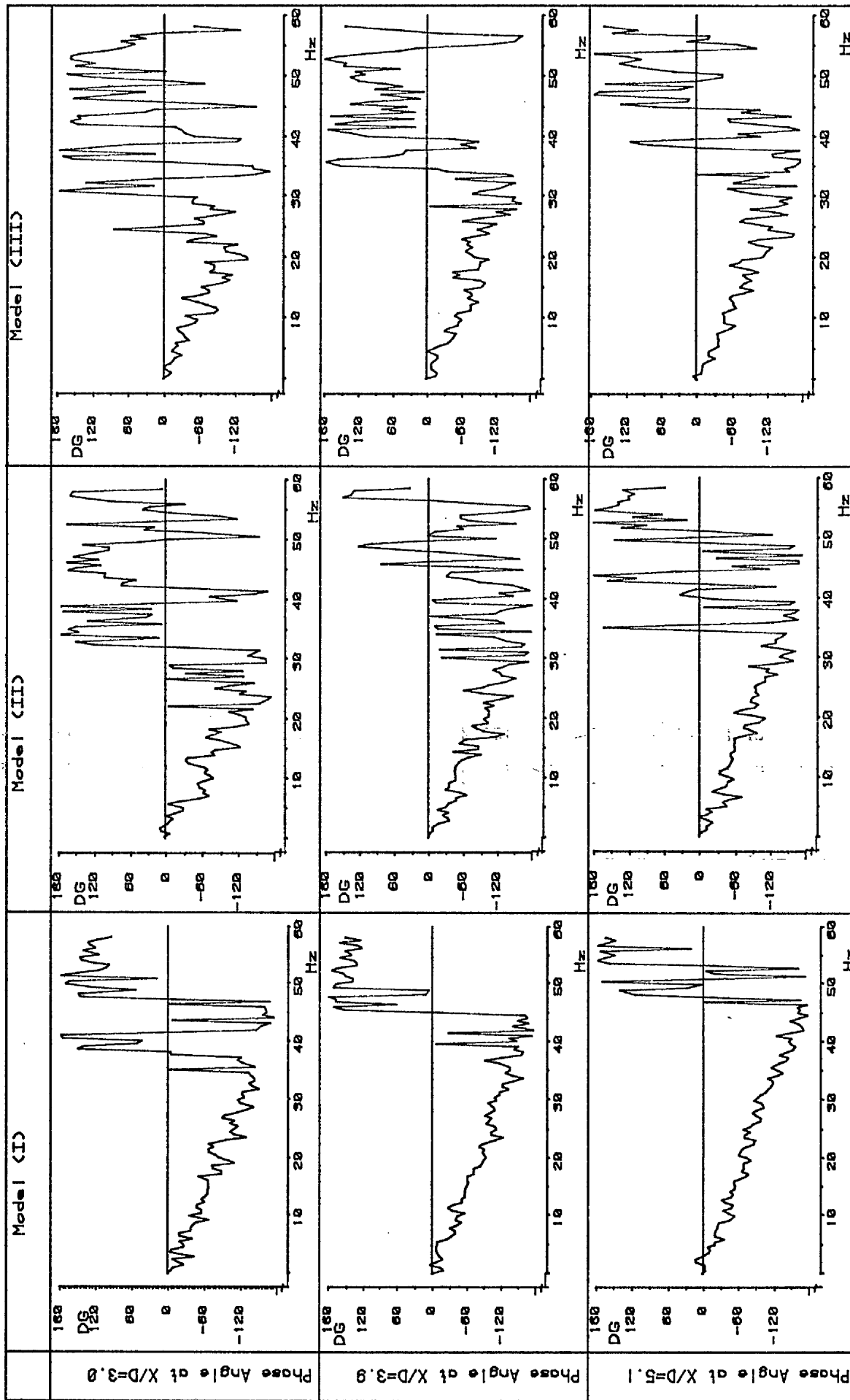
118

FIGURE (γ-3): (Continued)

119

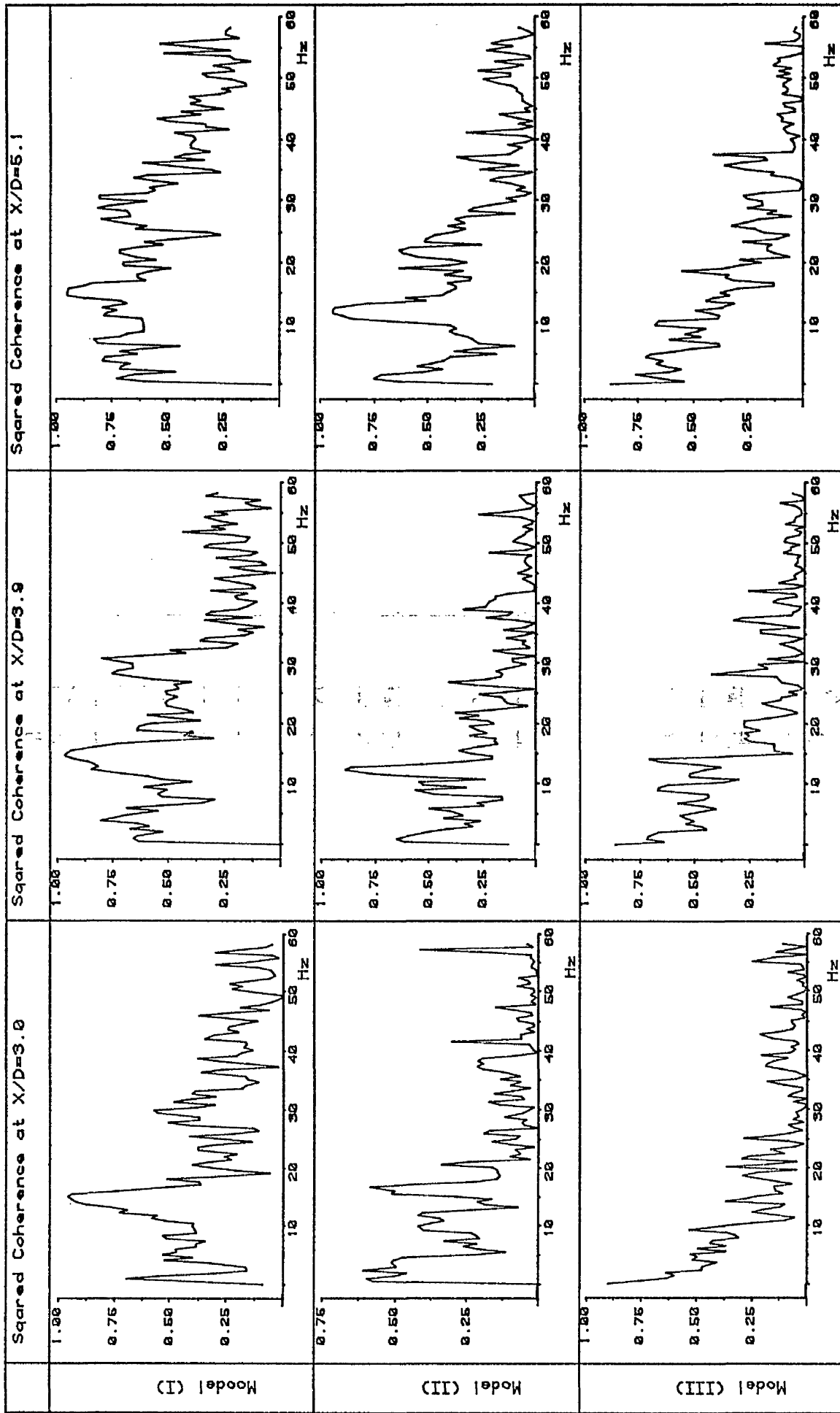FIGURE (Y-4): Phase Angle at selected positions along the wake (Y/D=0.6).
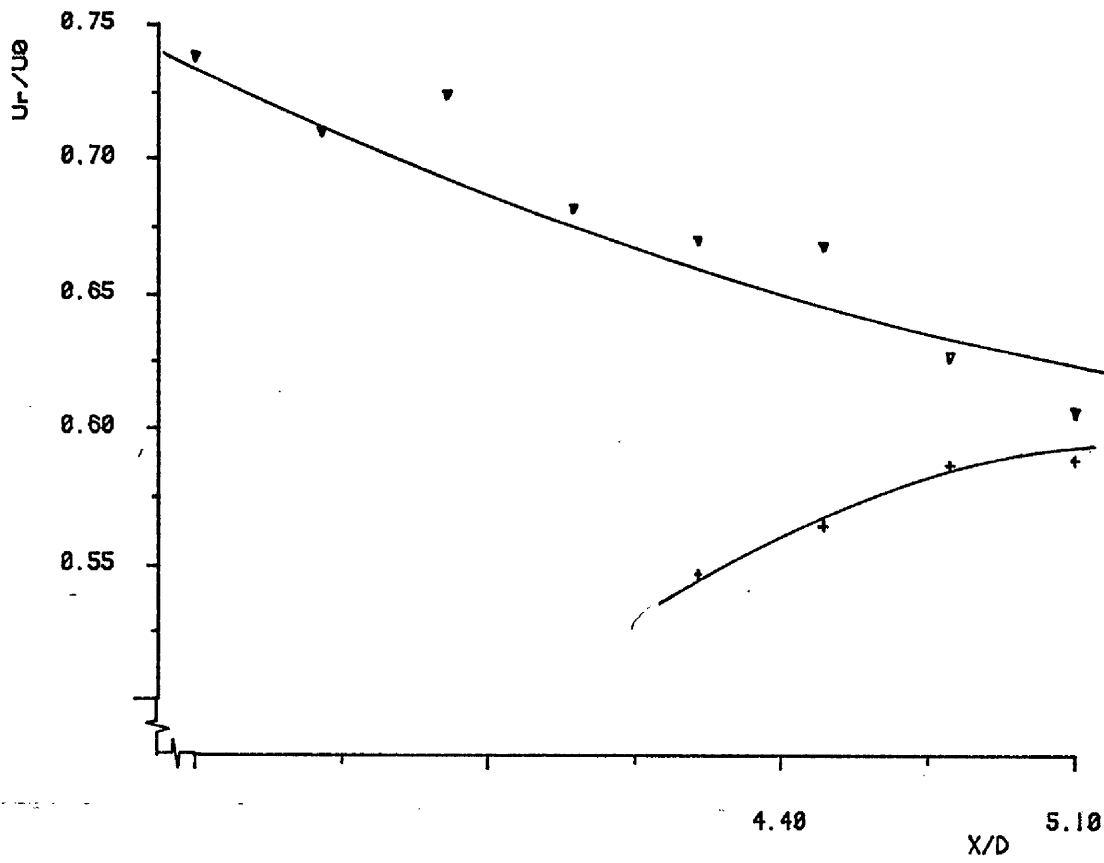
FIGURE (χ-5): Sqared Coherence at selected positions along the wake (Y/D=0.6) .
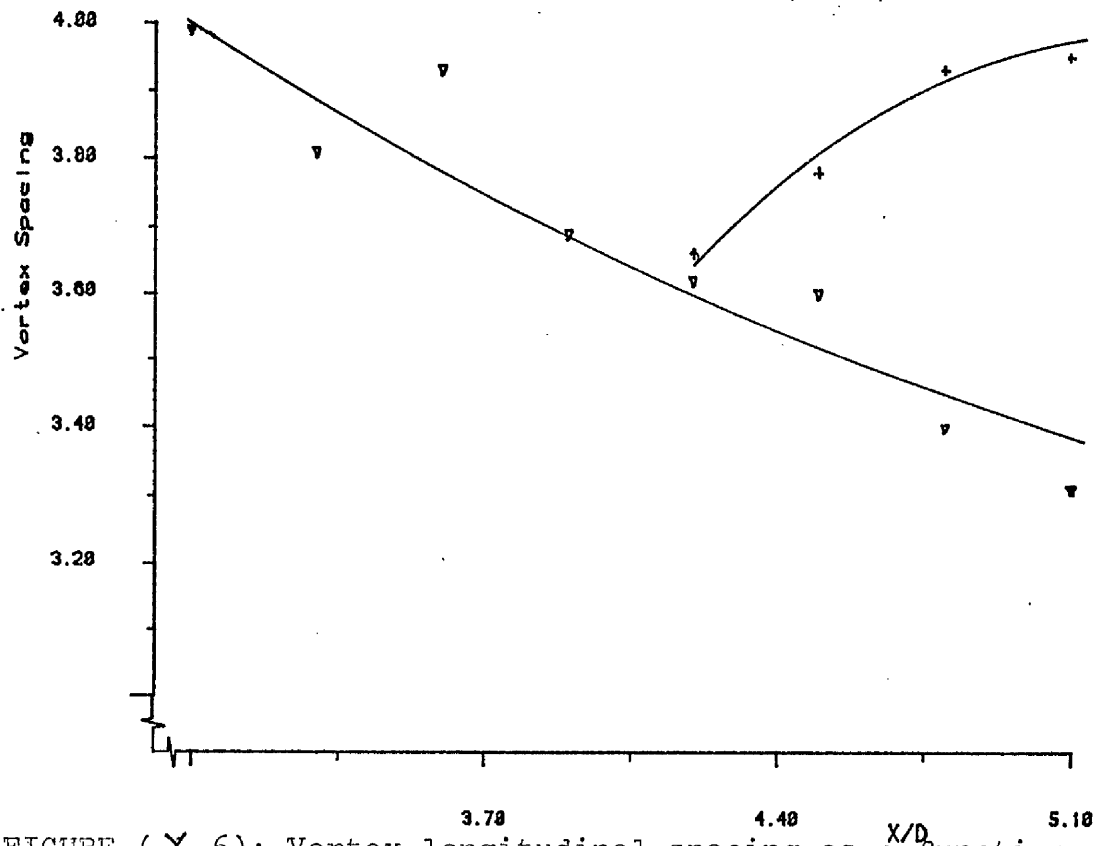
Vortex speed ratio as a function of downstream distance.

FIGURE (χ-6): Vortex longitudinal spacing as a function of downstream distance (Y/D=0.6).

REFERENCES

1. POPHAM, A.E. 'The Drawings of Leonardo de Vinci', Jonathan Cape, (1946).

2. KARMAN, T. von (mit Rubach H.), 'Uber den Mechanismus', Physikalishe Zeitschrift. 13, 49-59, (1912)

3. ABERNATHY. F.H. and KRONAUER, R.E., 'The formation of vortex streets', Journal of Fluid Mechanics, 13, 1-20,(1962).

4. BEARMAN. P.W.. 'Investigation into the effect of base bleed on the flow behing a two dimensional model with a blunt trailing edge', NPL AERO REPORT No. 1178, December 1965.

5. WOOD, C.J.. 'The effect of base bleed on a Periodic Wake', Journal of Royal Aeronautical Society, 68, 477-482, (1964).

6. GERRARD, J.H.. 'The mechanics of the formation region of vortices behind bluff bodies', Journal of Fluid Mechanics, 25, 401-413, (1966).

7. "Modern developments in Fluid Dynamics". Edited by S. Goldstein. Vol. II, pp 419, Oxford Press, (1950).

8. MORKOVIN, M.V., 'Flow around circular cylinder. A Kaleidoscope of challenging fluid phenomena', A.S.N.E. Symposium on Fully separated flows, Philadelphia, Pa., 1964.

9. BEARMAN, P.W., 'On vortex shedding from a circular cylinder in the critical Reynolds number regime',J. Fluid Mech., part 3, 37 , 577-585 (1969).

10. SCRUTON. C. and WALSHE, D.E.J., 'A means for avoiding wind-excited oscillations of structures with circular or nearly circular cross-section, NPL.

11. PRICE, P., 'Suppression of the fluid induced vibration of circular cylinders'. J. Engng. Mech. Div. Am. Soc. Cir. Engrs, Paper 1030, ^θ^θ, (1956).

12. ZDRAVKOVICH, M.M., 'Review and classification of various aerodynamic and hydrodynamic means for suppressing vortex shedding', Journal of Wind Engin. and Industrial Aerodynamics, 7. 145-189, (1981).

13. WONG, H.Y., 'An aerodynamic means of suppressing vortex excited oscillation', Proc. Instn. Civ. Engrs., Part 2, 63, 693-699, (1977).

14. WONG, H.Y., 'A means of controlling bluff body flow separation', Journal of Industrial Aerodynamics, 4, 183-201, (1979).

15. WONG, H.Y., 'Taming the vortices for Industry', University

of Glasgow, Report No. 8201, January 1982.

16. WONG, H.Y. & KOKKALIS, A., 'A comparative study of three aerodynamic devices for suppressing vortex induced oscillation', Journal of Wing Engin. and Industrial Aerodynamics, 10, 21-29, (1982).

17. WONG, H.Y. & COX, R.N.. 'The suppression of vortex induced oscillations on circular cylinders by aerodynamic devices', Proceedings of the 3rd Colloqium on Industrial Aerodynamics, ed. Carl Kramer u. Hans-J. Gerhardt, Aachen, F.D.R., Part 2, 185-204, (1978).

18. ROSHKO, -A., 'On the development of turbulent wakes from vortex streets', NACA TN 2913, 1952.

19. BLOOR, S.M. & GERRARD, J.H., 'Measurements on turbulent vortices in a cylinder wake', Proceedings of the Royal Society, A, 294, 319-342.

20. SIMMONS, J.E.L., 'Phase angle measurements between hot-wire signals in the turbulent wake of a two dimensional bluff body', Journal of Fluid Mechanics, 64, part 3, (1974).

21. BENDAT, J. & PIERSOL, A., 'Measurement and Analysis of Random Data', J. WILEY & SONS, 1966.

22. KING, L.V., 'On the convection of heat from small cylinders in a stream of fluid: Determination of the convection constants of small platinum wires with applications to Hot-Wire Anemometry', Phil. Trans. Roy. Soc., London, Series A, 214, 1914.

23. COLLIS, D.C. & WILLIAMS, M.J., 'Two dimensional convection from heated wires at low Reynolds numbers', Journal of Fluid Mechanics, 6, 357 (1959).

24. BRUUN, H.H., 'Interpretation of a hot-wire signal using a universal calibration law', J. Phys. E. Sci. Intrum., 4, 225, (1971a).

25. FROEBEL, E., 'DFVLR-Institut fur Turbulenz Forschung, Report, 1969.

26. ROSHKO, A., 'A new hodograph for free-streamline theory', NACA, Techn. Note 3168, 1953.

27. PERRY, A.E. et al, 'The vortex shedding process behind two dimensional bluff bodies', Journal of Fluid Mechanics, 116, 77-90, (1982).

28. SAUSTRUP KPISTENSEN, H., 'Hot-wire measurements in Turbulent Flows', DISA Publication.

29. BRUUN, H.H., 'Linearization and hot-wire anemometry',

Journal of Physics E: Scientific Instruments, 4, 815-820 (1971).

30. RICHTER, A. & NAUDASCHER, E., 'Fluctuating forces on a rigid circular cylinder in confined flow', Journal of Fluid Mechanics, 78, part 3, 561-576, (1976).

31. FAGE, A. & JOHANSEN, F.C., 'the structure of vortex streets', Philosophical Magazine V, 417-441, (1928).

32. FERGUSON, W., & PARKINSON, G.V., 'Surface and wake flow phenomena of the vortex-excited oscillation of a circular cylinder', Journal of Engineering for Industry (A.S.M.E.), 831-838, (1967).

33. SONNERVILE, P., 'Structure tridimensionnelle des ecoulements outour d'un cylindre circulaire', Bulletin Direction des Etudes et Recherches, Electricite de France, Serie A, No. 3, 1976.

34. TOEBES, G.H., 'The unsteady flow and wake near an oscillating cylinder', Journal of Basic Engineering, (A.S.H.E.), 493-505, September 1969.

35. ANGRILLI, F. et al, 'Investigation of wall inducted modifications to Vortex shedding from a circular cylinder', Journal of Fluids Engineering (A.S.H.E.), 104, 518-522, (1982).

36. McD. GALBRAITH, R.A., 'Flow pattern around a shrouded cylinder at Re = 5 X 103', Journal of Wing Engineering and Industrial Aerodynamics, 6, 227-242, (1980).

37. BEARMAN, P.W., 'On vortex street wakes', J. Fluid Mech., part 4, 28, 625-641, (1967).

38. EL. BAROUDI, M.Y., 'Measurement of two-point correlations of velocity near a circular cylinder shedding a Karman vortex street', UTIAS Report 76, (1960).